N73-18833

NASA TECHNICAL TRANSLATION

NASA TT F-747

NASA TT F-747

CASE FILE COPY

ASTROMETRY AND ASTROPHYSICS NO. 14

Physics of the Moon and Planets

Edited by I. K. Koval'

"Naukova Dumka" Press, Kiev, 1971

NATIONAL AERONAUTICS AND SPACE ADMINISTRATION • WASHINGTON, D. C. • FEBRUARY 1973

NASA TT F-747

ASTROMETRY AND ASTROPHYSICS NO. 14

Physics of the Moon and Planets

Edited by I. K. Koval'

Translation of "Astrometriya i Astrofizika 14. Fizika Luny i Planet." Edited by I. K. Koval'. "Naukova Dumka" Press, Kiev, 1971

For sale by the National Technical Information Service, Springfield, Virginia 22151
$3.00

Translated by Consultants Bureau, Inc.

Annotation

This collection contains the results of spectrometry investigations of the planets. Certain of the data are based on observations made with the 70-centimeter reflector at the Main Astronomical Observatory of the Academy of Sciences of the Ukrainian SSR and with the 2-meter reflector at the Shemakha Astrophysical Observatory. Much of the material in the collection is devoted to the study of ultraviolet absorption in the continuous spectrum of different sections of Jupiter and Saturn. The articles also reflect the results of photometric measurements of artificial planets made in the laboratories of the Main Astronomical Observatory of the Academy of Sciences of the Ukrainian SSR, and certain theoretical questions. While designed for scientific workers, astrophysicists, and geophysicists, the materials in this collection also can be helpful to students and graduate students in the respective specialties.

TABLE OF CONTENTS

Page

The Violet Clouds of Mars, N. B. Ibragimov, I. K. Koval' 1

Ultraviolet Absorption in the Continuous Spectrum of Jupiter, V. D. Krugov 10

Distribution of the Energy in the Shortwave Region of the Spectrum for Various Parts of Saturn's Disk, V. D. Krugov. 29

Results of Laboratory Photometric Measurements of Artificial Planets, O. I. Bugayenko, I. K. Koval', V. D. Krugov, A. V. Morozhenko, L. F. Slutskiy 42

Spectrophotometric Peculiarities of some Satellites of Planets, Yu. D. Davudov, I. K. Koval' 61

Glow from the Limb Side of a Spherical Planetary Atmosphere, E. G. Yanovitskiy. 70

The Possibility of Automatically Obtaining Statistical Morphological Characteristics of Sections of the Lunar Surface from their Photographic Images, L. A. Akimov, Yu. V. Korniyenko. 81

THE VIOLET CLOUDS OF MARS

N. B. Ibragimov, I. K. Koval'

ABSTRACT. Results are given of photometric investigations of Martian violet clouds based on observations carried out during 1958 - 1961, 1965, and 1969. Photometric data for the former three oppositions were obtained at the Astronomical Observatory of the Ukrainian Academy of Sciences. In 1969 the observations were made with the 2-meter reflector of the Shemakha Observatory using a grating spectrograph (dispersion 30 Å/mm). Monochromatic albedo was determined for an intense cloud observed near the terminator in the southern hemisphere on April 24, 1969. The values of optical thickness found in this investigation permitted the Junge parameter ($\nu = 3.9$) to be determined and a conclusion to be made that the violet cloud consists mainly of small particles.

The brightest violet clouds usually are seen at the eastern and western limbs of Mars when observations are in the shortwave region of the spectrum. They were first observed by Wright, the American astronomer in 1924, and since that time these formations have been under systematic observation by many observatories around the world. /3*

Slipher's photographic atlas [1] contains many excellent pictures of Mars, obtained over the past decade. This material leads to the conclusion that the violet clouds are not always seen. These clouds did not appear, except on rare occasions, during the favorable 1956 opposition. However, during most of the "ordinary" oppositions these formations cover up to 10 percent of the area of the visible disk of Mars, and sometimes are comparable in brightness to the polar caps.

Study of the activity of violet clouds in terms of heliocentric longitude of the planet has attracted the attention of astronomers for a comparatively long time, but not until 1958 [2], and again in 1961 [3], were the photometric characteristics of these formations obtained.

Violet clouds along the edges of the equatorial diameter of the Martian disk were a routine phenomenon in September - November 1958. The bright streak located along the equator and connecting the intense limb clouds was seen quite

---

* Numbers in the margin indicate pagination in the foreign text.

well at times in the blue and violet rays.

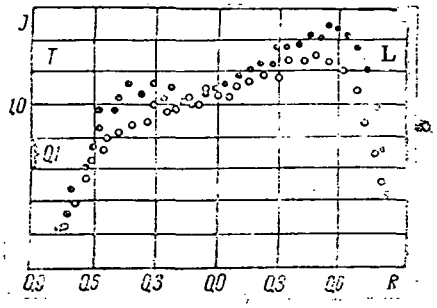

Figure 1. Photometric section of the Martian disk near the equator from 1958 photography (λ_{ef} = 3900 Å). The dots are the section passing through the violet clouds, the circles the comparison section (phase angle 21°).

Figure 1 is an example of the photometric sections parellel to the planet's equator and intersecting the violet clouds at the eastern and western limbs of the image. The section passes through along the bright streak mentioned, and this makes it possible to evaluate the contrast created by this streak with its surroundings. This contrast is very weak, a maximum of 5 to 7 percent for 3900 Å. The comparison section (the dots in Figure 1) was constructed by averaging the measurements along two directions inclined to the equator at an angle of about 15° because the clouds were located in the latitudinal direction quite distant from the equator (about ±10°).

TABLE 1. PHOTOMETRIC CHARACTERISTICS OF VIOLET CLOUDS FROM 1958 OBSERVATIONS

Date	λ micron	Terminator (W)			Limb (O)		
		ϱ_1	ϱ_2	$\Delta\varrho$	ϱ_1	ϱ_2	$\Delta\varrho$
October 8/9	0.40	0.102	0.077	0.025	0.118	0.110	0.008
„ 13/14	0.40	103	088	015	128	111	017
„ 14/15	0.40	085	050	033	128	112	016
„ 21/22	0.36	060	050	010	078	070	008
„ 28/29	0.36	058	048	010	067	054	012
November 4/5	0.40	107	103	004	125	115	010
„ 5/6	0.40	113	101	012	128	118	010
„ 9/10	0.40	103	077	026	119	110	009

Table 1 lists the results of 1958 violet cloud photometry. The relative measurements have been converted into absolute with respect to 1956 data. This is why the table lists the apparent albedo for the section of the planet near the cloud, ϱ_2, and for the cloud itself, ϱ_1. These data, obtained for different longitudes of the central meridian of Mars, show that the violet clouds are in no way connected with the details of the Martian surface, particularly the seas.

Yet the mean data (Table 2) show that a cloud on the terminator side (the setting limb) has a greater relative brightness than one on the limb side.

TABLE 2. MEAN PHOTOMETRIC CHARACTERISTICS OF VIOLET CLOUDS FROM 1958 OBSERVATIONS

λ microns	Terminator (W)		Limb (O)	
	contrast	Δϱ	contrast	Δϱ
0.36	0.16	0.010	0.13	0.09
0.40	0.17	0.18	0.11	0.012

Monochromatic sections passing through the Wright clouds [3] were obtained from spectrophotometry in 1960 - 1961. Reference [3] cites detailed data on /4 the distribution of brightness along the Martian equator, showing that the clouds begin to be perceived photometrically near 4800 Å. Figure 2 shows three photometric sections passing through the violet clouds and showing the increase in the cloud-background contrast on the shortwave side. Just as in 1958, the cloud on the setting limb was relatively brighter at this time.

The Wright clouds were not very bright in 1963, but were quite intense during the period of opposition in 1965 [4], standing out sharply on the photoelectric sections. The cloud on the setting limb was relatively brighter at this time. Figure 3 shows the photoelectric sections obtained on 6-7 April 1965, with a filter (maximum band pass about 3550 Å), and the fact that the cloud-continent contrast on the setting limb is 15 percent.

The mean photometric characteristics of the violet clouds, from 1958, 1961, and 1965 observations, are

λ, micron	0.36	0.40	0.45	0.50
k, W	0.20	0.20	0.17	0.04
k, O	0.13	0.10	0.07	0.03
ϱ_1, W	0.060	0.075	0.126	0.137
ϱ_2, W	0.050	0.067	0.118	0.128

The apparent albedo values for the clouds, ϱ_1, and for the adjacent continent, ϱ_2, show that the spectrum difference $\varrho_1 - \varrho_2$ changes little, although the contrast falls off quickly toward the red end of the spectrum.

The spectral limit of visibility of the clouds changes with their intensity (density). It usually puts in an appearance near 4500 Å, but at times of greatest development the visibility boundary shifts to the red end of the spectrum such that the presence of the clouds is photometrically perceptible near 5000 Å, /5 and their brightness near 3500 Å sometimes can be compared to the brightness of the polar caps.

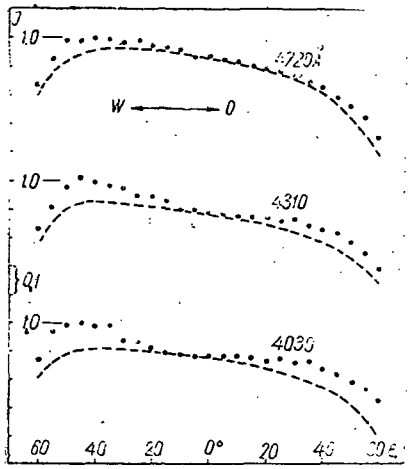

Figure 2. Photometric sections of the Martian disk near the equator from spectrograms obtained on 6-7 January 1961. Angles of reflection are plotted on the x-axis, relative intensities on the y-axis.

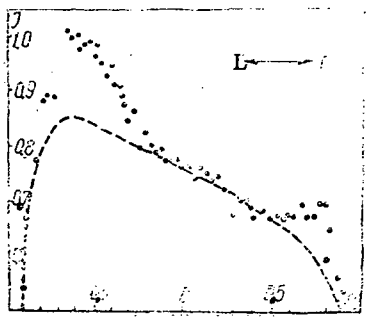

Figure 3. Photoelectric section of Martian disk near the equator, obtained 6-7 April 1965. The dashed line is the comparison section (continent). λ_{ef} = 3550 Å.

The mean size, and the number of particles in the cloud column, have been calculated from the 1958 and 1965 observations [5]. It was assumed that the refractive index of the particles was 1.5 (aerosol of the terrestrial atmosphere), that particle distribution by size was in accordance with Junge's law, and that the particles themselves were spherical. It was found that the particle radius was $r \approx 0.05$ micron, and that the number of particles was of the order of 10^{11} cm^{-2} for a mean observed cloud contrast near 4000 Å of 20 percent ($\tau \approx 0.1$).

Mars was observed in 1969 at the Shemakha Astrophysical Observatory of the Academy of Sciences of the Azerbaydzhan SSR in the Cassegrain focus of a 2-meter reflector. N. B. Ibragimov obtained scores of spectrograms of Mars with a dispersion of 30 Å/mm on Kodak OaF plates with an image scale of 7"/mm. The 24

April 1969, observations were made when the slit of the spectrograph was positioned along the chord of the planet's disk and intersected the south polar cap, the continent adjacent to it, and the intense cloud formation located near the terminator in the part of the southern hemisphere near the equator. We used the spectrograms obtained on that date to make a spectrophotometric study of the cloud formation. Photometry of the spectrograms was performed across, as well as along, the dispersion in the 3800-6600 Å region.

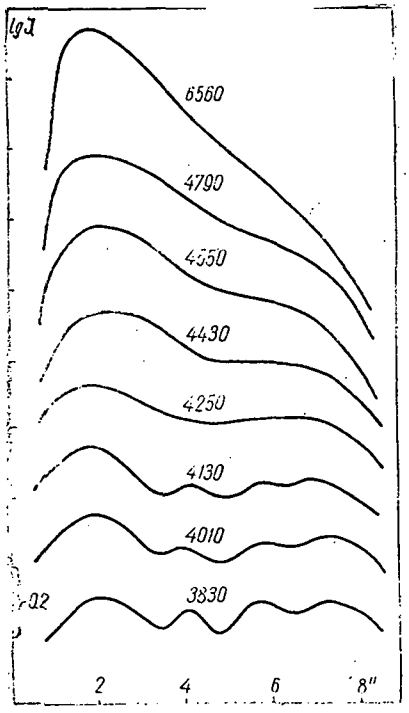

Figure 4. Photometric sections along the chord of the Martian disk intersecting the polar cap (left) and the cloud (right). Spectral observations of 24 April 1969, using the Shemakha Astrophysical Observatory's 2-meter reflector.

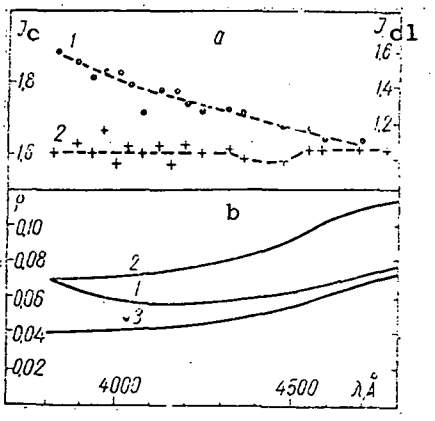

Figure 5. Photometric characteristics of a violet cloud from spectral observations on 24 April 1969.
a - cloud brightness (1) and south polar cap brightness (2) in terms of wavelength compared to continents;
b - monochromatic albedo of cloud (1), cap (2), and continents (3).

Figure 4 shows the transverse photometric section of one of the spectrograms obtained for the longitude of the central meridian of Mars near 150°. Logarithms of the intensity are plotted along the y-axis, and seconds of arc along the x-axis. As we see, the cloud becomes photometrically perceptible near 4800 Å, and near 3800 Å is comparable in brightness to the south polar cap. If the effect of

limb darkening (the phase angle at the time of observation was about 26°) is taken into consideration, and if the relative measurements obtained are made absolute in terms of the 1960 - 1961 observations [3], we obtain monochromatic values of cloud and south polar cap albedo as shown in Figure 5b. This figure shows that the cloud has a lower apparent albedo than does the polar cap, and only near 3800 Å are their albedoes comparable.

Figure 5a shows the brightness of the cloud and of the polar cap compared to /6
that of the continent. We see that the cap-continent contrast remains constant in the 3800 - 4800 Å region, whereas cloud brightness rises steadily toward the violet end of the spectrum. We further note that the data for the violet cloud observed on 24 April 1969, were photographed at the point of maximum cloud brightness (density), although (as will be seen from Figure 4) the structure of this formation becomes better defined with reduction in wavelength. Evidently a system of violet clouds with different densities was observed at the time of observation near the planet's terminator.

Let us attempt to use the data from the photometric observations of the violet clouds to determine some of the optical parameters of these formations.

Unfortunately, we cannot use the spectral observations made in 1969 at the Shemakha Astrophysical Observatory because the spectrophotometric chracteristics of the clouds obtained apparently were badly distorted by the influence of atmosphere dispersion because of the large south declination of Mars at the time of observation. We should point out that unfortunately the Cassegrain system of the 2-meter reflector at the Shemakha Astrophysical Observatory does not include positional rotation of the spectrograph to permit observations with minimum influence exerted by atmospheric dispersion. This comment applies in part as well to the 1960 - 1961 observations, but these were made with Mars high enough above the horizon and were limited to a minimum wavelength at 0.4 micron.

Let us, therefore, use the data from the 1958, 1960 - 1961, and 1965 observations to determine the optical parameters of the violet clouds. The measured cloud-adjacent mainland contrasts contained in reference [2-4] were recalculated for a phase angle of $\alpha = 10°$ and a value of the cosine of the angle

of reflection for light of $\zeta = 0.71$. We used for this purpose the calculated /7 data on the distribution of brightness along the equator of Martian intensity for different α as set forth in reference [8].

Table 3, which lists the mean spectral values for the brightness coefficient for the western and eastern clouds, also lists the values for the scattering indicatrix of light, and the optical thickness for "average" Martian atmosphere, according to reference [6]. There is very little change in indicatrix values, according to data on the spectrum in reference [6], so we took a mean value of $\chi_a(\pi - \alpha) = 0.65$ for the region considered.

TABLE 3. MEAN SPECTRAL VALUES OF THE BRIGHTNESS COEFFICIENT FOR THE WESTERN AND EASTERN CLOUDS

λ, micron	0.36		0.40		0.45		0.50	
	W	O	W	O	W	O	W	O
$\bar{r}_0$	0.095	0.083	0.108	0.087	0.128	0.112	0.150	0.131
$\bar{r}_a$	0.078	0.71	0.091	0.076	0.118	0.104	0.144	0.126
$\chi_a(\pi-\alpha)$	0.65		0.65		0.65		0.65	
τ_a	0.064		0.048		0.038		0.032	

Let us use known expressions for the brightness coefficient, without including multiple scattering

$$r(\eta, \zeta, \alpha) = \frac{\omega\chi(\pi-\alpha)}{4(\eta+\zeta)}\left[1 - e^{-\tau\left(\frac{1}{\eta}+\frac{1}{\zeta}\right)}\right] + f(\eta, \zeta)\, e^{-\tau\left(\frac{1}{\eta}+\frac{1}{\zeta}\right)} \qquad (1)$$

where

ω is the probability of survival of a quantum;

$\chi(\pi - \alpha)$ is the scattering indicatrix of light in the atmosphere;

α is the planet's phase angle;

τ is the atmosphere's optical thickness;

η, ζ are the cosines of the angles of incidence and reflection of light;

f is the brightness coefficient for the planet's own surface.

From two such equations, written for the center of the cloud, and for the point of comparison (with the same η and ζ values), eliminating $f(\eta, \zeta)$, and taking $\omega = 1$, we obtain

$$e^{-\tau_0 c} = \frac{\varkappa_0 - r_0}{\varkappa_a - r_a - \tau(\varkappa_0 - \varkappa_a)e^{-\tau_a c}}, \qquad (2)$$

where

$$c = \frac{1}{\eta} + \frac{1}{\zeta}, \quad \varkappa = \frac{\chi(\pi-\alpha)}{4(\eta+\zeta)}.$$

Here the subscript a is the atmosphere and o is the cloud, and the optical thickness in Eq. (1), written from the center of the cloud, is equal to $\tau = \tau_a + \tau_o$.

Let us assume that the shape of the particles contained in the cloud is spherical, and that the density of particle distribution by size is determined by Junge's law.

$$dN = \frac{\bar{C}}{r^{\nu+1}} dr,$$

where

dN is the number of aerosol particles, the radii of which are in the limits r to r + dr;

C is the normalization constant;

ν is the so-called Junge distribution parameter.

Junge's law is well justified for terrestrial aerosols, as special research has shown (see reference [7] for a survey of the literature apropos of this). In this case the spectral behavior of the optical thickness of the aerosol is determined by $\tau_\lambda = b\lambda^{-n}$, where b is some constant, and $n = \nu - 2$. The magnitude ν lies in the limits $2 < \nu < 6$, and the larger ν, the greater part the smaller particles have in scattering the light. /8

τ_{01}, n, and $\varkappa_0$ are determined by taking $\lambda_1 = 0.36$ micron, $\tau_0 = \tau_{01}$, $\varkappa_{0\lambda} =$ = constant, and $\tau_{0\lambda} = (\frac{\lambda}{\lambda_1})^{-n}\tau_{01}$, using Eq. (2) and the data listed in Table 4. The results, obtained using a "Promin'" electronic computer, are $\varkappa_0 = 0.15$ or $\varkappa_0(\pi - \alpha) = 0.77$, $n = 1.9$ for the western and eastern clouds.

The following values were obtained for the optical thickness of the clouds

λ, micron	0.36	0.40	0.45	0.50
$\tau_{0\lambda}$, W	0.073	0.060	0.048	0.038
$\tau_{0\lambda}$, O	0.057	0.046	0.37	0.030

The values n = 1.9, or $\nu = 3.9$, we obtained within the framework of the assumptions used bespeak the big part played by the fine aerosol in the violet cloud.

The mean values of $\tau_{0\lambda}$ for the violet clouds we found for 1958, 1960 - 1961, and 1965 evidently are the low limit because the atmospheric image tremor of the planet always reduces the surface brightness of comparatively small disk

details. It would thus seem that the cloud-adjacent continent contrasts we measured were most likely too low. Moreover, the 1959 observations evidently provide a greater relative violet cloud intensity than was the case in 1958-1965.

Thus, the rough approximation for the violet clouds of Mars is $\tau(0.36 \text{ micron}) \approx 0.1$ when $\nu = 3.9$. Comparing this ν value with the mean value $\nu = 4.25$ for a "homogeneous" Martian atmosphere [6], we can conclude that the mean size of the particles in the violet cloud, within the context of the assumption we have made, is very close to the mean size of the aerosol particles in the homogeneous Martian atmosphere. It can be supposed, naturally, that the violet clouds are "bunches" of aerosol particles constantly present in the Martian atmosphere and creating the known effect of violet haze.

REFERENCES

1. Slipher, E. C., Ph. St. of brigh. Pl., Lowell Obs., 1964.

2. Barabashov, N. P., Koval', I. K., Chekirda, A. T., Izv. Komissii po fiz. pl., No. 3, 1961.

3. Didychenko, Ye. I., Koval', I. K., Morozhenko, A. V., Izv GAO AN UkSSR, 1, 1963, 5.

4. Bugayenko, L. A., Bugayenko, O. I., Koval', I. K., Morozhenko, A. V., Fizika Luny i planet [Physics of the Moon and Planets], "Naukova dumka" Press, Kiev, 1966.

5. Koval', I. K., Doctoral Dissertation, Kiev, 1968.

6. Morozhenko, A. V., Astron. zhurn, 46, 5, 1969.

7. Zuyev, V. Ye., Prozrachnost' atmosf. dlya vidimykh i IK-luchey [Transparency of the Atmosphere to Visible and Infrared Rays], "Sovetskoye radio" Press, Moscow, 1960.

8. Morozhenko, A. V., Yanovitskiy, E. G., Astron. zhurn, 48, 1971.

ULTRAVIOLET ABSORPTION IN THE CONTINUOUS SPECTRUM OF JUPITER[1]

V. D. Krugov

ABSTRACT: The results of the spectrophotometric investigation of Jupiter (range 3300-4800 Å) for the purpose of determining ultraviolet absorption for different regions of Jupiter's disk region are presented. The observations were made with a 70-cm reflector and ASP-7 spectrograph (dispersion 230 Å/mm at H and K). About 100 spectrograms were taken during 1969 (January-April). It is shown that ultraviolet absorption in Jupiter's atmosphere is real and the quantity of effect for positions of the spectrograph's vision slit 1, 2, 3, 5 (as shown in Figure 2) is an average lg I(0.33) - lg I(0.48) = -0.33. Time variations are observed in the course of reflectivity for different regions of Jupiter's disk. The quantity of ultraviolet absorption is approximately the same for Jupiter's northern and southern polar regions (range 4800-3300 Å).

A Short History of the Question

Many authors have obtained chromatic photometry of the planets in the solar /9 system, particularly of Jupiter and Saturn, in the past 40 years. This originally was in the form of visual and photographic measurements, followed by spectrophotometric measurements, but it was not until recently that photoelectric measurements were obtained. N. P. Barabashov and A. T. Chekirda [1] were among the first to obtain spectrophotometry of Jupiter, and of other planets.

Jupiter's spectrum was photographed with an objective prism on a 6-inch reflector (focal length of the objective lens was 55 cm). The aperture in the objective prism was 110 mm, and the angle of refraction was 12°. Three spectrograms, measurement of which was made with a Hartmann microphotometer, were obtained for Jupiter. Measurements were in the 4100-6000 Å region. The results showed a slight drop in intensity from 6000 to 5000 Å, and a sharply defined drop in intensity in the 5000-4100 Å region. The work was done at the Astronomical Observatory of Khar'kov State University in 1948.

V. G. Teyfel' [2], in 1959, used an ASP-9 slit spectrograph (dispersion 143 Å/mm at H_γ) on a 200-mm AZT-7 mirror-lens telescope to obtain the spectra

---

1. Figure 8 is an appendix and illustrates the relative spectral energy distribution for different regions of Jupiter.

of the equatorial (EZ) and temperate zones of Jupiter, north (NTZ) and south (STZ). The spectrograph slit was 0.050 mm wide and cut out a band $\varphi = \pm 12°$ in the focal image of Jupiter's disk in the equatorial zone, and one approximately $\varphi = 30\text{-}60°$ in the temperate zones. Thirty-two spectrograms were obtained and measured to make a photometric study of the continuous spectrum. Spectrograms of the Moon in the Mare Vaporum region were obtained in May 1959, in order to complete the photometric closure of Jupiter's spectrum.

A drop in the intensity to 0.10(lg I) [2] will be observed in the spectral distribution in the 3900-500 Å region. Some authors find strong ultraviolet absorption, others find none [2].

Two series of spectrograms of Jupiter and of the Moon were obtained with this same telescope in 1962 at the Astrophysical Institute of the Academy of Sciences of the Kazakh SSR [3]. The author provides a curve that shows quite clearly just how precipitous is the drop in intensity in the UV region of Jupiter's spectrum. Intensification of absorption in the spectrum begins at 4100-4200 Å, and near 3600 Å the effect achieves a magnitude of 0.36(lg I), where $\lg I = \lg I_J - \lg I_M$. Observations were made on 13-14 September, and again on 11-12 October 1962. Different photometric gradients were obtained for these dates, but these differences were less than those between the observations made by V. G. Teyfel' and those by the Kiesses and Corliss [4].

V. G. Teyfel' has no doubt that there is strong UV absorption in Jupiter's spectrum. It appears that here we have a matter of the absorption of aerosol in Jupiter's atmosphere. The spectrograms of Jupiter's dark equatorial band and light temperate zones obtained by V. G. Teyfel' on 20-21 November 1962, showed no significant differences in the behavior of the spectral reflectivity of these regions in the UV region. So we cannot say that strong UV absorption is inherent only for the material of the dark or light zones of the planet. /10

I. N. Glushneva [5] investigated the dependence of Jupiter's monochromatic albedo in the 4500-3200 Å region of the spectrum in 1963. The spectrograms were obtained with an ASP-5 slitless spectrograph at the P. K. Shternberg State Astronomical Institute, a high-mountain station. The dispersion at H_γ was 150 Å/mm, at 3000 Å - 50 Å/mm. The observations were made in January-February 1963, and 10 spectrograms of Jupiter were obtained. Comparison spectra of the

planet and of stars were photographed at identical zenith distances to preclude the influence of absorption of light in the Earth's atmosphere. No direct comparison of spectra of planet and Sun was made; instead the Sun's spectral energy distribution was taken from Johnson [12]. Jupiter's monochromatic albedo decreases by a factor of 1.5 in the interval 3900-3500 Å. The albedo begins to increase with further shortening of the wavelength. Comparing the results obtained by Younkin [6] and Glushneva, we can conclude that the behavior of the albedo, according to Younkin, can be characterized by a monotonic decrease, and this is different from the results obtained by I. N. Glushneva.

According to I. N. Glushneva, the sharp reduction in the albedo begins at 4100-4200 Å. Increase in the albedo in the region shorter than 3500 Å obviously is real because it is obtained by comparing Jupiter with α Lyrae and α Ursae Majoris.

V. F. Kartashov [7] made observations in August 1965, and studied UV absorption in Jupiter's spectrum, using a slit spectrograph with a dispersion of 143 Å/mm on an AZT-7 mirror-lens telescope. The spectrograph slit was oriented in the plane of the planet's equator (width 0.05 mm). Data on solar energy distribution were taken from I. N. Glushneva [5]. If the gradients obtained for the entire period of the observations are compared, one notes the variations in Jupiter's gradient in the ultraviolet. We therefore can conclude that the time-dependent change in the relative spectrometric gradient is real.

V. V. Avramchuk [8] too made a spectrophotometric study of Jupiter. His observations were made at the Main Astronomical Observatory of the Academy of Sciences of the Ukrainian SSR in 1965, using a 70-cm reflector in the Cassegrain focus (F = 30 m) with an ASP-21 diffraction-grating spectrograph. Jupiter's spectrograms were tied in with stars with known energy distributions.

When orientation of the spectrograph slit was along the central meridian it was found that there was a reduction in the albedo toward the UV end of the spectrum for all zones of Jupiter investigated. Minimum absorption in the UV rays was observed in the polar regions of the planet, and the maximum in the northern, light, tropical zone. The observations were made on 27-28 August 1965. The periods 25-26 January 1965, and 12-13 February 1965, can be characterized by absence of UV absorption. Nevertheless, the polar regions were more "blue" than

the equatorial regions at these times.

The author concludes that UV absorption is variable and can cause the changes observed in the color of Jupiter. The absorption is not associated with light or dark bands, but is global in nature, increasing toward the center of the disk. Younkin [6] used the 60-inch telescope with scanning monochromator at the Mount Wilson Observatory for photoelectric investigations of UV absorption in 1961. An RCA 1P21 photomultiplier was used to record the spectrum in the 3300-5200 Å region, and an RCA 7265 photomultiplier was used for the same purpose in the 4800-8000 Å region. Observation conditions were such that the investigations in these two regions had to be made on different nights. Direct measurements of the solar spectrum were not made, so Johnson's data [12] were used for the 4100-8000 Å region, and Shkol'nik's data were used for $\lambda < 4100$ Å. Overlapping of spectral intensity curves for Jupiter was in the 4800 and 5200 Å /11 regions. The slit was positioned near the center of the planet's image.

The spectral energy distribution curve obtained for Jupiter can be characterized by the monotonic reduction in the albedo in the UV region of the spectrum and the attainment of a value of 0.25(lg I) in the 3300-4800 Å region.

Jupiter's spectrum was measured, including that of the UV region, in January and September 1967, by Isakson [9], who used a monochromator with 16- and 36-inch telescopes. A synchronous motor, running at a speed of 250 Å/min, was used to rotate the scanner grating. Numerous observations were made with a 20" entrance slit and an 80 Å exit slit. The principal purpose was to determine the relationship between the reflectivity and the wavelength of the continuous spectrum. This was because of the spectrometer's low resolution. The slit was oriented with respect to the center of the planet's disk. A direct comparison between the planet's spectrum and that of the sun was difficult, so observations of Jupiter were standardized with respect to the stars most nearly resembling the sun in spectral class.

The author posed for himself the task of obtaining the relationship between the mean reflectivity for the planet, and the wavelength. Possible temporary variations in this relationship were not studied.

Isakson's data show the following peculiarities in Jupiter's spectral energy distribution. An energy minimum, such that lg I(3750) - lg I(4800) = -0.23,

is observed in the 3750 Å region. Some increase in the albedo is observed beyond this wavelength. These results differ somewhat from those in references [5, 6]. Isakson tends to believe that these differences are the result of study of different sections of the planet's disk.

Irvine's paper [10] contains the results of photoelectric investigations of Jupiter and Saturn in 1963-1965. The observations were made with 10 interference filters in the 3150 Å - 1.06 micron region, as well as in the UBV system. The observations were made through the 16-inch telescope at the Bowden Observatory in South Africa, and through a 12-inch telescope in France. Stars with known energy distributions were measured for each filter. Phase curves for Jupiter, and for its geometric albedo, were obtained. Irvine's data, when plotted, failed to show a maximum at 4000 Å, or a minimum at 3500 Å, on Jupiter's spectral energy distribution curve, as had been the case in I. N. Glushneva's paper [5]. What can be observed is a smooth drop in energy toward the UV end of the spectrum such that lg I(3300) - lg I(4800) = -0.24. Hopkins and Irvine [11] studied the variations in Jupiter's spectral energy distribution as they analyzed their data and concluded that the annual and monthly variations were, as a whole, insignificant. There are variations from date to date, and this has been noted repeatedly by other authors. Table 1 lists the values of the magnitude of the UV absorption effect as derived by the different authors.

TABLE 1. VALUES OF THE MAGNITUDE OF THE UV ABSORPTION EFFECT

Year	Author	λ	$\lg I(\lambda) - \lg I(4800)$
1948	N.P.Barabashov		
	A.T.Chekirda	0.41	—0.16
1961	L. Younkin	0.33	—0.25
1962	V.G. Teyfel'	0.36	—0.35
1963	I.N.Glushneva	0.33	—0.13
1963—1965	M. Irvine	0.33	—0.24
1967	M. Isakson	0.33	—0.14

If one disregards the intensity minimum near 3600 Å for some observations, the data in Table I are such that one can say there is quite a great difference in the magnitude of the absorption effect in the 3300-4800 Å region. /12

What follows from this survey of the work in the field of spectrophotometry

of Jupiter in the shortwave region of the spectrum is that there is UV absorption in Jupiter's atmosphere, and this has been noted by many authors. The magnitude of this effect has different values during different periods of observation. However, the variability of this effect stems from the difference in the observations, each of which is burdened by its own systematic errors. Unfortunately, it is impossible to cite a single study (with the possible exception of Irvine's) in which the fact of the variability of Jupiter's UV absorption could be established with complete reliability. Nor is there any evidence to establish a behavior pattern in the variations in the absorption effect. Some researchers associate the variability in UV absorption with solar activity, others with change in the planet's atmosphere. It is obvious that all these questions can be answered only by lengthy, systematic, observations using a unified procedure.

Statement of the Problem

The results of the majority of the work done to study UV absorption in Jupiter's atmosphere are based on data obtained over several nights, or over a period of one or two months. Then too, all the observations listed in the survey refer to the planet as a whole, or to the central region of its disk. Still not understood is how UV absorption is distributed in terms of the planet's disk, although some observers have noted a different energy distribution for polar and central regions. In no case has this author found a single paper based on the results of systematic, simultaneous, investigation of UV absorption by Jupiter for the central and limb regions of the disk (polar regions, east and west limbs).

Yet investigations such as these are of great interest, particularly in connection with established disk and time-dependent variations in the intensity of the molecular CH_4 and NH_3 absorption bands [14]. It can be anticipated that if the variation in the intensity of the CH_4 and NH_3 molecular bands is associated with change in aerosol diffusion properties, it also can cause a change in UV absorption.

High dispersion spectrographs are not needed, obviously, to investigate UV absorption and determine its magnitude at different times. On the contrary, systematic work on UV absorption for different regions of Jupiter's disk can be more effective if low dispersion equipment is used, permitting observations to be made at short exposures for all regions of the disk.

Our goal was to conduct long-term, systematic, monitoring of the spectral energy distribution for Jupiter and Saturn in the shortwave region of the spectrum, using the 70-cm reflector and the ASP-7 spectrograph at the Main Astronomical Observatory of the Academy of Sciences of the Ukrainian SSR. Observations were begun in January 1969. The program was to last for several years. Some 100 spectrograms of different regions of Jupiter's disk for the period January-April 1969, have been obtained.

Equipment and Observation Procedure /13

The observations to determine the magnitude of the UV absorption in different regions of Jupiter's disk were made using a 70-cm reflector in the Cassegrain focus (F = 10.5 m) and a prism spectrograph that could be rotated around its axis by a position bearing. The spectrograph was usable at 3000-7000 Å, and slit limits were 0.001-0.4 mm. The spectrograph's linear dispersion at 3000 Å was 90 Å/mm, and 230 Å/mm near the H and K lines. Plotting of a dispersion curve was a requirement for the work. An iron arc spectrum was obtained for this purpose, as was that of the Sun, for great certainty. We identified 11 absorption lines very nearly uniformly located in the 3300-4800 Å region and constructed the dispersion curve in Figure 1.

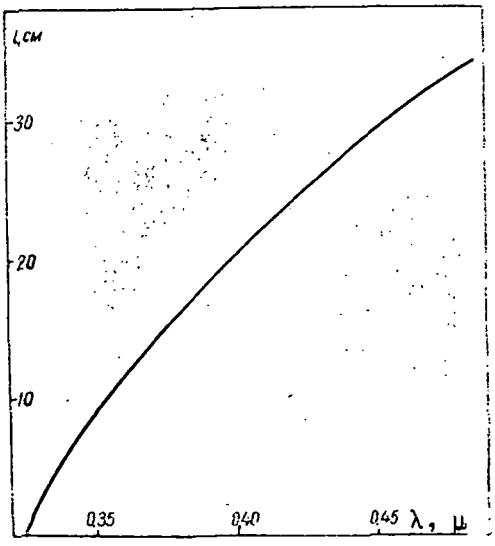

Figure 1. ASP-7 spectrograph dispersion curve.

Slit width was selected as 0.13 mm (≈2.6") for the Jupiter spectrograms. Calibration, star spectra for comparative purposes, and spectra of the Sun and of the planet, all were made and obtained at the same exposures at this slit width, and this, in our opinion, is mandatory for this type of observation. Two conditions were satisfied in the selection of the stars to be used for comparative purposes. First of all, the star, standard in order to preclude extinction, was selected for small angular distance from the planet. Second, its spectral class was selected as close as possible to that of the Sun. A star of the class

AO(η Vir) could be used as the standard when the first of these conditions was observed more closely. This latter fact proved convenient, in that the spectrograms of the planet, as well as of the comparison star, could be made at the same exposure. Moreover, the continuous spectrum suffers less distortion by absorption lines in the star of an early spectral class. The spectrograph slit was oriented so as to avoid the influence of atmospheric dispersions when obtaining star spectrograms (in the meridian perpendicular to the horizon). The comparison star then was tied to the center of the solar disk.

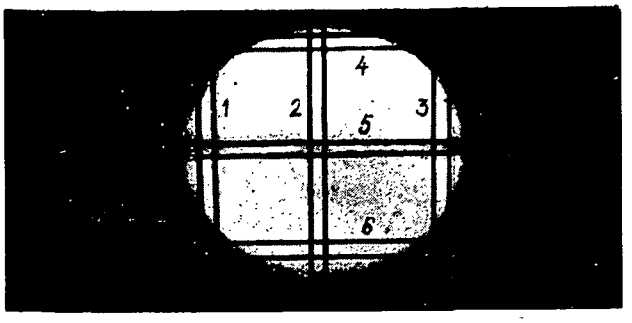

Figure 2. Orientation of slit for studying the UV absorption in Jupiter's spectrum (6 is the south polar region).

The program for one night's observations was as follows. The spectrograph slit was oriented on Jupiter's equator and along the central meridian. S and N, the polar regions, and the west and east limbs, were cut off. Figure 2 shows the position of the slit on the planet's disk. All spectrograms were obtained at the same exposures (10 sec, 30 sec, 90 sec, 3 min) for Jupiter and for the comparison star. The comparison star was observed before and after exposure (depending on the position of the planet after the upper culmination) of the particular section of the planet. It was customary to take 3 or 4 spectrograms in one night for all positions of the slit near the planet's culmination shown in Figure 2, thus providing normal density of blackening in the 3300-4800 Å region. In addition, 5 to 6 series of spectrograms were made on one plate for a particular region of the disk, and these then were used to find the observation error. Each region of Jupiter's disk, and the comparison stars, were exposed on /14 the same plate (6 to 7 spectrograms). A diaphragm with a central shutter was placed in front of the spectrograph slit. The accuracy of the 10 second exposure was of the order of 1 percent, with the accuracy of the other exposures very much better, naturally. A step attenuator was used for calibration. An

incandescent lamp, supplied from a stabilized source of supply, was used. Emulsion grade ZU-2 was selected because UV absorption in the 3300-4800 Å region was studied. The limbs of the disk were studied with the slit $r \approx 0.7R_J$ from the center of the disk.

The following considerations were involved in selecting this distance. The observations were made for zenith distances $Z \leq 50°$. Table 2 shows that when observations of polar regions of the planet are made there is a shift in the slit of 2.20" ($Z = 50°$) caused by atmospheric dispersion in the band of wavelengths we were studying. This shift actually differs from the true shift because the slit is exposed without filter. The spectrograph slit is between 0.7 and $0.85R_J$ (shift of 3") when observing the south polar region for the Z value taken. The extreme position of the slit corresponds to the distance from the center of the disk, $r_1 \approx 17"$ (~3" from the limb). This also had a hand in the selection of the height of the microphotometer window when measuring the spectrograms.

All plates were developed using D-19 developer at +19°C. We also used a special adapter so 30 plates with spectrograms of Jupiter, stars, and four calibration plates could be developed simultaneously.

Processing the Spectrograms

The first thing to be established is which of the characteristic curves to use to correctly study the continuous spectrum in the 3300-4800 Å region we selected. ZU-2 plates were studied to determine the contrast in terms of wavelength and exposure. Measurements were made every 30 Å for all exposures. The result was to establish that contrast, γ, depends on wavelength and exposure. Contrast changes slowly from 4800-4200 Å, but beginning at 4200 Å drops rapidly toward the shortwave side. In the 4500 Å region $\gamma \approx 2.00$ for exposures from 40 seconds to 3 minutes, whereas $\gamma \approx 1.60$ in this same region for exposures from 10 seconds to 30 seconds. Figure 3 shows the $\gamma(\lambda, t)$ relationship. These curves were obtained from study of 10 plates in each ZU-2 batch (three batches).

Characteristic curves then were plotted for 16 values of the wavelength (every 100 Å) with overlapping of the spectrograms at four points in the continuous spectrum (Figure 4). The curves were plotted with confidence because the scatter in the points was slight (number of points per curve 5 to 8). The spectrograms were measured by an MF-4 microphotometer with an FEU-15B photomultiplier as the radiation receiver, and darkening was recorded on recorder graph paper. The

photomultiplier supply was from a stabilized source. The measurements of the spectrograms were made along the dispersion in 16 sections of the continuous spectrum free of absorption lines. The microphotometer window cut out spectrogram sections 0.05 x 0.10 mm (5 Å/mm at 3300 Å x 8"). This window width was selected such that first, resolution of the spectrograms obtained would not deteriorate during photometry, and second to eliminate the fluctuations caused by graininess of the plates. The window height indicated was selected in order to reduce the influence of atmospheric dispersion when processing the spectrograms of the south polar region. The extreme position of the spectrograph slit near 3300 Å corresponds to $\approx 0.85R_J$. The length of the corresponding chord is 10". Thus, with a window height of 8", the influence of atmospheric dispersion on the measurement of the relative spectral energy distribution for the south polar region can be determined by the distribution of the brightness along the planet's central meridian (along the direction of the shift in the slit occasioned by atmospheric dispersion). /15

All spectrograms obtained for the same region of Jupiter's disk, but with different exposures, were subjected to photometry. Subsequent

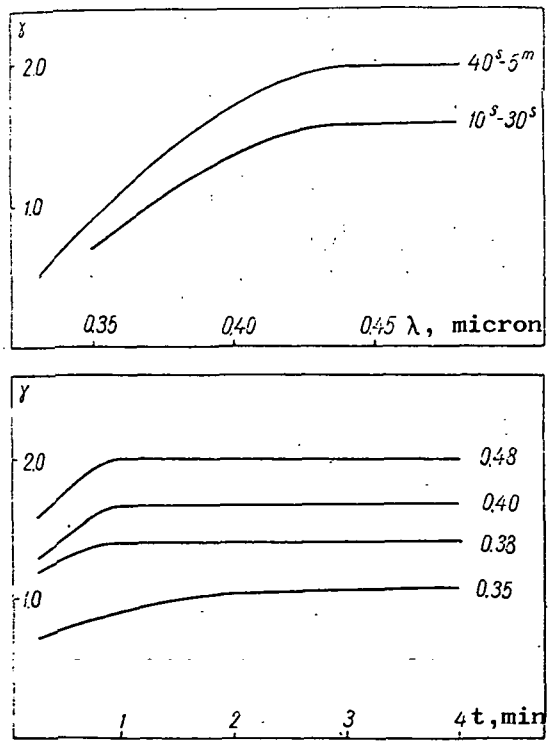

Figure 3. The $\gamma(\lambda, t)$ relationship for study of the ZU-2 plates.

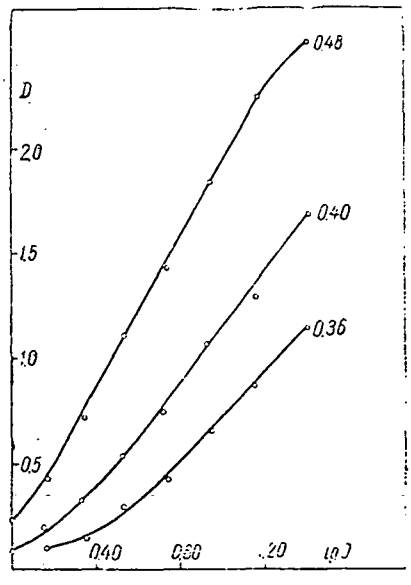

Figure 4. Characteristic curves.

processing usually used the recordings of two spectrograms that reliably overlapped the whole of the region of the spectrum studied (1-4800-3900 Å; 2-4200-3300 Å).

Thus, the photometric tie (overlap) to two spectrograms obtained with different exposures was made at four points (four characteristic curves). Finally, the recordings of blackening obtained were converted into intensity in accordance with the 16 characteristic curves in all regions of the spectrum we studied. The angular recession of η Virginis, the comparison star, from Jupiter usually was a maximum of 1° during the observations, and the time between star exposure and that of the particular region of Jupiter's disk was a maximum of 10 minutes. Hence, the values $\lg I_J - \lg I_*$ were not distorted by the influence of extinction. Although η Virginis is stationary, its photometric comparison with α Leonis, the spectral distribution for which is well known, was made in passing. As should have been expected (these stars are comparable in terms of spectral class) the energy distribution in η Virginis proved to be very nearly that for α Leonis. We deemed it undesirable to use existing data on solar spectral energy distribution to compare η Virginis with the Sun, because to do so obviously could introduce additional errors. /18 The correct tie to the Sun should be made with the same equipment for the concrete purpose of studying the planet's spectral energy distribution. We made the photometric tie between star and Sun as follows. When atmospheric conditions were favorable, and when the star observation program was completed, the sun was observed on the same morning, at the same distances as the stars.

A Hartmann diaphragm with a 3-mm diameter opening was placed over the telescope tube when observing the Sun. The working alignment of the openings was located along the refracting edge of the spectrograph prism. A 25-mm diameter diaphragm was placed in front of the hole in the main mirror to attenuate the flux of energy arriving from the Cassegrain mirror. This flux can be varied by the magnitude of the diaphragm, as well as by the distance of the diaphragm from the Cassegrain mirror.

Thus, the densities of the spectrograms of the center of the solar disk were obtained very close to those of the spectrograms of the comparison star and planet. The tie of star to Sun was made in 5 days in April 1969. The solar spectrograms obtained were measured under the same conditions as were the spectrograms of the planet. The calculations made of monochromatic intensities of Jupiter assumed, in accordance with Allen [13], a solar limb darkening, and used the formula

TABLE 2. MONOCHROMATIC VALUES OF REFRACTION FOR VARIOUS Z AND λ

Z/λ	ΔR															
	0.33	.34	.35	.36	.37	.38	.39	.40	.41	.42	.43	.44	.45	.46	.47	.48
30°	1″.01	0″.85	0″.70	0″.63	0″.60	0″.47	0″.40	0″.26	0″.10	0″.08	0″.05	0″.02	0″.01	0″.01	0″.01	0″.00
40	1 .60	1 .40	1 .35	1 .15	1 .00	0 .85	0 .75	0 .55	0 .40	0 .15	0 .10	0 .06	0 .03	0 .01	0 .01	0 .00
50	2 .20	1 .90	1 .85	1 .50	1 .40	1 .15	0 .90	0 .85	0 .60	0 .40	0 .30	0 .22	0 .14	0 .09	0 .05	0 .00
60	2 .85	2 .55	2 .35	1 .65	1 .55	1 .45	1 .25	0 .80	0 .55	0 .40	0 .28	0 .22	0 .17	0 .13	0 .10	0 .00
70	4 .47	4 .10	3 .70	3 .20	2 .70	2 .20	1 .95	1 .70	1 .30	1 .10	0 .90	0 .70	0 .50	0 .35	0 .20	0 .00

TABLE 3. ULTRAVIOLET ABSORPTION IN THE CONTINUOUS SPECTRUM OF JUPITER

Disk region number	λ, microns															
	UT	0.33	.34	.35	.36	.37	.38	.39	.40	.41	.42	.43	.44	.45	.46	.47	.48
								1969, 5.I									
1	2ʰ23ᵐ	51	54	47	47	27	33	21	13	10	05	05	06	02	04	08	0
2	2 40	11	13	14	23	09	17	04	08	05	03	01	+01	+02	01	03	0
3	2 55	33	44	48	45	37	43	33	25	24	18	11	17	10	09	07	0
4	3 15	38	54	52	54	36	33	33	31	29	19	13	14	11	06	04	0
6	3 56	77	67	52	44	42	43	35	29	25	17	13	02	02	00	00	0
								7.I									
1	0 37	40	46	37	36	38	33	28	28	26	17	04	01	+04	+03	+01	0
4	2 20	50	50	44	40	30	27	13	06	06	07	04	08	05	05	06	0
5	2 51	40	40	42	45	34	28	29	25	19	17	14	+01	01	02	05	0
6	3 02	56	51	41	45	33	30	12	04	06	06	04	03	06	05	03	0

TABLE 3 continued

Disk region number	UT	λ, microns 0.33	.34	.35	.36	.37	.38	.39	.40	.41	.42	.43	.44	.45	.46	.47	.48
								7. III									
1	21 00	+01	+01	15	10	04	11	00	07	03	03	03	01	01	+01	+02	0
2	21 23	06	20	18	25	19	26	15	20	09	08	15	05	03	02	01	0
3	21 43	28	32	35	34	24	20	16	15	18	14	12	10	04	02	02	0
4	22 58	13	08	10	06	12	17	03	01	03	01	05	03	06	+01	+01	0
5	22 27	20	26	26	31	20	19	15	15	08	08	13	+03	+02	04	01	0
6	22 06	21	29	31	34	16	22	09	15	09	08	07	02	+01	01	+02	0
								8. III									
1	22 24	17	19	26	33	25	30	18	26	16	23	15	07	05	02	04	0
2	22 41	05	05	06	22	13	16	13	29	15	10	12	07	+06	+03	00	0
3	22 54	27	27	30	35	21	16	22	17	21	18	18	16	03	04	11	0
4	21 29	07	22	15	18	18	13	11	11	05	09	08	05	03	03	+01	0
5	21 44	03	12	05	12	15	17	08	11	07	01	09	02	02	01	+01	0
6	22 04	53	48	35	31	32	30	29	13	16	16	09	10	04	00	09	0
								20. III									
1	23 14	45	52	61	57	46	49	38	30	22	14	08	06	04	01	02	0
2	23 36	32	39	34	38	33	27	27	23	16	19	11	06	01	00	01	0
4	22 47	30	53	47	36	34	36	20	16	09	10	07	00	+04	+06	+02	0
5	22 21	51	49	45	40	39	35	27	24	18	25	12	06	00	+01	+04	0
								10. IV									
1	20 00	23	28	26	32	20	19	17	14	10	08	04	03	+05	+06	+01	0
2	20 11	45	49	49	45	40	38	22	27	26	21	17	09	11	09	05	0
3	20 40	32	32	39	36	25	23	18	15	17	11	10	06	02	+01	+03	0
4	18 35	32	33	38	29	27	19	12	06	03	+04	02	02	00	+01	+03	0
5	19 03	19	22	21	30	28	33	26	24	20	14	18	08	01	01	+05	0
6	19 33	50	55	50	48	41	35	29	19	16	18	15	09	01	05	+03	0
								28. IV									
4	19 16	40	52	54	45	35	32	25	20	17	12	09	08	02	+02	00	0
5	19 39	35	37	45	41	32	28	24	26	17	19	17	10	04	00	03	0
6	20 01	47	45	52	36	38	40	30	24	19	15	09	08	01	+03	+02	0

$$\lg \frac{I_J}{I_\odot} = \lg \frac{I_J}{I_*} - \lg \frac{I_\odot}{I_*}.$$

Because atmospheric dispersion has a significant effect on spectrophotometric investigations of the planets (we have the polar regions in mind here), the formula given in reference [15] was used to calculate the monochromatic values of refraction for various Z and λ (Table 2), and these then were used to determine the magnitudes of the UV absorption for Jupiter's polar regions.

Results of Observations

Table 3 lists the results of the relative spectral energy distribution for different regions of Jupiter's disk for all dates of observations. The first column in Table 3 shows the number of the region on the planet's disk for each date and the positions of the spectrograph slit as shown in Figure 2; that is, 1- east limb; 2- central meridian; 3- west limb; 4- north polar region; 5- planet's equator; 6- south polar region. The second column lists universal time for the middle of the observation interval for each region. The table then lists 10^2[lg I(λ) - lg I(0.48)] for each wavelength in 0.1 increments. All values without signs are negative. The nature of the dependence of the monochromatic albedo of the regions of Jupiter's disk that were observed can be judged from the curves in the appendix. Figure 5 shows the combined data on relative spectral energy distribution for each region of Jupiter's disk for the whole of the observation period (January-May 1969). These curves show the difference in the reflectivity of Jupiter with respect to the spectrum for individual observation dates. Figure 5 compares the mean energy distribution curves for groups 1, 2, 3, and 4, 5, 6. Ten spectrograms were obtained in a 30 minute period on 20 March 1969, near the culmination of Jupiter with the slit oriented along the planet's central meridian, in order to determine energy distribution errors. Ten spectrograms of the comparison star were taken during this same period. Curve 1 in Figure 6 is the mean curve for Jupiter's spectral energy distribution as obtained from the 10 spectrograms. The vertical segments show the root-mean-square error in one measurement (5-7 percent). The error was found from

/20

$$\sigma^2 = \frac{\sum |\varepsilon_i|^2}{\sum n_i - N},$$

where

ε_i is the modulus of the deviation from the mean arithmetical error;

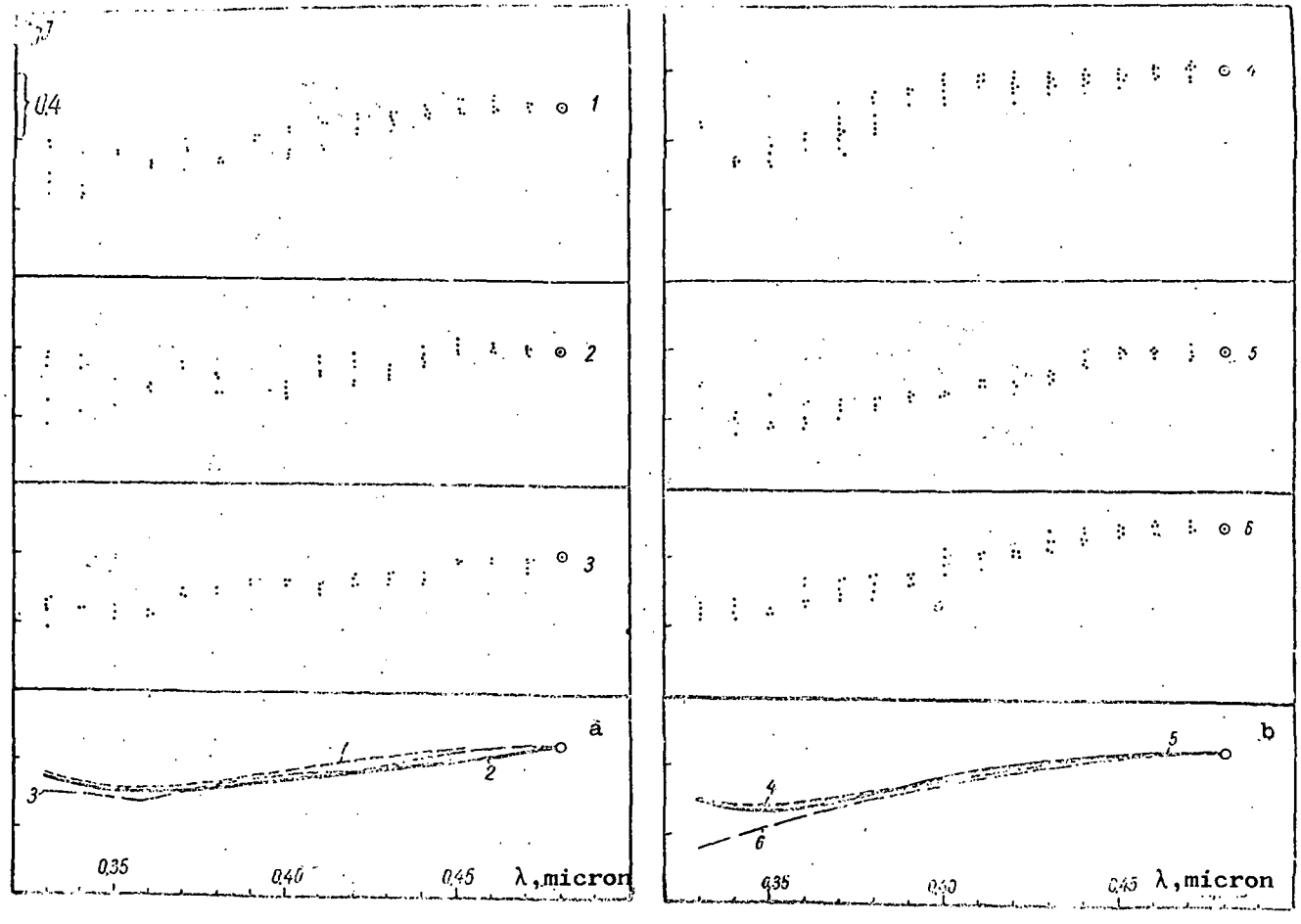

Figure 5. Comparison of mean energy distribution curves.
a- regions 1, 2, 3, 6-4, 5, 6; 1- east; 2- meridian;
3- west; 4- north; 5- equator; 6- south.

Σn_i is the total number of measurements for the spectrograms;

N is the number of points measured on each of the spectrograms.

Curve 2 in Figure 6 shows the scatter in the lg I(λ) - lg I(0.48) values, and gives some idea of the error in the behavior of Jupiter's relative spectral energy distribution (observation errors).

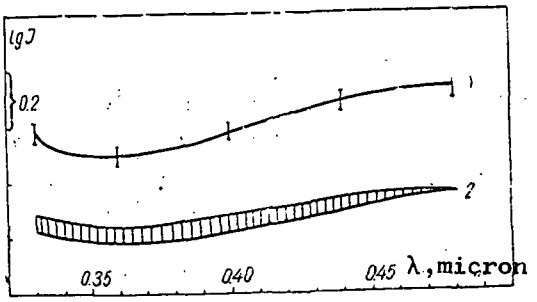

Figure 6. Jupiter's spectral energy distribution to determine observation error. 1- root-mean-square error in one measurement; 2- scatter of lg I(λ) - lg I(0.48) values during one night.

Discussion of Results and Conclusions

Our spectrophotometric study of the relative spectral energy distribution for individual sections of Jupiter's disk in the 3300-4800 Å region revealed that the existence of UV absorption in Jupiter's atmosphere is real, and as follows from Figures 5 a, b, the magnitude of the absorption effect, within the limits of observational errors, is the same for all sections of the planetary disk, on the average, as lg I(0.33) - lg I(0.48) = -0.33. The following needs consideration with respect to variations in UV absorption. Figure 6 and the appendix show that variations in the observed relative distribution of energy in the shortwave region of Jupiter's spectrum greatly exceeds observational errors from date to date. The curves for 7 and 8 March (Figure 6, 2) are much flatter than for the other dates, for example. The difference is lg I(0.33) - lg I(0.48) = -0.15 for 7 March, but is an average -0.45 for the other dates. Still, it is difficult to say that we are, or are not, dealing here with variations in the UV absorption for the same observed sections of the planet's disk (meridian, equator, west and east limbs), or whether what is involved here is that, because of the rotation of Jupiter, we observed different regions of the planet with different energy distributions (the longitudinal effect) on each individual date. Only a specially conducted sampling of lengthy, systematic,

observations can explain just how significant the latter of these is. Our observations clearly are inadequate for these purposes. Time should be taken, in particular, to determine the magnitude of the UV absorption in Jupiter's polar regions.

As will be seen from the appendix, the magnitude of the UV absorption for region 6 (south) is systematically larger than for region 4 (north). Figure 5b shows that the magnitude /21

$$\lg I(0.33) - \lg I(0.48) = \Delta I$$

is equal, approximately, to -0.5 for the south polar region, and to -0.3, approximately, for the north polar region. It already has been noted that atmospheric dispersion increases UV absorption for the south polar region, and decreases it for the north.

Let us evaluate the approximate magnitude of the effect created by atmospheric dispersion on the distribution of brightness along the planet's central meridian.

1. South polar region. According to reference [16], the distribution of brightness along the planet's meridian has little to do with the wavelength up to $r_1 = 0.85R_J$ in the 4300-6480 Å band. The brightness ratio for $r_1 = 0.85R_J$ and $r = 0.7R_J$ is close to 0.7. Considering the tendency toward some increase in this ratio on the short wavelength side, let us take $I(r_1)/I(r) \approx 0.80$, or $\lg I(r_1) - \lg I(r) \approx 0.10$, for 3300 Å.

Thus $\Delta I \approx -0.4$ for the south polar region (instead of -0.5 with the atmospheric dispersion disregarded).

2. North polar region. The brightness ratio for $r = 0.7$ and $r_2 = 0.55$ is close to 0.8, using the same measurements [16]. Let us take $I(r)/I(r_2) \approx 0.9$, or $\lg I(r) - \lg I(r_2) \approx -0.05$ for 3300 Å. Thus $\Delta I = -0.35$ for the north polar region (instead of -0.3 with the atmospheric dispersion disregarded).

The overall influence of atmospheric dispersion in the measurement of UV absorption is quite significant for the polar regions of Jupiter when the planet's zenith distance is near 50°, as we see, and the magnitude of the UV absorption is approximately the same for the north and south polar regions.

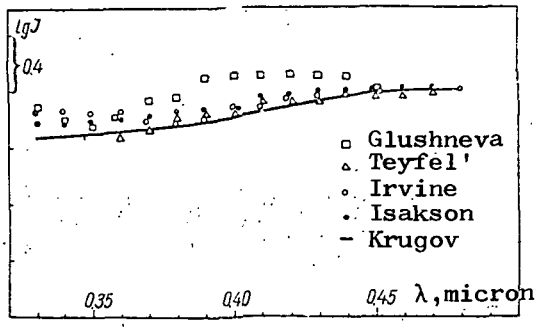

Figure 7. Comparison of our results with those obtained by other authors.

In conclusion, let us compare our results with those from similar investigations made earlier by other authors. Figure 7 shows curves of Jupiter's relative spectral energy distribution obtained by us, and by other authors (region 2, the meridian, was taken from our observations for the comparison). As we see, our data are in good concordance with the data provided by other authors, with the exception of those obtained by I. N. Glushneva, who made the observations using spectrophotometry for the entire disk.

The author is indebted to I. K. Koval' for his constant attention to the work, as well as to V. V. Avramchuk and A. V. Morozhenko for consultations.

/22

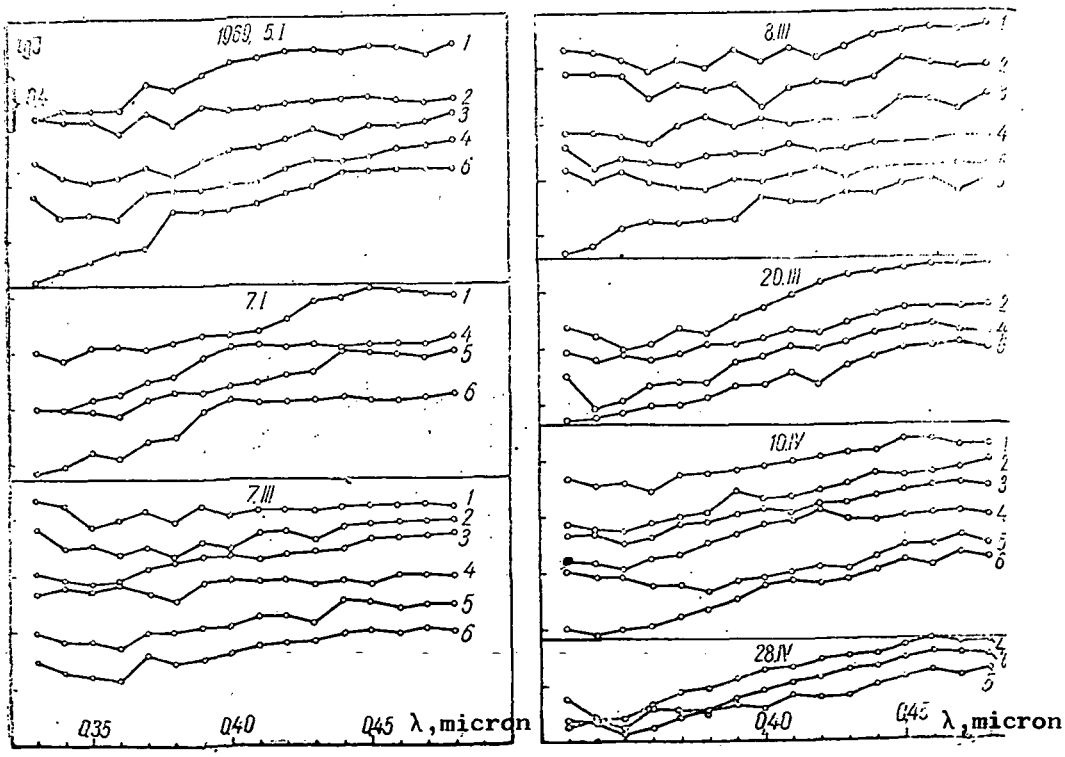

Figure 8.

REFERENCES

1. Barabashov, N. P., Chekirda, A. T., Trudy Astron. Observatorii KhGU, 1, 9, 1950, pp. 19-23.

2. Teyfel', V. G., Izv. Astrofiz. in-ta, Vol. 13, 1962, pp. 54-61.

3. Teyfel', V. G., Izv. AN Kaz. SSR, No. 1, 1963, pp. 74-77.

4. Kiess, C. C., Corliss, C. H., Kiess, H. K., Ap. J., 132, N 1, 1960, pp. 221-231.

5. Glushneva, I. N., Astron. zhurn., 41, No. 4, 1964, pp. 720-723.

6. Younkin, L., Munch, Mem. Society Roy. Sci., Liege, 7, No. 1, 1963, pp. 125.

7. Kartashov, V. F., Trudy Astrofiz. in-ta AN Kaz. SSR, IX, 1967, pp. 47-50.

8. Avramchuk, V. V., Trudy Astrofiz. in-ta AN Kaz. SSR, IX, 1967, p. 51, (thesis).

9. Isakson, M., Departamento de Astronomia, Publicaciones, No. 7.

10. Irvine, M., Aj., 73, 1968, p. 9.

11. Hopkins, B., Irvine, W. M., IAU Symposium 40, October 1969.

12. Johnson, F. S., J. Meteor, 11, 6, 1959, p. 436.

13. Allen, C. W., Astrophysical Magnitudes, 1960, pp. 167-168.

14. Avramchuk, V. V., Fizika Luny i planet [Physics of the Moon and Planets], 1968, pp. 126-160.

15. Teyfel', V. G., Trudy Astrofiz. in-ta AN Kaz. SSR, IX, 1967, pp. 98-103.

16. Lebedinets, V. N., Trudy Astron. observatorii KhGU, 12, 1957, pp. 168-239.

DISTRIBUTION OF THE ENERGY IN THE SHORTWAVE REGION OF THE SPECTRUM FOR VARIOUS PARTS OF SATURN'S DISK[2]

V. D. Krugov

ABSTRACT. The results are presented of measuring ultraviolet absorption for Saturn's disk in a range of 3300 - 4800 Å taken in 1968 - 1969. The observations were carried out with the 70-cm reflector and spectrograph ASP-7 (dispersion 230 Å/mm at H and K). It is found out that the quantity of ultraviolet absorption for various regions of Saturn's disk (equator, meridian, the southern polar region, eastern and western limbs) is lg I(0.33) - lg I(0.48) = 0.30 on the average. Time variations are observed in the course of reflectivity for various regions of Saturn's disk. The data for the rings show a more neutral motion of albedo along the spectrum and time variations are shown rather less.

Virtually no study has been made as yet of the relative spectral energy /23 distribution for different regions of Saturn's disk, and this is, to some degree, associated with the presence of a ring around the planet's disk. Nevertheless, such investigations, as those of Jupiter, are of great interest.

We began to study the relative spectral energy distribution for different regions of Saturn's disk in the 3300-4800 Å range with a 70-cm reflector and ASP-7 spectrograph at the Main Astronomical Observatory of the Academy of Sciences of the Ukrainian SSR, in August 1968. The slit in the spectrograph measured 0.18 mm, and the MF-4 window cut out a section $\Delta\lambda \sim 12$ Å/mm near the H and K lines on the spectrogram. Figure 1 shows the position of the slit on Saturn's disk and ring. The spectrograph slit was at a distance of $r \approx 0.6Rc$ in order to reduce the influence of atmospheric dispersion during the study of the south polar region. The height of the microphotometer window when measuring the corresponding spectrograms was selected with the considerations cited in the paper on the spectrophotometry of Jupiter's south polar region in mind.[3] The star ξ^2 Ceti, of spectral class AO, and at the same zenith distance as the

---

2. Figures 6-9 are appendices and illustrate the relative spectral energy distribution for different regions of Saturn.

3. V. D. Krugov, "Ultraviolet Absorption in the Continuous Spectrum of Jupiter." This collection, p. 9.

planet, was observed for purposes of standardization and to exclude the influence of extinction. The procedures used for the observations, and for processing the spectrograms, were those used for Jupiter.

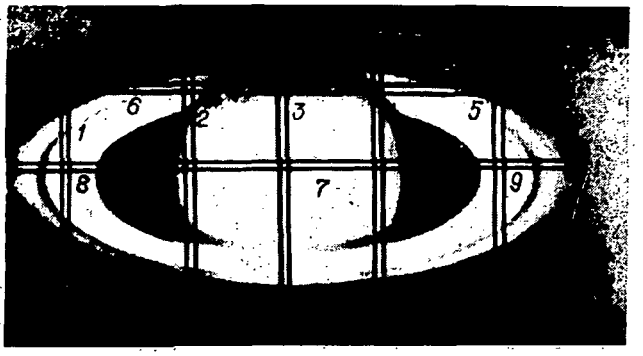

Figure 1. Position of spectrograph slit on Saturn's disk (6 - south polar region).

A total of 300 spectrograms of Saturn and of the comparison star were obtained between 5 August 1968 and 21 November 1969, and 100 were processed for different regions of the planet's disk and ring. The relative spectral energy distribution for Saturn's disk and ring can be given by the magnitudes $\lg I_J/\lg I_\odot$.

Measurement results are listed in the table, and in the appendix. The first column lists the numbers of the regions of the planet's disk corresponding to those in Figure 1; that is, 1, 8 are the ring's west eye, 2 is the west limb, 3 is the central meridian, 4 is the east limb, 5, 9 are the ring's east eye, 6 is the south polar region, and 7 is the planet's equator. The second column is universal time for the midpoint in the interval of observations for each region. The values of $10^2[\lg I(\lambda) - \lg I(0.48)]$ are given every 100 Å for each wavelength. Unsigned values are negative.

The shapes of the relative energy distribution curves for the observed regions of Saturn's ring and disk are shown in the appendix (see Figures 6-9).

RESULTS OF MEASUREMENTS OF ENERGY DISTRIBUTION IN THE CONTINUOUS SPECTRUM OF SATURN

Disk region no.	UT	λ, microns															
		0.33	.34	.35	.36	.37	.38	.39	.40	.41	.42	.43	.44	.45	.46	.47	.48
								1968, 5. IX									
2	21h18m	14	12	18	06	25	27	26	30	28	20	16	08	08	06	03	0
3	22 24	27	23	30	38	39	40	35	35	30	23	20	14	11	10	05	0
4	23 37	57	52	55	49	47	50	43	36	26	20	16	11	10	02	08	0
								7. IX									
2	21 08	52	55	48	41	44	52	47	37	31	21	14	08	05	03	04	0
3	22 18	46	44	47	47	33	45	42	38	35	26	30	17	08	05	02	0
4	23 24	56	52	56	54	54	48	42	32	27	24	19	13	07	06	04	0
								9. IX									
2	22 18	48	42	45	42	38	39	32	30	25	19	13	06	01	02	02	0
3	23 19	50	44	42	44	40	43	39	35	28	22	17	10	03	05	05	0
4	0 22	47	48	46	43	47	58	49	43	35	37	16	11	05	04	05	0
								9. X									
2	22 00	37	37	37	36	36	43	42	33	27	22	13	11	07	06	06	0
3	23 07	37	37	37	42	43	51	43	30	24	20	16	04	05	06	06	0
								10. X									
2	20 45	34	34	31	40	49	49	49	37	32	26	20	13	08	06	07	0
3	21 41	21	25	24	31	35	47	35	23	20	19	12	11	11	08	06	0
4	19 49	07	01	07	07	06	12	28	17	17	13	10	05	01	02	05	0
								30. X									
2	19 22	48	43	41	36	40	45	31	27	24	16	11	10	09	06	04	0
3	20 20	07	08	09	07	21	17	16	07	10	05	05	07	05	06	04	0
4	21 11	36	35	35	35	28	35	23	24	18	12	09	09	08	05	02	0
								24. XI									
2	17 00	44	41	40	41	43	51	48	36	35	28	21	12	08	08	02	0
3	17 44	35	25	25	34	34	34	33	24	19	16	09	03	06	05	03	0
4	18 25	13	13	25	17	20	23	26	20	15	11	10	13	11	10	09	0

Disk region no.	UT	λ, microns															
		0.33	.34	.35	.36	.37	.38	.39	.40	.41	.42	.43	.44	.45	.46	.47	.48
								1968, 13. XII									
1	19h40m	29	26	26	15	25	17	09	05	08	11	13	10	11	09	06	0
2	18 00	70	56	56	56	59	54	44	37	32	31	23	24	10	07	07	0
3	18 29	69	59	56	53	55	49	43	34	38	28	25	17	07	04	01	0
4	18 51	52	58	41	39	52	50	41	36	34	29	25	16	10	10	05	0
5	20 10	15	11	06	02	03	17	33	10	07	06	09	12	11	12	05	0
6	16 42	40	41	38	38	40	31	25	25	25	24	14	12	03	07	06	0
								15. XII									
1	16 19	38	31	29	19	21	20	09	03	02	00	+03	+03	+04	+03	+01	0
								1969, 4. I									
1	16 20	55	53	53	48	44	48	44	37	34	32	26	15	09	07	04	0
5	17 14	63	63	55	50	47	44	44	38	37	31	23	19	13	07	02	0
6	18 06	35	30	23	31	34	27	25	28	24	21	14	+03	00	00	+07	0
								5. I									
1	15 06	46	53	44	34	27	27	29	19	18	13	14	06	01	+02	01	0
2	15 50	64	47	53	57	56	48	33	57	43	32	31	22	16	10	06	0
3	16 31	49	43	49	44	52	43	45	34	24	26	24	14	06	01	00	0
4	16 21	54	55	45	52	50	65	46	38	31	31	26	19	13	12	08	0
5	15 38	54	50	54	50	42	23	36	42	26	21	16	17	07	06	04	0
6	17 04	55	66	57	45	50	53	51	40	35	31	23	11	07	07	04	0
								6. I									
2	18 39	37	42	43	44	42	36	46	34	39	28	24	19	07	08	05	0
4	19 18	63	53	45	49	51	55	42	38	33	29	20	08	+03	+02	+05	0
								30. VIII									
1	23 27	37	34	30	29	29	14	04	07	08	07	05	02	+01	+01	+01	0
5	0 17	30	24	23	20	25	09	04	08	09	05	02	01	+02	+01	+02	0
								31. VIII									
3	0 31	33	31	33	33	37	22	22	20	19	16	12	07	01	00	01	0
								7. IX									
1	23 38	42	42	37	40	28	30	27	19	20	19	17	11	08	06	+01	0
5	23 48	42	28	27	10	16	14	11	14	24	03	+03	+05	+04	00	+01	0

Disk region no.	UT	λ, microns															
		0.33	.34	.35	.36	.37	.38	.39	.40	.41	.42	.43	.44	.45	.46	.47	.48
								1969, 8. IX									
1	2h40m	50	38	37	34	28	24	37	21	26	22	18	13	11	09	09	0
3	21 47	19	25	35	35	41	30	35	27	21	22	14	07	04	09	08	0
								10. IX									
3	21 53	44	47	53	55	56	46	30	20	17	02	02	05	02	04	07	0
6	21 30	+05	+10	04	02	11	00	00	+08	00	+06	+04	+08	+10	+04	+07	0
7	21 40	10	22	22	26	33	11	17	15	20	13	07	+03	+08	+04	03	0
8	21 40	04	02	03	+02	08	09	+11	02	13	07	00	+12	+02	03	07	0
9	21 40	+13	+13	+08	+08	+11	+10	+12	+07	00	+03	+26	+13	+05	03	08	0
								11. IX									
2	23 58	39	36	34	38	37	28	27	20	22	14	10	07	+05	+02	+02	0
4	0 06	47	45	47	51	47	45	39	32	30	29	23	19	08	09	11	0
5	23 00	58	45	36	31	25	30	20	14	21	12	00	+04	00	03	03	0
								24. IX									
1	22 23	46	41	38	36	27	23	15	13	09	04	05	+01	+03	+02	+01	0
2	1 53	23	15	13	15	18	26	21	12	09	04	00	02	01	03	02	0
3	1 46	45	33	33	38	34	32	26	24	26	18	11	06	02	02	00	0
4	1 40	25	25	25	25	28	22	23	12	16	10	07	03	00	02	01	0
5	22 33	25	28	33	21	15	14	13	07	00	01	00	02	+01	01	01	0
6	21 20	07	07	11	18	16	16	13	08	12	04	10	05	00	02	04	0
7	21 33	02	11	09	18	24	18	27	17	18	15	15	13	06	08	05	0
								27. IX									
6	20 01	27	33	34	34	37	33	24	19	13	13	16	08	05	00	02	0
7	20 36	31	34	28	37	33	40	34	28	28	17	17	10	03	02	02	0
8	20 36	22	18	20	19	07	14	04	03	00	02	01	00	+02	+01	+02	0
9	20 36	28	26	22	14	08	14	12	05	06	05	05	04	02	03	02	0

Disk region no.	UT	λ, microns															
		0.33	.34	.35	.36	.37	.38	.39	.40	.41	.42	.43	.44	.45	.46	.47	.48
								13. X									
1	19h16m	37	31	20	27	19	13	08	19	15	13	11	09	00	01	01	0
2	19 41	00	+05	+08	+08	+13	+08	+12	+09	+09	+04	00	+01	+04	00	+02	0
3	20 06	+02	+02	08	14	17	15	08	06	04	+01	+01	+02	+04	+02	+03	0
4	20 34	16	24	25	24	25	32	18	24	17	16	10	08	00	01	10	0
5	20 59	+03	+16	+15	+18	+13	+16	+23	+17	+14	+00	+01	+02	+02	+00	00	0
6	21 24	08	04	09	00	+01	00	+06	+09	+06	+08	+06	+04	+07	+04	+06	0
7	21 49	41	33	34	34	34	41	27	30	25	19	19	06	+01	+04	+03	0
8	21 49	42	30	26	20	22	24	+03	11	12	09	09	02	+03	+02	+01	0
9	21 49	50	51	41	29	24	31	13	16	08	10	10	03	+04	+06	+01	0
								14. X									
7	22 43	21	11	10	14	16	15	12	08	04	+01	+02	+03	+04	+02	+02	0
8	22 43	21	12	16	09	12	11	00	00	01	01	+02	+04	+05	+04	+03	0
9	22 43	30	21	20	14	13	07	03	+12	+03	+05	+07	+06	+05	+05	+04	0
								15. X									
1	23 30	08	03	00	+07	+03	+09	+12	+14	+11	+09	+07	+05	+04	+03	+02	0
2	21 03	05	+04	02	00	+03	+11	+05	+08	+09	+08	+09	+08	+06	+04	+03	0
3	21 25	13	02	12	10	09	07	01	06	06	04	01	+01	+01	00	+01	0
4	21 50	08	20	07	02	10	00	+02	+01	+04	+04	+03	+01	+01	00	+02	0
6	19 21	17	09	08	07	12	13	07	01	+01	+04	+06	+08	+07	+05	+02	0
7	19 53	07	01	11	18	19	10	10	11	10	07	04	02	+01	+01	+03	0
								16. X									
7	20 58	31	26	26	25	29	28	25	21	15	14	11	06	01	02	00	0
8	20 58	28	24	16	17	08	06	02	+04	+04	+01	+01	00	+03	00	+02	0
9	20 58	23	16	16	10	14	09	02	+01	00	01	+01	+01	+04	+02	+02	0
								21. X									
1	21 25	02	02	01	+03	+02	+12	+12	+11	+11	+07	+01	+01	02	04	05	0
2	20 10	21	22	23	27	34	30	24	19	17	12	06	02	+03	+04	+03	0
3	21 47	56	51	53	52	54	51	39	32	26	18	12	04	01	+01	00	0
4	22 35	23	22	25	21	27	27	24	12	14	12	08	02	+02	+03	+06	0
5	23 05	07	07	11	07	07	03	+19	+06	+02	+01	+02	03	04	06	06	0
6	19 43	29	29	38	29	27	24	20	15	12	07	04	01	+01	+02	+07	0
7	19 10	37	45	48	47	50	45	41	43	37	26	20	16	07	02	09	0
8	19 10	42	36	35	29	29	18	19	18	17	+01	01	01	+03	+04	00	0
9	19 10	44	34	27	28	32	28	23	21	18	08	05	05	01	+01	+01	0

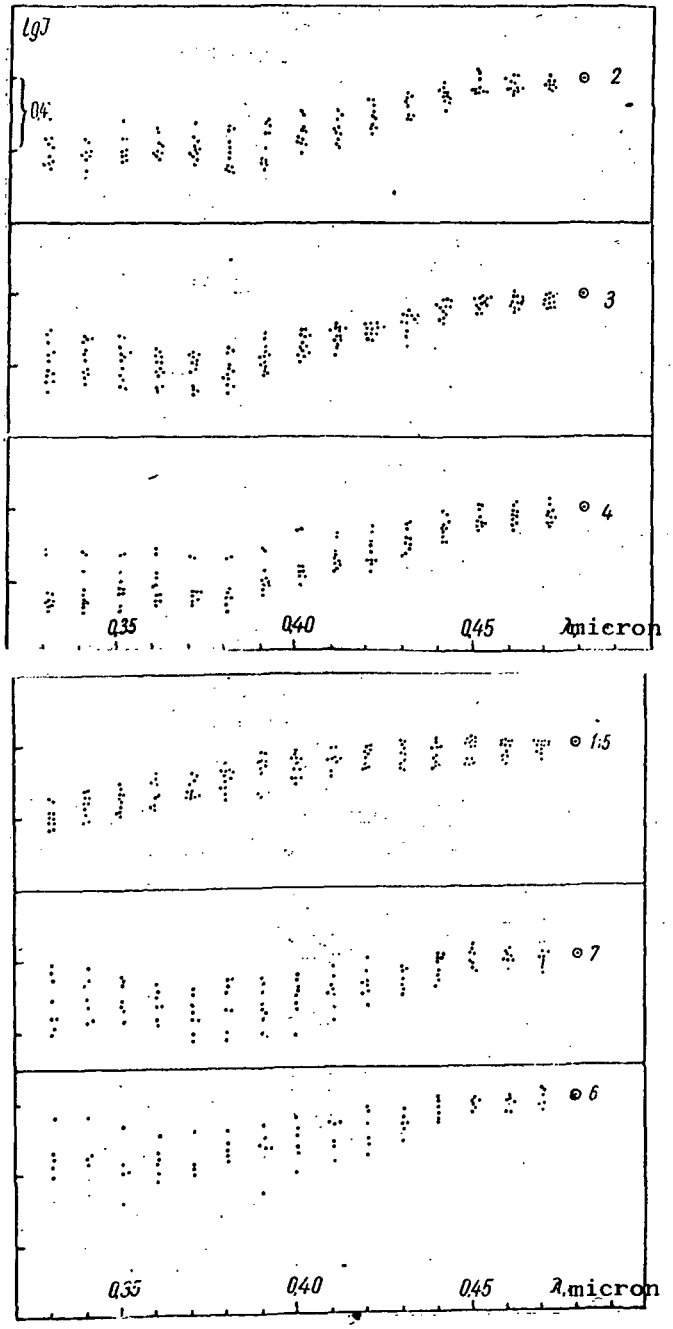

Figure 2. Relative energy distribution in different regions of Saturn's disk (composite data): 1 and 5 are the ring.

Figure 2 shows composite data on the relative spectral energy distribution /29 for each region of Saturn's disk and ring for the entire observation period. These graphics are a visual display of the difference in the behavior of the reflectivity between regions of Saturn's disk and ring for individual observation dates. It has been assumed that the time-dependent relative spectral energy distribution for the ring is constant. This fact is at the basis of determinations made of the errors in spectral energy distribution for different regions of Saturn's disk and ring. Eight spectrograms of the east and west eyes of the ring were obtained within 40 minutes on 27 September 1969, near Saturn's culmination in order to determine the errors. Sixteen spectrograms of the comparison star were obtained at the same time. Figure 3 I is the mean spectral energy distribution curve for the ring, from the 16 spectrograms. The vertical segments show the root-mean-square error of one measurement (5 percent). Figure 3 II is the scatter in the $\lg I(\lambda) - \lg I(0.48)$ values and gives some idea of the error in the behavior of the relative spectral energy distribution for Saturn and the ring (observation errors). Figure 4 I shows data for the planet's equator and ring, obtained simultaneously for the same position of the slit (measurements were made from details on the same spectrogram). Figure 5 I shows the mean relative spectral energy distribution curves for Saturn's equator and ring. What follows from Figure 5 I is that the magnitude of the UV absorption is the same, on the average, within the limits of observation error, for the equator and for the ring, $\lg \bar{I}(0.33) - \lg \bar{I}(0.48) \approx -0.30$. There are significant differences in the behavior of the reflectivity for equator and ring, however. The magnitude of the absorption for the equator drops sharply, beginning at λ 4500 Å, with the minimum near λ 3800 Å. The corresponding magnitude of the absorption in this band of wavelengths is -0.36. The peculiarity noted in the spectral behavior of reflectivity for Saturn's equator extends to other regions of the planet's disk as well. The magnitude of the UV absorption for the latter differ little from data for the equator.

The spectral energy distribution curve for the ring subsides monotonically to λ = 3300 Å, and there is no minimum in the λ = 3800 Å region. The behavior of the reflectivity of Saturn's rings is, overall, more neutral.

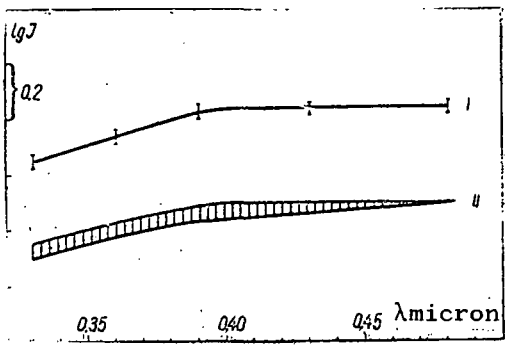

Figure 3. Relative spectral energy distribution for the ring.
I - root-mean-square error for one measurement;
II - observation error for 16 spectrograms.

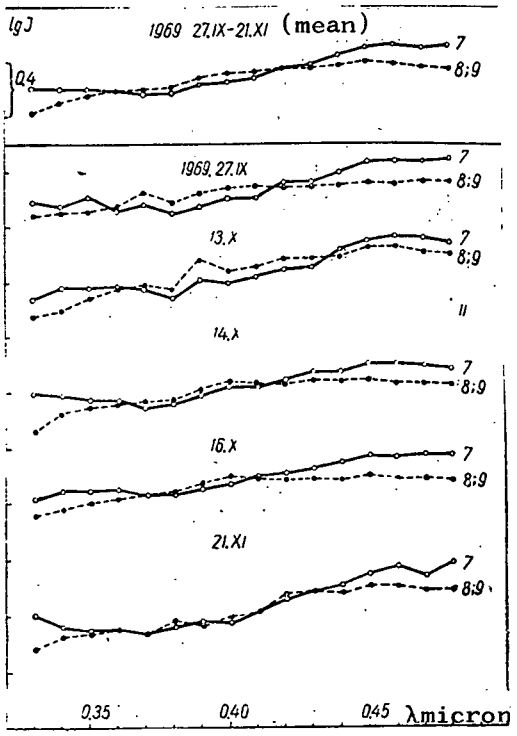

Figure 4. Spectral energy distribution for planet's equator and ring. I - mean curves; II - energy distribution for regions; 7, 8, 9 - for different observation dates.

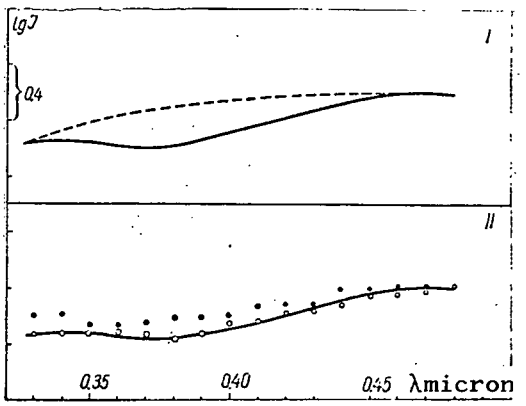

Figure 5. Reflectivity curves for the planet's equator and ring, reduced to 4800 Å. I - ring and equator comparison, ---- ring, —— equator; II - comparison of data obtained by different authors (with our results, given for the planet's equator); • - Irvine's data; o - Isakson's data; —— Krugov's data.

The curves in Figures 6-9 and 2 show that the variation in the observed relative energy distribution in the shortwave region of Saturn's spectrum is greatly in excess of the observation error. On 15 October 1969 (Figures 2, 2; 3; 4; 6; 7) lg I(0.33) - lg I(0.48) $\approx$ -0.20, whereas the difference was a mean of $\approx$ -0.50 for the other dates. As should have been expected, the temporal variations in the behavior of the spectral reflectivity for the rings were much smaller than for the planetary disk region (Figures 2, 1; 5), although there were occasional cases when these variations exceeded the observation errors noted. /30

Let us, in conclusion, compare our results with those obtained by other authors (Figure 5, II). Irvine [1] and Isakson [2] made photoelectric studies of the reflectivity of the whole of Saturn's disk between 1963 and 1965. The effect of the ring was not included. Our results (Figure 2 7) agree well with Isakson's results, but differ somewhat from Irvine's, the result, apparently, of the fact that the ring makes a definite contribution to the reflectivity of the planet's disk. The ring, as a whole, is more neutral than the planet's disk (Figures 4 and 5 I). We should point out that Isakson's period of observations coincide with small ring openings, and it is to this that its minor contribution during the observation interval can be attributed.

V. G. Teyfel' [3] made the first experiments to study the spectra of individual details in 1957. He established in particular that in the red the center of the planet's disk is much brighter than the ring, and that in the violet the ring and disk have almost the same brightness. Our results are in good concordance with his data (Figure 4 I and II).

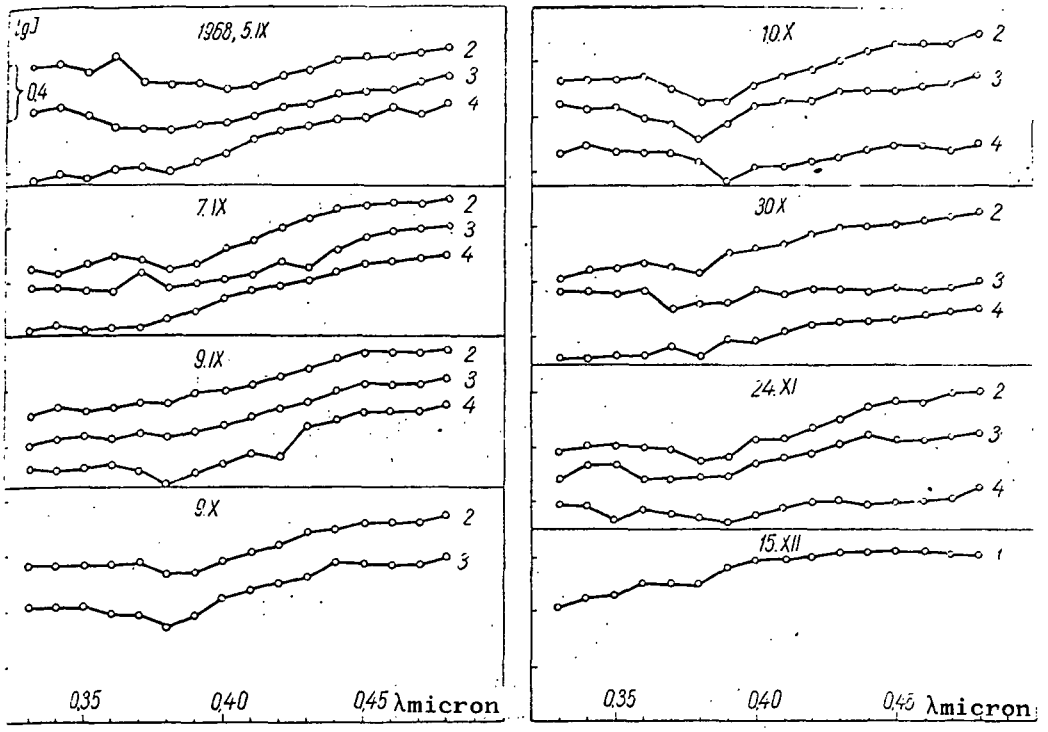

Figure 6.

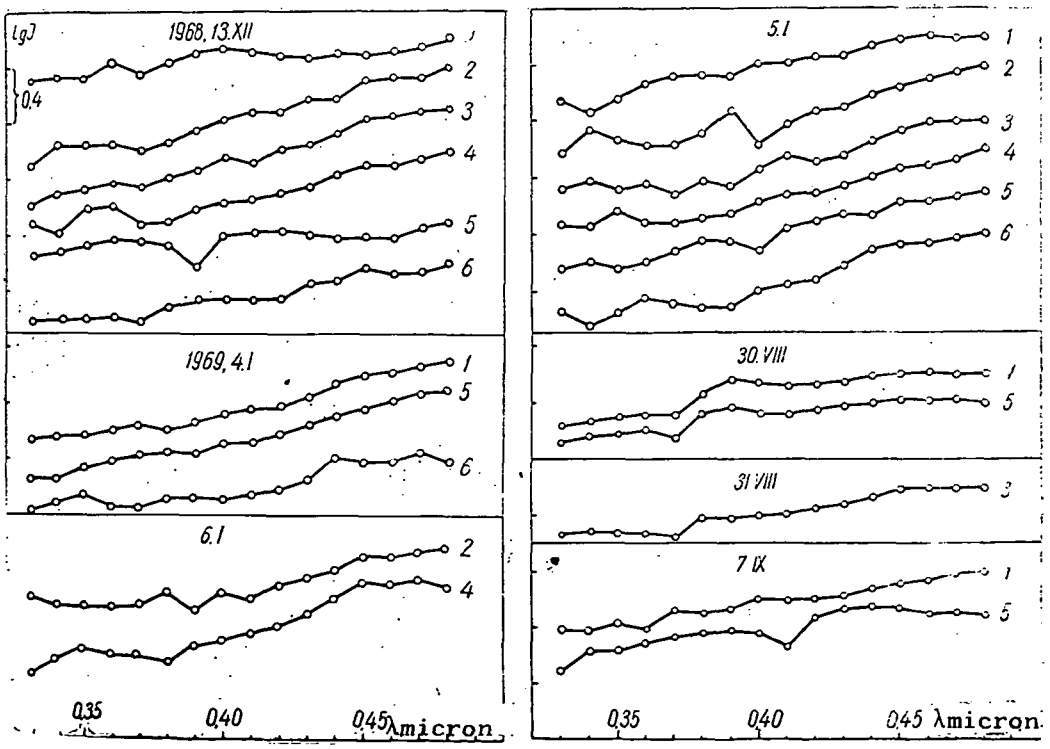

Figure 7.

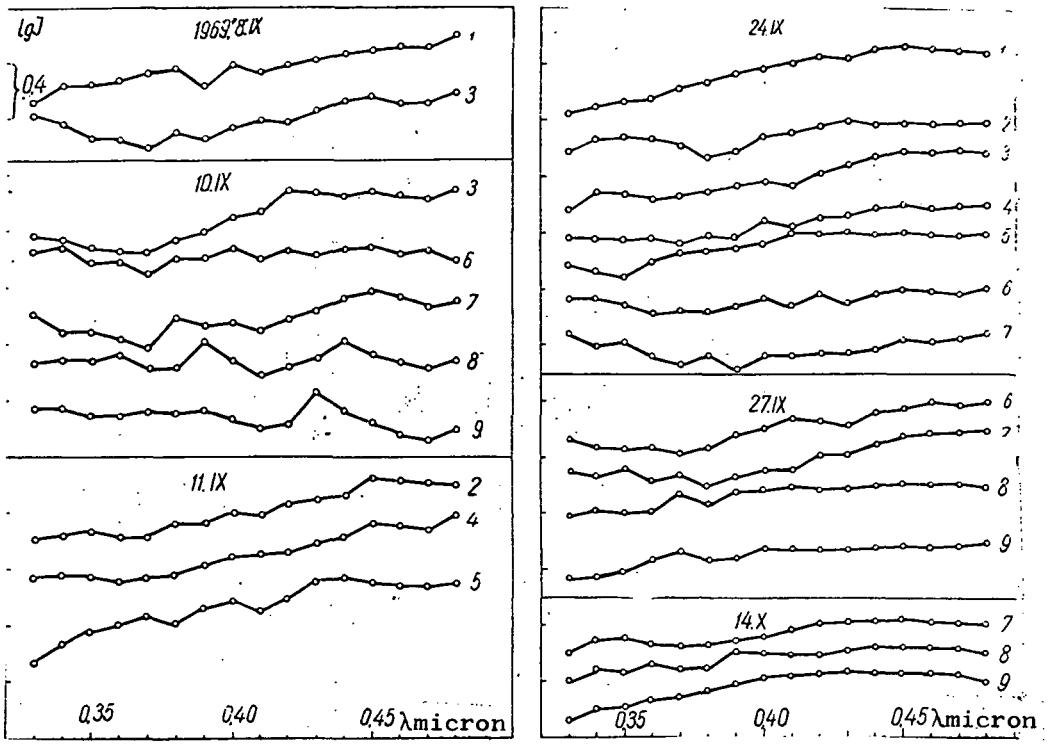

/32

Figure 8.

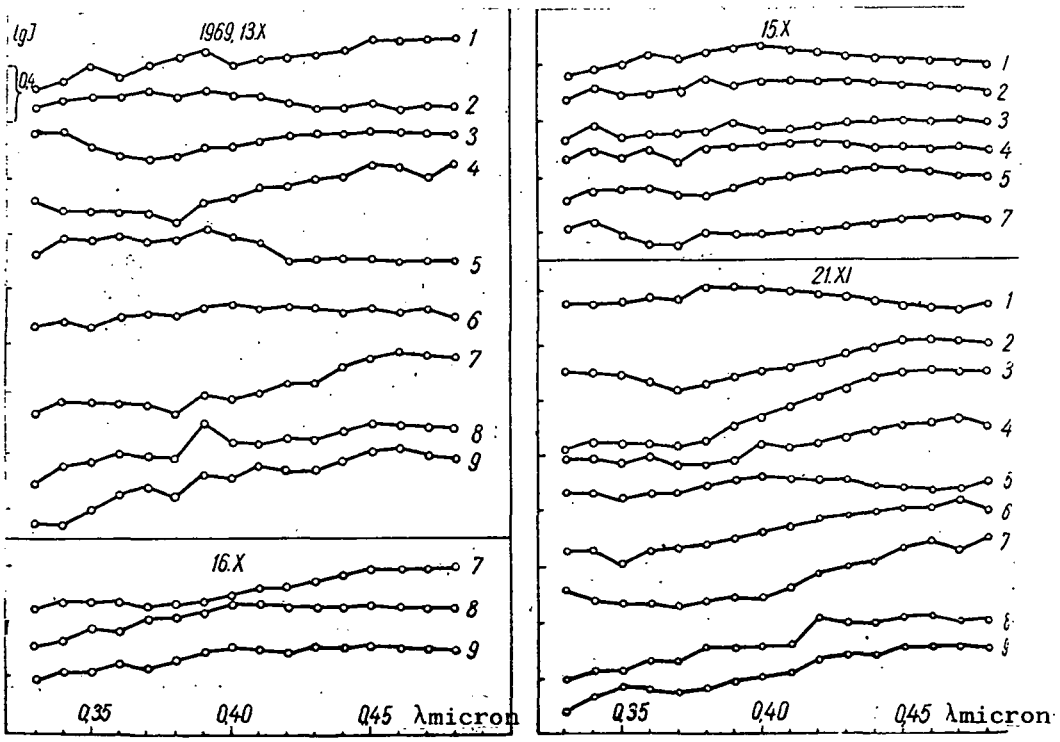

Figure 9.

REFERENCES

1. Irvine, W. M., AJ, 73, November, 1968, 9, N 1364.

2. Isakson, M., Departamento de Astronomia, Publicaciones N 7.

3. Teyfel', V. G., Teyfel', Ya. A., Trudy Sektora astrobotaniki AN Kaz. SSR, VII, 1959, 64 - 68.

RESULTS OF LABORATORY PHOTOMETRIC MEASUREMENTS OF ARTIFICIAL PLANETS

O. I. Bugayenko, I. K. Koval', V. D. Krugov
A. V. Morozhenko, L. F. Slutskiy

ABSTRACT. Results are given of photoelectric measurements of brightness distribution and brightness-phase dependence for six spheres whose surfaces have different colors and roughness. These results (Tables 1 and 2) are applied to verify validity of some empirical formulas used earlier for determining optical parameters of the Martian surface.

Reference [1] hypothesized that the surface layer of a planet consists of /33 not too densely packed semitransparent particles of a size greatly in excess of that of the length of a light wave. This was done to explain the change that takes place in the phase curves of Martian brightness with wavelength $\tilde{\lambda}$. In this case the spectral shape of the phase curves can be explained quite well, qualitatively speaking, by the presence of the shadow effect in the particles, by the spectral behavior of the single scattering albedo, λ, and the degree of transparency, $\varkappa$, of the particles, as well as by the influence of the atmosphere in the short-wavelength region of the spectrum.

Reference [2] considered the following model of the surface layer structure:

1. the surface layer consists of small elements, spheres of radius r, not too tightly packed, so that light can penetrate the layer to some depth $h > 2r$ from any direction, and will be scattered and absorbed by these particles;

2. particle dimensions exceed the length of the light wave, $\tilde{\lambda}$, such that a well-defined shadow forms behind each particle;

3. the particles are transparent. The degree of transparency is determined by the magnitude $\varkappa$, which indicates how much of the luminous flux entering the contour of the particle leaves a parallel beam absorbed and scattered to the side;

4. diffraction of the light by the particles can be ignored.

Reference [2] then used this model to obtain an approximate formula for /34 the intensity, $I(\eta, \zeta, \alpha)$ of the light diffusely reflected by the surface

(the reflection law)

$$I(\eta, \zeta, \alpha) = I_1(\eta, \zeta, \alpha) + \Delta I(\eta, \zeta, \alpha), \tag{1}$$

where

$$I_1(\eta, \zeta, \alpha) = \frac{\lambda}{4}\frac{\zeta}{\eta + \zeta}\chi(\pi - \alpha)\exp\left[\frac{\varkappa^2}{\pi}\left(\frac{g}{2}\right)^{3/2}\operatorname{ctg}\frac{\alpha}{2}\right] \times J(y, \varkappa), \tag{2}$$

$$\Delta I(\eta, \zeta, \alpha) = \frac{\lambda}{4}\frac{\zeta}{\eta + \zeta}\left\{\varphi_0^0(\eta)\,\varphi_0^0(\zeta) - 1 - x_1\left[\varphi_1^0(\eta)\,\varphi_1^0(\zeta) - \frac{\eta\zeta - \cos\alpha}{\sqrt{(1-\eta^2)(1-\zeta^2)}}\,\varphi_1^1(\eta)\,\varphi_1^1(\zeta) - \cos\alpha\right]\right\}, \tag{3}$$

where

$\chi(\pi - \alpha)$ is the particle scattering indicatrix;

α is the phase angle;

ζ, η are the cosines of the angles of incidence and reflection of light, respectively;

g is a factor for particle packing density in a layer

$$y(\eta, \zeta, \alpha) = \frac{3\varkappa}{4}\left(\frac{g}{2}\right)^{3/2}\left(\frac{1}{\eta} + \frac{1}{\zeta}\right)\sqrt{1 + \eta\zeta\operatorname{cosec}^2\frac{\alpha}{2}}. \tag{4}$$

Numerical values of the function $j(y, \varkappa)$ are given in reference [2], and precise values of the Ambartsumyan function, $\varphi_i^k(\eta)$, when $|x_1| \leq 1$, can be taken from the tables compiled by I. N. Minin et al. [3]. The Ambartsumyan function scattering indicatrix can be calculated for the other values of the elongation, x_1, by using the approximate formulas derived by E. G. Yanovitskiy [4].

As will be seen from Eqs. (2) and (3), the optical model of the surface layer can be determined by the assignment of parameters g, λ, $\varkappa$, and by the scattering indicatrix $\chi(\pi - \alpha)$, which can be found by comparing the observed and calculated intensity values. At the same time, data on planetary disk brightness distribution can be used, as can data on the integral brightness phase relationship. The maximum phase angle for Mars is, as we know, 47°, so the observed phase curve for the brightness of this planet cannot be fully used to determine the scattering indicatrix, $\chi(\pi - \alpha)$. However, the parameter λ can be found [5] from the data on the Martian disk brightness distribution.

Reference [5] proposed an interpolation formula for determining a planet's phase function, $\Phi(\alpha)$, for $0 \leq \alpha \leq 180°$, if this function is known within a limited range of phase angles $0 \leq \alpha \leq \alpha_0$ ($\alpha_0 = 47°$ for Mars). But if the phase

function is completely known, the scattering indicatrix, $\chi(\pi - \alpha)$, and all the optical parameters can be determined quite readily.

We made laboratory measurements of the phase relationship and disk brightness distribution for artificial planets with different surface colors and roughnesses in December 1969, in order to verify the validity of the interpolation formula in reference [5]. The task assigned the experiment also included (1) a check on the degree of agreement between λ values found from disk brightness distribution on the one hand, and with respect to the planet brightness phase relationship on the other, and (2) study of the relationship between planetary disk brightness distribution and λ. It was of interest, in passing, to check the validity of Russell's empirical formula [6].

Six spheres, 60 mm in diameter, covered with a layer of powder as follows, /35 were used in the experiment: (I) crocus (mean grain size d = 200 microns); (II) brown hematite (d = 100 microns); (III) brown hematite + sand (d = 150 microns); (IV) chrome carborundum (d = 100 microns); (V) chrome carborundum (d = 250 microns); and (VI) chrome carborundum (d = 400 microns). The coatings were applied to spheres I, II, and III by the laboratory at the Belgorod Experimental Industrial Abrasive Plant. The powders were applied in a casein binder in several layers such that the backing was not translucent. A similar technology was used by the laboratory at the Main Astronomical Observatory of the Academy of Sciences of the Ukrainian SSR to coat spheres IV, V, and VI. Figure 1 is a photograph of the side-lighted surfaces of the spheres, magnified 6 times.

The equipment described in reference [7] was used to measure the integral brightness-phase relationship for the spheres, as well as the brightness distribution along the intensity equator.

The surfaces of the spheres were illuminated by a parallel beam of light from a ribbon filament lamp supplied by a stabilized power source. Steps were taken to do away with extraneous illumination. Phase relationships were measured between phase angles 0.7° - 170° in 10° increments. Brightness distribution was measured with a diaphragm with a diameter of $0.2R_s$, with a spacing of approximately $0.1R_s$ for phase $\alpha = 0.7°$, and for sphere III for $\alpha = 10$ and 37.5° as well. All measurements of spheres I, II, and III were made in four regions

of the spectrum defined by interference filters. Spheres IV, V, and VI were measured in one region of the spectrum (596 millimicrons). Measurements of a white screen with the following values of reflectivity, ρ, were made to determine surface reflectivity:

$\tilde{\lambda}$, millimicrons	416	503	596	750	б/ф
ρ	0.74	0.84	0.89	0.90	0.86

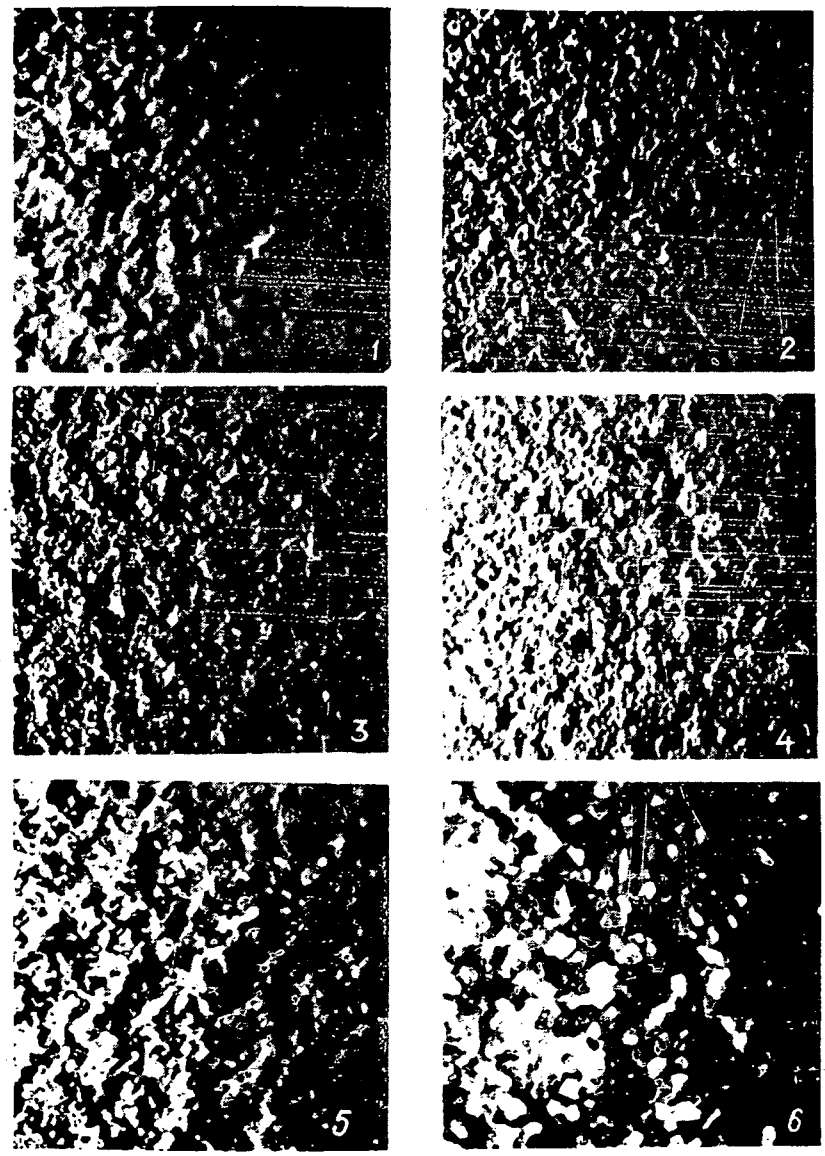

Figure 1. Views of surface of spheres (I-VI) magnfied 6 times.

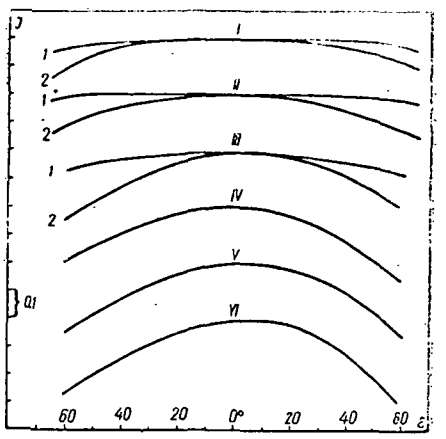

Figure 2. Distribution of brightness along the intensity equator for spheres with $\alpha = 0.7°$. For spheres I-III 1 - 416 millimicrons, 2 - 750 millimicrons; for spheres IV-VI - 596 millimicrons.

The results of the measurement of brightness distribution along the intensity equator are listed in Tables 1 and 2. Reflectivity, ρ, for each sphere is listed at the end of the table. Figure 2 shows the brightness distribution for $\alpha = 0.7°$ for the spectral extremes (I, II, III) and in one spectral region for spheres IV, V, and VI. Table 3 lists the results of the measurements of the phase-brightness relationship for the spheres for extreme wavelength values. The values of the geometric albedo, A_g, and phase integral, q, are listed at the end of the table.

As we see from Figure 2 and Table 3, sphere disk brightness distribution, and the value of the phase functions and the phase integral depend on the wavelength, $\tilde{\lambda}$ (that is, on surface reflectivity). The reflectivity of the models studied decreased with decrease in the limb opacity. L. A. Akimov and N. P. Barabashov [8, 9] obtained similar results from measuring a great many laboratory models.

This peculiarity in the reflection law is readily explained (within the context of the model adopted for the structure of a ploughed up surface) by the change in the parameters λ and $\varkappa$ with wavelength in Eqs. (1) - (3), which provide a quantitative description of the reflection law for a ploughed up surface. /36

Let us now move on to the indirect purpose of the experiment, that of ascertaining the validity of the procedure used [5] to determine the phase function and the parameter λ. One is readily persuaded that the product /37

$\chi(\pi-\alpha)\exp\left[\frac{\varkappa^2}{\pi}\left(\frac{\sigma}{2}\right)^3 \operatorname{ctg}\frac{\alpha}{2}\right] J(y,\varkappa)$ has practically no dependence on η and ζ when α is small ($\alpha \leq 30°$). In this case change in the function $\frac{\eta-\zeta}{\zeta} I(\eta,\zeta,\alpha)$ with change in η and ζ is almost entirely attributable to multiple particle scattering of the surface layer, and this permits the determination of the value of the

parameter λ in terms of the magnitude $\Delta I(\eta, \zeta, \alpha)$ quite confidently.

TABLE 1. BRIGHTNESS DISTRIBUTION ALONG THE INTENSITY EQUATOR OF ARTIFICIAL PLANETS (α = 0.7°).

ε	I				II				IV	V	VI
	$\tilde{\lambda}$, millimicron										
	416	503	596	750	416	503	596	750	596	596	596
65°	0.95	0.97	0.94	0.86	0.98	0.98	0.95	0.86	0.77	0.69	0.67
60	0.97	0.98	0.96	0.91	0.99	0.99	0.97	0.90	0.80	0.75	0.72
50	0.98	0.99	0.98	0.95	1.00	1.00	0.98	0.93	0.86	0.82	0.80
40	0.99	1.00	0.99	0.97	1.00	1.00	0.99	0.95	0.91	0.88	0.85
30	1.00	1.00	1.00	0.99	1.00	1.00	1.00	0.96	0.94	0.94	0.89
25	1.00	1.00	1.00	1.00	1.00	1.00	1.00	0.97	0.97	0.96	0.92
20	1.00	1.00	1.00	1.00	1.00	1.00	1.00	0.98	0.99	0.98	0.95
15	1.00	1.00	1.00	1.00	1.00	1.00	1.00	0.99	1.00	0.99	0.97
10	1.00	1.00	1.00	1.00	1.00	1.00	1.00	1.00	1.00	1.00	0.98
5	1.00	1.00	1.00	1.00	1.00	1.00	1.00	1.00	1.00	1.00	0.99
0	1.00	1.00	1.00	1.00	1.00	1.00	1.00	1.00	1.00	1.00	1.00
5	1.00	1.00	1.00	1.00	1.00	1.00	1.00	1.00	1.00	1.00	1.00
10	1.00	1.00	1.00	1.00	1.00	1.00	1.00	1.00	1.00	1.00	0.99
15	1.00	1.00	1.00	1.00	1.00	1.00	0.99	0.99	0.99	0.99	0.99
20	1.00	1.00	1.00	0.99	1.00	1.00	0.98	0.98	0.98	0.98	0.98
25	1.00	1.00	0.99	0.98	1.00	1.00	0.97	0.97	0.96	0.97	0.96
30	1.00	1.00	0.98	0.97	1.00	1.00	0.96	0.95	0.93	0.95	0.92
40	1.00	1.00	0.97	0.96	1.00	1.00	0.95	0.93	0.88	0.90	0.86
50	1.00	1.00	0.95	0.95	1.00	1.00	0.94	0.90	0.82	0.83	0.79
60	0.99	0.99	0.93	0.93	0.99	0.99	0.93	0.88	0.74	0.75	0.70
65	0.97	0.97	0.90	0.90	0.98	0.98	0.91	0.85	0.69	0.69	0.64
ϱ	0.039	0.042	0.117	0.190	0.035	0.087	0.256	0.352	0.453	0.324	0.255

TABLE 2. BRIGHTNESS DISTRIBUTION ALONG THE INTENSITY EQUATOR OF ARTIFICIAL PLANETS

ε	III, α=0°.7				III, α=10°				III, α=37°.5			
	$\tilde{\lambda}$, millimicron											
	416	503	596	750	416	503	596	750	416	503	596	750
60	0.94	0.93	0.85	0.78	0.98	1.00	0.94	0.86	1.27	1.24	1.22	1.16
50	0.95	0.95	0.88	0.82	1.00	1.01	0.96	0.88	1.24	1.22	1.19	1.16
40	0.96	0.96	0.91	0.86	1.00	1.01	0.96	0.92	1.21	1.20	1.16	1.12
30	0.97	0.97	0.94	0.90	1.00	1.01	0.98	0.96	1.15	1.16	1.13	1.12
25	0.98	0.98	0.97	0.94	1.00	1.01	0.98	0.98	1.12	1.13	1.12	1.11
20	0.99	0.99	0.98	0.96	1.00	1.00	1.00	1.00	1.09	1.10	1.11	1.09
15	0.99	1.00	0.99	0.98	1.00	1.00	1.00	1.00	1.06	1.08	1.08	1.06
10	1.00	1.00	1.00	0.99	1.00	1.00	1.00	1.00	1.03	1.06	1.05	1.05
5	1.00	1.00	1.00	1.00	1.00	1.00	1.00	1.00	1.02	1.03	1.02	1.03
0	1.00	1.00	1.00	1.00	1.00	1.00	1.00	1.00	1.00	1.00	1.00	1.00
5	1.00	1.00	0.99	1.00	0.98	0.98	0.98	0.98	0.96	0.95	0.94	0.96
10	0.99	1.00	1.99	0.99	0.96	0.97	0.98	0.96	0.90	0.91	0.88	0.90
15	0.99	0.99	0.98	0.99	0.94	0.96	0.96	0.94	0.84	0.87	0.83	0.83
20	0.98	0.98	0.98	0.98	0.92	0.94	0.94	0.92	0.78	0.83	0.77	0.80
25	0.98	0.98	0.97	0.96	0.90	0.93	0.92	0.88	0.72	0.77	0.72	0.70
30	0.97	0.97	0.96	0.94	0.88	0.92	0.90	0.84	0.63	0.71	0.61	0.61
40	0.96	0.96	0.94	0.91	0.86	0.89	0.86	0.78	0.54	0.63	0.47	0.41
50	0.94	0.95	0.91	0.86	0.84	0.86	0.80	0.73				
60	0.93	0.94	0.87	0.81	0.80	0.80	0.74	0.65				
ϱ	0.051	0.104	0.263	0.340								

TABLE 3. SPHERE PHASE-BRIGHTNESS RELATIONSHIP

α	I		II		III		IV	V	VI
	λ, millimicron								
	416	750	416	750	416	750	596	596	596
0°.7	1.00	1.00	1.00	1.00	1.00	1.00	1.00	1.00	1.00
10	0.73	0.78	0.70	0.73	0.70	0.74	0.87	0.91	0.93
20	0.60	0.64	0.53	0.64	0.60	0.65	0.82	0.86	0.88
30	0.50	0.54	0.41	0.55	0.48	0.56	0.73	0.76	0.79
40	0.41	0.45	0.35	0.48	0.40	0.49	0.65	0.69	0.70
50	0.34	0.38	0.28	0.40	0.33	0.42	0.57	0.60	0.62
60	0.29	0.32	0.22	0.33	0.27	0.35	0.48	0.53	0.54
70	0.25	0.27	0.18	0.27	0.23	0.29	0.41	0.45	0.47
80	0.20	0.22	0.14	0.22	0.18	0.23	0.34	0.37	0.39
90	0.16	0.18	0.11	0.17	0.15	0.18	0.26	0.30	0.31
100	0.13	0.14	0.08	0.12	0.12	0.13	0.19	0.24	0.25
110	0.10	0.11	0.06	0.09	0.09	0.10	0.14	0.19	0.20
120	0.08	0.09	0.05	0.06	0.07	0.08	0.10	0.15	0.16
130	0.07	0.08	0.04	0.05	0.06	0.06	0.07	0.10	0.13
140	0.06	0.07	0.03	0.04	0.05	0.04	0.04	0.07	0.10
150	0.04	0.05	0.02	0.03	0.04	0.03	0.03	0.05	0.08
160	0.03	0.04	0.02	0.02	0.03	0.02	0.02	0.03	0.06
170	0.02	0.03	0.01	0.01	0.02	0.01	0.01	0.02	0.04
A_g	0.028	0.194	0.024	0.356	0.035	0.342	0.388	0.270	0.204
q	0.81	0.87	0.62	0.82	0.75	0.88	1.22	1.37	1.43

Let us find the value of λ, using the data on brightness distribution for spheres II and III ($\tilde{\lambda}$ = 750 millimicrons - Table 1 and 2). The size of the diaphragm for measuring the brightness distribution was $\sim 0.2R_s$, so the maximum reflection angle $\varepsilon \approx 65°$ ($\alpha = 0.7°$) is the mean for the interval $52° \leq \varepsilon \leq 90°$. Now

$$\Delta\bar{I}(\bar{\varepsilon}) = \int_{\varepsilon_1}^{\varepsilon_2} \Delta I(\varepsilon)\, d\varepsilon. \tag{5}$$

Making all the necessary calculations we obtain $\lambda = 0.76$ for sphere III, and $\lambda = 0.68$ for sphere II.

On the other hand, if the brightness phase curve is known, λ can be determined from

$$2\int_0^{\pi} \frac{h(\alpha)}{G(\alpha, g, \varkappa)} \sin\alpha d\alpha = \lambda + 2\int_0^{\pi} \frac{\Delta G(\alpha, \lambda, X_1)}{G(\alpha, g, \varkappa)} \sin\alpha d\alpha, \tag{6}$$

where

$$h(\alpha) = \frac{\pi}{2} A_g(\alpha); \tag{7}$$

$A_g(\alpha)$ is the apparent geometric albedo. /38

$$G(\alpha, g, \varkappa) = \exp\left[\frac{\varkappa^2}{\pi}\left(\frac{g}{2}\right)^{3/2}\operatorname{ctg}\frac{\alpha}{2}\right]\int\limits_{\alpha-\frac{\pi}{2}}^{\pi/2}\frac{\eta\zeta}{\eta+\zeta}\,d\omega\int\limits_{0}^{\pi/2}J(y,\varkappa)\cos\psi d\psi; \tag{8}$$

$$\Delta G(\alpha, \lambda, X_1) = \int\limits_{\alpha-\frac{\pi}{2}}^{\pi/2}\eta d\omega\int\limits_{0}^{\pi/2}\Delta I(\eta, \zeta, \alpha)\cos\psi d\psi; \tag{9}$$

$$\eta = \cos\omega\cos\psi,\ \zeta = \cos(\alpha-\omega)\cos\psi; \tag{10}$$

ω and ψ are the planetocentric longitude and latitude of a point on the planet's surface. The numerical values of the functions $G(\alpha, g, \varkappa)$ and $\Delta G(\alpha, \lambda, x_1)$ are listed in Tables 4 and 5. Approximation formulas [4] for the Ambartsumyan function φ_i^k were used to calculate the $\Delta G(\alpha, \lambda, x_1)$.

Analysis reveals that the λ values obtained using Eq. (6) are little dependent on x_1, g, and $\varkappa$. Their roughly approximate values therefore can be taken in this case. Eq. (6) yielded $\tilde{\lambda} = 0.74$ and $\lambda = 0.68$, respectively, for spheres III and II, and these values agree well with the λ values found from the disk brightness distribution. /47

The maximum phase angle when observing Mars is 47°. But there are cases when the requirement is for knowledge of the planet's spherical albedo, $A_s = A_g q$, or its brightness for any phase angle value $0° \leq \alpha \leq 180°$. Russell [6] has suggested an empirical formula in which $A_s = aA_g\Phi(50°)$, where $a \approx 2.2$, for finding the spherical albedo. Let us check the validity of this expression, using the results of the measurements made of the spheres. In our case, according to the calculations, $a = 2.29 \pm 0.11$.

The following formula has been suggested for use in finding the Martian phase function for $\alpha > 47°$ [5] /48

$$\Phi(\alpha) = a\alpha^3 + b\alpha^2 + c\alpha + d, \tag{11}$$

in which the constants a, b, c, and d are found from the following family of equations

$$\Phi(\alpha_0) = a\alpha_0^3 + b\alpha_0^2 + c\alpha_0 + d,$$
$$\left.\frac{d\Phi}{d\alpha}\right|_{\alpha=\alpha_0} = 3a\alpha_0^2 + 2b\alpha_0 + c,$$
$$\Phi(180°) = 0, \qquad (12)$$
$$\left.\frac{d\Phi}{d\alpha}\right|_{\alpha=180°} = 0.$$

TABLE 4.

$G(\alpha, g, \varkappa) \cdot 10^3$

α	g								
	0.1	.2	.3	.4	.5	.6	.7	.8	.9
					$\varkappa=1$				
0°	1571	1571	1571	1571	1571	1571	1571	1571	1571
1	1017	1212	1321	1385	1425	1452	1471	1485	1497
2	919	1077	1193	1273	1328	1367	1396	1417	1434
3	878	1004	1112	1194	1255	1300	1335	1361	1382
4	854	959	1056	1135	1198	1246	1283	1313	1336
5	839	927	1014	1089	1151	1200	1239	1271	1296
10	797	846	900	953	1002	1045	1083	1115	1143
	768	801	839	879	916	951	982	1010	1035
20	741	765	794	823	853	881	906	930	951
25	713	732	754	777	801	823	844	864	881
30	684	699	716	735	754	772	789	805	819
35	653	665	680	695	710	725	738	751	763
40	622	632	643	656	668	680	691	701	710
45	589	598	607	617	627	637	646	654	661
50	556	563	571	580	588	596	602	609	614
60	490	494	500	505	511	516	519	523	525
70	423	427	430	434	437	440	441	443	443
80	359	361	363	365	367	368	368	368	368
90	297	298	300	301	301	301	300	299	298
100	239	240	240	241	240	240	238	237	234
110	186	186	186	186	185	184	182	180	178
120	138	139	138	138	137	135	133	131	128
130	97.2	97.2	96.7	96.0	94.7	93.2	91.2	89.0	86.4
140	62.8	62.6	62.1	61.2	60.0	58.6	56.7	54.7	52.5
150	35.5	35.3	34.8	34.8	32.9	31.6	30.1	28.7	27.8
160	15.8	15.6	15.2	14.5	13.7	13.7	11.8	10.8	9.8
170	3.9	9.8	3.5	3.1	2.7	2.3	1.9	1.7	1.4
					$\varkappa=0.9$				
0°	1428	1428	1428	1428	1428	1428	1428	1428	1428
1	976	1139	1230	1282	1314	1336	1351	1362	1370
2	894	1025	1123	1189	1235	1367	1291	1308	1321
3	860	964	1055	1124	1175	1212	1241	1263	1279
4	841	927	1007	1074	1126	1167	1198	1223	1242
5	828	900	972	1035	1087	1128	1162	1188	1209
10	791	831	876	920	960	997	1029	1056	1079
15	765	792	822	855	886	915	942	966	986
20	738	758	782	806	830	854	875	895	913
25	711	726	744	764	783	802	819	836	850
30	682	694	709	724	740	755	769	783	795

TABLE 4 CONTINUED

a	$\varkappa$								
	0.1	.2	.3	.4	.5	.6	.7	.8	.9
35°	652	662	674	686	699	711	722	735	743
40	620	629	638	649	659	669	678	687	695
45	588	595	603	611	620	628	636	642	648
50	556	561	568	575	582	588	594	599	604
60	489	495	498	502	507	511	514	517	519
70	423	426	429	432	434	437	438	440	440
80	538	360	362	364	365	366	367	367	366
90	297	298	299	300	300	301	300	299	298
100	239	240	240	240	240	240	239	237	236
110	186	186	186	186	186	185	183	182	180
120	138	139	138	138	137	136	134	133	130
130	97.2	97.2	96.9	96.3	95.3	94.1	92.5	90.7	88.6
140	62.8	62.6	62.2	61.6	60.6	59.4	58.0	56.3	54.3
150	35.5	35.4	34.9	34.3	33.5	32.4	31.2	29.9	28.4
160	15.9	15.7	15.3	14.8	14.1	13.4	12.6	11.6	10.7
170	3.95	3.81	3.58	3.28	2.91	2.55	2.21	1.91	1.64
	$\varkappa=0.8$								
0°	1309	1309	1309	1309	1309	1309	1309	1309	1309
1	938	1073	1149	1192	1219	1236	1249	1257	1264
2	872	979	1060	1116	1154	1181	1200	1214	1225
3	845	929	1003	1061	1103	1135	1159	1177	1191
4	829	898	964	1019	1063	1097	1123	1144	1160
5	818	876	935	987	1030	1065	1092	1115	1132
10	786	818	854	890	923	953	980	1003	1023
15	761	783	808	834	859	883	905	925	943
20	736	752	770	790	810	829	847	864	879
25	709	721	736	751	767	783	797	811	823
30	681	690	702	714	727	740	751	763	773
35	651	659	668	678	688	699	708	717	725
40	619	626	634	642	650	659	667	674	680
45	587	593	599	606	613	620	626	632	637
50	554	559	565	570	576	581	586	591	595
60	489	492	495	499	503	506	509	512	514
70	423	425	427	430	432	434	436	437	438
80	358	360	361	363	364	365	366	366	366
90	297	298	298	299	300	300	300	299	298
100	239	239	240	240	240	240	239	238	237
110	186	186	186	186	186	185	184	183	181
120	138	139	138	138	138	137	136	134	132
130	97.2	97.2	97.0	97.5	95.8	94.9	93.7	92.3	90.7
140	62.8	62.6	62.3	61.9	61.1	60.3	59.2	57.7	56.4
150	35.5	35.5	35.0	34.7	34.0	33.1	32.1	31.0	30.0
160	15.9	15.8	15.4	15.0	14.5	13.9	13.2	12.4	11.6
170	3.96	3.85	3.65	3.42	3.12	2.81	2.50	2.27	2.02
	$\varkappa=0.7$								
0°	1208	1208	1208	1208	1208	1208	1208	1208	1208
1	905	1015	1078	1114	1136	1150	1160	1167	1172
2	852	937	1004	1050	1082	1104	1120	1132	1141
3	831	897	957	1004	1040	1066	1086	1101	1113
4	818	872	925	970	1006	1035	1057	1074	1088
5	809	855	901	943	978	1007	1031	1050	1064
10	782	806	834	863	890	914	936	956	972
15	758	775	794	815	835	855	873	889	904
20	734	746	761	776	792	807	822	835	848
25	707	717	728	740	753	765	777	788	790
30	679	687	696	706	716	726	735	744	752
35	650	656	663	671	679	687	695	702	709
40	619	624	630	636	643	650	656	662	667
45	587	591	596	601	607	612	617	622	627
50	554	558	562	566	571	575	579	583	587
60	488	491	494	497	499	502	505	507	509
70	422	424	426	428	430	431	433	434	435
80	358	359	360	362	363	364	364	364	364
90	296	297	298	299	299	299	299	299	299

TABLE 4 CONTINUED

α	ξ								
	0.1	.2	.3	.4	.5	.6	.7	.8	.9
100°	239	239	240	240	240	240	239	239	238
110	186	186	186	186	186	186	185	184	183
120	138	138	138	138	138	137	136	135	134
130	97.2	97.2	97.1	96.8	96.3	95.6	94.7	93.7	92.5
140	62.8	62.7	62.5	62.2	61.6	61.0	60.1	59.1	58.1
150	35.5	35.5	35.2	35.0	34.4	33.8	33.1	32.2	31.4
160	15.9	15.8	15.6	15.3	14.9	14.4	13.9	13.3	12.6
170	3.97	3.89	3.75	3.56	3.33	3.07	2.80	2.63	2.39
				$\varkappa=0.6$					
0°	1122	1122	1122	1122	1122	1122	1122	1122	1122
1	875	963	1015	1045	1063	1075	1083	1089	1093
2	835	900	954	992	1018	1037	1050	1060	1068
3	819	869	916	954	983	1005	1022	1035	1045
4	808	849	890	926	955	979	997	1012	1023
5	801	836	871	904	933	956	976	991	1004
10	778	796	817	839	860	879	897	913	926
15	756	768	783	798	814	829	843	856	868
20	732	741	752	764	776	788	799	810	820
25	706	713	721	731	740	750	759	768	776
30	678	684	690	698	705	713	721	728	735
35	649	653	659	665	671	677	683	689	695
40	618	622	626	631	636	641	646	651	656
45	586	589	593	597	601	605	609	613	617
50	554	556	559	563	566	570	573	576	579
60	488	490	492	494	496	499	501	503	504
70	422	423	425	426	428	429	430	431	432
80	358	359	360	361	361	362	363	363	363
90	296	297	297	298	298	299	299	299	299
100	239	239	239	240	240	240	239	239	238
110	186	186	186	186	186	186	185	185	184
120	138	138	138	138	138	138	137	136	136
130	97.2	97.2	97.1	96.9	96.6	96.1	95.5	94.8	94.0
140	62.8	62.7	62.6	62.4	62.0	61.5	61.0	60.3	59.5
150	35.6	35.5	35.4	35.1	34.8	34.3	33.8	33.2	32.5
160	15.9	15.8	15.7	15.5	15.2	14.8	14.4	14.0	13.5
170	3.97	3.82	3.68	3.51	3.31	3.10	2.88	2.68	2.53
				$\varkappa=0.5$					
0°	1047	1047	1047	1047	1047	1047	1047	1047	1047
1	850	916	958	983	999	1009	1015	1020	1024
2	820	868	909	940	961	977	968	997	1003
3	808	844	879	909	933	951	965	975	984
4	800	830	860	887	910	929	944	956	966
5	795	819	845	870	892	911	926	939	950
10	774	787	802	818	834	849	862	874	885
15	754	762	773	784	795	806	817	827	837
20	730	737	744	753	762	770	779	787	795
25	705	710	716	722	729	736	743	750	756
30	677	681	686	690	697	702	708	712	718
35	648	651	655	659	664	668	673	677	682
40	617	620	623	627	630	634	638	641	645
45	586	588	590	593	596	599	602	605	608
50	553	555	557	560	562	565	567	570	572
60	488	489	490	492	494	495	497	498	500
70	422	423	424	425	426	427	428	429	430
80	358	358	358	359	360	360	361	361	362
90	296	297	297	298	297	298	298	298	298
100	239	239	239	239	239	239	239	239	239
110	186	186	186	186	186	186	186	185	185
120	138	138	138	138	138	138	138	137	137
130	97.2	97.2	97.2	97.0	96.9	96.6	96.2	95.7	95.2
140	62.8	62.8	62.7	62.5	62.3	62.0	61.6	61.2	60.6
150	35.6	35.5	35.4	35.3	35.1	34.8	34.4	34.0	33.6
160	15.9	15.8	15.8	15.6	15.4	15.2	14.9	14.6	14.3
170	3.98	3.94	3.88	3.78	3.66	3.52	3.36	3.20	3.03

TABLE 4 CONTINUED

α	g								
	0.1	.2	.3	.4	.5	.6	.7	.8	.9
					$\varkappa=0.4$				
0°	982	982	982	982	982	982	982	982	982
1	828	876	908	929	941	950	956	960	963
2	808	840	870	893	911	924	933	940	945
3	799	824	848	870	888	902	914	922	929
4	794	813	834	853	870	885	897	907	915
5	790	806	823	841	857	871	883	893	902
10	772	780	790	801	811	822	832	841	849
15	752	757	764	772	779	787	795	802	809
20	729	733	738	744	750	756	762	767	773
25	704	707	711	715	720	725	729	734	739
30	676	679	682	685	689	693	697	701	704
35	647	649	652	655	658	661	664	667	670
40	617	618	620	623	625	628	630	633	635
45	585	587	588	590	592	594	596	599	601
50	553	554	556	557	559	561	562	564	566
60	487	488	489	490	491	493	494	495	496
70	422	422	423	424	424	425	426	427	427
80	357	358	358	359	359	360	360	361	361
90	296	296	297	297	297	297	298	298	298
100	238	239	239	239	239	239	239	239	239
110	186	186	186	186	186	186	186	186	185
120	138	138	138	138	138	138	138	138	138
130	97.2	97.2	97.2	97.1	97.0	96.9	96.6	96.4	96.1
140	62.8	62.8	62.7	62.7	62.5	62.4	62.1	61.9	61.6
150	35.6	35.5	35.5	35.2	35.1	35.2	34.9	34.7	34.4
160	15.9	15.9	15.8	15.7	15.6	15.5	15.3	15.1	14.9
170	3.98	3.96	3.92	3.87	3.79	3.70	3.60	3.48	3.42
					$\varkappa=0.3$				
0°	924	924	924	924	924	924	924	924	924
1	810	841	864	880	890	897	902	906	908
2	798	818	837	853	866	876	884	889	894
3	792	807	822	836	849	859	868	875	881
4	789	800	812	825	836	846	855	863	869
5	785	795	805	816	826	836	845	852	859
10	770	774	780	787	793	800	806	812	818
15	750	754	758	762	767	771	776	781	785
20	728	730	733	737	740	744	747	751	755
25	703	705	707	710	712	715	718	721	724
30	676	677	679	681	683	685	688	690	692
35	647	648	649	651	653	655	657	658	660
40	616	617	618	620	621	623	624	626	627
45	585	586	587	588	589	590	591	593	594
50	553	553	554	555	556	557	558	559	560
60	487	488	488	489	489	490	491	492	492
70	422	422	422	423	423	424	424	424	425
80	357	358	358	358	359	359	359	359	360
90	296	296	297	297	297	297	297	297	297
100	238	239	239	239	239	239	239	239	239
110	186	186	186	186	186	186	186	186	186
120	138	138	138	138	138	138	138	138	138
130	97.2	97.2	97.2	97.2	97.2	97.1	97.0	96.8	96.7
140	62.8	62.8	62.8	62.7	62.7	62.6	62.5	62.4	62.2
150	35.6	35.6	35.5	35.5	35.4	35.4	35.3	35.1	35.0
160	15.9	15.9	15.9	15.8	15.8	15.7	15.6	15.5	15.4
170	3.98	3.97	3.95	3.92	3.89	3.84	3.78	3.72	3.64
					$\varkappa=0.2$				
0°	873	873	873	873	873	873	873	873	873
1	797	813	827	837	845	851	855	857	860
2	790	800	810	819	828	834	840	844	848
3	787	794	802	809	817	823	829	834	838
4	785	790	796	803	809	815	820	825	829
5	782	787	792	797	803	808	813	817	822
10	768	770	773	776	779	782	786	789	792

TABLE 4 CONTINUED

α	g								
	0.1	.2	.3	.4	.5	.6	.7	.8	.9
15°	749	751	753	755	757	759	762	764	766
20	727	728	730	731	733	735	736	738	740
25	703	703	704	705	707	708	710	711	712
30	675	676	677	678	679	680	681	682	683
35	646	647	648	648	649	650	651	652	653
40	616	616	617	618	618	619	620	621	621
45	585	585	585	586	586	587	588	588	589
50	552	553	553	554	554	554	555	556	556
60	487	487	487	488	488	488	489	489	489
70	421	422	422	422	422	422	423	423	423
80	357	357	358	358	358	358	358	358	358
90	296	296	296	296	296	296	296	297	297
100	238	238	239	239	239	239	239	239	239
110	186	186	186	186	186	186	186	186	186
120	138	138	138	138	138	138	138	138	138
130	97.1	97.2	97.2	97.2	97.2	97.1	97.1	97.0	97.0
140	62.8	62.8	62.8	62.8	62.7	62.7	62.7	62.6	62.6
150	35.6	35.6	35.6	35.6	35.6	35.5	35.5	35.4	35.4
160	15.9	15.9	15.9	15.9	15.8	15.8	15.8	15.8	15.7
170	3.98	3.98	3.97	3.96	3.95	3.93	3.91	3.88	3.85
	$\varkappa=0.1$								
0°	827	827	827	827	827	827	827	827	827
1	788	793	798	802	806	810	812	814	816
2	786	789	792	795	798	801	803	806	808
3	784	786	788	791	793	795	798	800	802
4	782	784	786	787	788	791	793	795	797
5	780	782	783	784	786	788	789	791	793
10	767	768	768	769	770	771	772	773	774
15	749	749	750	750	751	751	752	753	754
20	727	727	728	728	728	729	729	730	730
25	702	702	703	703	704	704	704	704	705
30	675	675	675	676	676	676	677	677	677
35	646	646	646	647	647	647	647	648	648
40	616	616	616	616	616	617	617	617	617
45	574	584	584	585	585	585	585	585	586
50	552	552	552	553	553	553	553	553	553
60	487	487	487	487	487	487	487	487	488
70	421	421	421	421	422	422	422	422	422
80	357	357	357	357	357	357	357	358	358
90	296	296	296	296	296	296	296	296	296
100	238	238	238	238	238	238	238	239	239
110	186	186	186	186	186	186	186	186	186
120	138	138	138	138	138	138	138	138	138
130	97.1	97.1	97.1	97.2	97.2	97.2	97.2	97.1	97.1
140	62.8	62.8	62.8	62.8	62.8	62.8	62.8	62.7	62.7
150	35.6	35.6	35.6	35.6	35.6	35.6	35.6	35.5	35.5
160	15.9	15.9	15.9	15.9	15.9	15.9	15.9	15.9	15.9
170	398	3.98	3.98	3.98	3.98	3.97	3.97	3.97	3.95

TABLE 5.

$\Delta G(\alpha\lambda\chi_1) \cdot 10^3$

α	x_1						
	—0.5	—1.0	—0.5	0.0	0.5	1.0	1.5
	$\lambda=0.1$						
0°	0.337	0.747	0.998	1.08	1.00	0.745	0.306
5	0.339	0.745	0.994	1.08	0.998	0.742	0.307
10	0.345	0.741	0.983	1.07	0.986	0.735	0.309
15	0.355	0.734	0.966	1.05	0.965	0.724	0.314
20	0.368	0.726	0.944	1.02	0.941	0.711	0.320
25	0.382	0.715	0.917	0.984	0.911	0.694	0.329
30	0.398	0.702	0.886	0.946	0.877	0.676	0.338

TABLE 5 CONTINUED

α	x_1						
	−1.5	−1.0	−0.5	0.0	0.5	1.0	1.5
35°	0.414	0.687	0.852	0.904	0.840	0.650	0.349
40	0.429	0.670	0.815	0.859	0.800	0.635	0.356
45	0.442	0.651	0.755	0.812	0.759	0.612	0.370
50	0.453	0.630	0.734	0.763	0.715	0.588	0.378
60	0.464	0.580	0.647	0.662	0.626	0.536	0.389
70	0.459	0.522	0.556	0.561	0.535	0.478	0.388
80	0.435	0.456	0.466	0.463	0.446	0.416	0.372
90	0.393	0.386	0.378	0.369	0.361	0.351	0.342
100	0.338	0.313	0.295	0.284	0.281	0.285	0.297
110	0.272	0.241	0.219	0.209	0.209	0.220	0.243
120	0.204	0.173	0.153	0.144	0.146	0.160	0.185
130	0.139	0.114	0.099	0.092	0.094	0.106	0.128
140	0.083	0.066	0.056	0.052	0.054	0.062	0.077
150	0.040	0.032	0.026	0.024	0.026	0.030	0.038
160	0.014	0.011	0.009	0.008	0.009	0.010	0.013
170	0.002	0.002	0.001	0.001	0.001	0.001	0.002
				$\lambda=0.2$			
0°	1.72	3.32	4.31	4.67	4.35	3.31	1.48
5	1.73	3.31	4.30	4.65	4.33	3.29	1.48
10	1.75	3.29	4.25	4.59	4.28	3.26	1.49
15	1.78	3.26	4.17	4.50	4.20	3.21	1.50
20	1.82	3.21	4.08	4.38	4.09	3.15	1.53
25	1.86	3.16	3.96	4.24	3.96	3.08	1.55
30	1.91	3.09	3.82	4.07	3.81	2.99	1.59
35	1.95	3.02	3.67	3.89	3.65	2.90	1.62
40	1.99	2.94	3.51	3.70	3.47	2.80	1.65
45	2.03	2.84	3.34	3.50	3.29	2.70	1.68
50	2.05	2.74	3.16	3.28	3.10	2.58	1.71
60	2.05	2.51	2.78	2.85	2.71	2.34	1.73
70	1.99	2.24	2.39	2.41	2.31	2.08	1.71
80	1.86	1.95	1.99	1.98	1.92	1.80	1.62
90	1.66	1.64	1.61	1.58	1.55	1.51	1.47
100	1.41	1.32	1.26	1.22	1.20	1.22	1.27
110	1.13	1.01	0.932	0.891	0.893	0.940	1.04
120	0.843	0.726	0.650	0.614	0.623	0.678	0.782
130	0.571	0.478	0.416	0.390	0.400	0.448	0.537
140	0.340	0.277	0.236	0.220	0.228	0.262	0.323
150	0.165	0.132	0.111	0.102	0.107	0.126	0.159
160	0.056	0.044	0.037	0.034	0.036	0.043	0.055
170	0.008	0.006	0.005	0.005	0.005	0.006	0.008
				$\lambda=0.3$			
0°	4.83	8.34	10.6	11.4	10.7	8.34	4.07
5	4.84	8.31	10.5	11.4	10.7	8.31	4.07
10	4.87	8.26	10.4	11.2	10.5	8.23	4.08
15	4.92	8.16	10.2	11.0	10.3	8.10	4.10
20	4.98	8.04	9.98	10.7	10.1	7.94	4.14
25	5.04	7.89	9.69	10.4	9.74	7.74	4.18
30	5.10	7.71	9.36	9.95	9.38	7.52	4.23
35	5.16	7.51	8.99	9.51	8.98	7.28	4.28
40	5.21	7.28	8.59	9.04	8.54	7.02	4.33
45	5.23	7.03	8.16	8.54	8.09	6.74	4.37
50	5.23	6.76	7.71	8.02	7.62	6.44	4.40
60	5.14	6.15	6.77	6.95	6.65	5.82	4.39
70	4.90	5.47	5.80	5.88	5.65	5.14	4.26
80	4.51	4.72	4.84	4.83	4.70	4.43	4.00
90	3.98	3.95	3.90	3.85	3.78	3.70	3.60
100	3.36	3.17	3.03	2.95	2.93	2.97	3.08
110	2.67	2.41	2.24	2.15	2.16	2.22	2.49
120	1.97	1.72	1.56	1.48	1.50	1.63	1.87
130	1.33	1.13	0.995	0.937	0.960	1.07	1.28
140	0.784	0.651	0.563	0.526	0.544	0.621	0.764
150	0.382	0.309	0.263	0.244	0.255	0.297	0.374
160	0.130	0.103	0.086	0.080	0.084	0.100	0.128
170	0.018	0.014	0.012	0.011	0.012	0.014	0.018

TABLE 5 CONTINUED

α	x_1						
	−1.5	−1.0	−0.5	0.0	0.5	1.0	1.5
				$\lambda=0.4$			
0°	10.06	16.7	20.7	22.2	21.1	16.8	8.93
5	10.6	16.6	20.6	22.1	21.0	16.8	8.93
10	10.6	16.5	20.3	21.9	20.7	16.6	8.93
15	10.6	16.3	20.0	21.4	20.3	16.3	8.94
20	10.7	16.0	19.5	20.9	19.8	16.0	8.96
25	10.7	15.7	18.9	20.2	19.2	15.6	9.00
30	10.8	15.3	18.3	19.4	18.4	15.1	9.03
35	10.8	14.9	17.5	18.5	17.6	14.6	9.06
40	10.8	14.4	16.7	17.6	16.8	14.1	9.10
45	10.7	13.9	15.9	16.6	15.9	13.5	9.10
50	10.6	13.3	15.0	15.6	15.0	12.9	9.08
60	10.2	12.0	13.2	13.5	13.0	11.5	8.91
70	9.59	10.6	11.2	11.4	11.1	10.1	8.52
80	8.71	9.12	9.35	9.37	9.17	8.69	7.90
90	7.61	7.58	7.52	7.45	7.35	7.21	7.03
100	6.34	6.04	5.82	5.70	5.67	5.75	5.97
110	5.00	4.58	4.29	4.15	4.17	4.37	4.78
120	3.68	3.26	2.97	2.84	2.88	3.11	3.56
130	2.46	2.12	1.89	1.79	1.83	2.03	2.41
140	1.45	1.22	1.06	1.00	1.03	1.17	1.43
150	0.701	0.576	0.495	0.462	0.480	0.557	0.696
160	0.237	0.191	0.162	0.150	0.157	0.185	0.236
170	0.034	0.027	0.022	0.021	0.022	0.026	0.034
				$\lambda=0.5$			
0°	20.2	29.6	35.9	38.6	37.0	30.3	17.5
5	20.2	29.6	35.8	38.4	36.9	30.2	17.5
10	20.2	29.3	35.4	37.9	36.4	29.9	17.5
15	20.2	28.9	34.8	37.2	35.7	29.4	17.4
20	20.1	28.4	33.9	36.2	34.8	28.8	17.4
25	20.1	27.8	32.9	35.0	33.6	28.0	17.4
30	20.0	27.0	31.7	33.6	32.4	27.2	17.3
35	19.8	26.2	30.4	32.2	31.0	26.2	17.2
40	19.6	25.3	29.0	30.5	29.4	25.2	17.1
45	19.4	24.3	27.5	28.8	27.8	24.1	17.0
50	19.0	23.2	26.0	27.1	26.2	22.9	16.8
60	18.0	20.9	22.7	23.4	22.8	20.5	16.2
70	16.7	18.3	19.3	19.7	19.3	17.9	15.2
80	15.0	15.6	16.1	16.2	15.9	15.2	13.9
90	12.9	12.9	12.9	12.8	12.7	12.5	12.2
100	10.6	10.2	9.94	9.78	9.78	9.93	10.3
110	8.33	7.72	7.30	7.10	1.16	7.49	8.16
120	6.07	5.45	5.04	4.85	4.93	5.30	6.02
130	4.04	3.53	3.19	3.04	3.11	3.44	4.05
140	2.37	2.02	1.78	1.69	1.74	1.96	2.38
150	1.14	0.948	0.825	0.773	0.804	0.924	1.15
160	0.383	0.313	0.268	0.250	0.261	0.305	0.386
170	0.054	0.044	0.037	0.034	0.036	0.042	0.054
				$\lambda=0.6$			
0°	35.8	49.3	58.6	62.8	60.9	51.4	32.3
5	35.8	49.2	58.4	62.5	60.6	51.2	32.3
10	35.7	48.7	57.7	61.7	59.8	50.6	32.1
15	35.5	48.0	56.6	60.5	58.7	49.8	32.0
20	35.3	47.1	55.3	58.9	57.1	49.7	31.7
25	35.0	46.0	53.6	57.0	55.3	47.3	31.5
30	34.6	44.7	51.7	54.8	53.2	45.8	31.2
35	34.1	43.3	49.5	52.3	50.8	44.1	30.8
40	33.5	41.6	47.2	49.6	48.3	42.3	30.4
45	32.7	39.9	44.7	46.9	45.7	40.4	29.9
50	31.9	38.0	42.2	43.9	42.9	38.3	29.2

TABLE 5 CONTINUED

α	x_1						
	−1.5	−1.0	−0.5	0.0	0.5	1.0	1.5
60°	29.8	34.0	36.8	37.8	37.2	34.0	27.7
70	27.1	29.6	31.3	32.0	31.5	29.5	25.7
80	24.0	25.1	25.8	26.1	25.9	24.9	23.1
90	20.5	20.6	20.7	20.7	20.6	20.4	20.0
100	16.7	16.2	15.9	15.7	15.8	16.0	16.6
110	12.9	12.1	11.6	11.4	11.5	12.0	13.0
120	9.36	8.52	7.96	7.72	7.84	8.40	9.49
130	6.18	5.48	5.01	4.81	4.92	5.40	6.31
140	3.60	3.11	2.79	2.65	2.73	3.06	3.68
150	1.72	1.45	1.28	1.21	1.25	1.43	1.76
160	0.574	0.476	0.412	0.386	0.402	0.465	0.584
170	0.081	0.066	0.056	0.052	0.054	0.064	0.081
				$\lambda=0.7$			
0°	60.9	79.4	92.5	99.0	97.2	84.8	58.3
5	60.8	79.2	92.2	98.6	96.8	84.5	58.2
10	60.5	78.4	91.1	97.4	95.6	83.6	57.8
15	60.1	77.3	89.5	95.5	93.8	82.1	57.3
20	59.4	75.7	78.2	92.9	91.3	80.2	56.7
25	58.6	73.8	84.6	89.9	88.3	78.0	55.9
30	57.6	71.6	81.5	86.4	84.9	75.3	55.0
35	56.4	69.1	78.0	82.0	81.1	72.4	53.9
40	55.0	66.4	74.3	78.3	77.1	69.3	52.7
45	53.4	63.4	70.4	73.8	72.8	65.9	51.3
50	51.7	60.2	66.3	69.2	68.3	62.4	49.9
60	47.5	53.5	57.6	59.7	59.1	55.0	46.4
70	42.7	46.3	48.9	50.1	49.8	47.4	42.2
80	37.2	39.0	40.2	40.9	40.8	39.7	37.3
90	31.4	31.7	32.0	32.2	32.3	32.2	31.8
100	25.3	24.8	24.4	24.4	24.6	25.1	25.9
110	19.4	18.4	17.8	17.5	17.8	18.6	20.0
120	13.9	12.8	12.1	11.8	12.1	12.9	14.4
130	9.08	8.18	7.58	7.33	7.51	8.19	9.43
140	5.23	4.60	4.18	4.01	4.13	4.59	5.47
150	2.48	2.13	1.90	1.80	1.87	2.11	2.58
160	0.821	0.691	0.606	0.570	0.592	0.680	0.845
170	0.115	0.094	0.081	0.076	0.079	0.092	0.116
				$\lambda=0.8$			
0°	103	128	146	156	156	141	107
5	103	127	146	156	155	140	106
10	102	126	144	154	153	139	106
15	101	124	141	151	150	136	104
20	99.5	121	138	147	146	133	103
25	97.6	118	133	142	141	129	101
30	95.4	114	128	136	136	125	98.6
35	92.9	110	122	130	130	120	96.0
40	90.0	105	117	123	123	114	93.1
45	86.9	100	110	116	116	108	89.9
50	83.4	95.2	104	109	109	102	86.9
60	75.6	83.9	90.1	93.7	93.9	89.6	78.8
70	66.9	72.1	76.0	78.4	78.8	76.5	70.1
80	57.5	60.1	62.3	63.7	64.2	63.4	60.7
90	47.7	48.5	49.3	50.0	50.5	50.8	50.7
100	38.0	37.5	37.4	37.6	38.1	39.1	40.6
110	28.7	27.6	27.0	26.9	27.4	28.6	30.8
120	20.3	19.0	18.2	18.0	18.4	19.6	21.8
130	13.2	12.9	11.3	11.0	11.3	12.3	14.1
140	7.47	6.68	6.17	5.97	6.15	6.78	7.99
150	3.49	3.06	2.77	2.66	2.74	3.07	3.70
160	1.14	0.980	0.871	0.827	0.856	0.973	1.20
170	0.158	0.132	0.115	0.108	0.112	0.121	0.161

TABLE 5 CONTINUED

α	x_1						
	—1.5	—1.0	—0.5	0.0	0.5	1.0	1.5
				$\lambda=0.9$			
0°	183	216	243	260	264	250	211
5	182	216	242	259	263	250	210
10	181	213	239	256	260	247	208
15	178	210	235	251	255	242	205
20	175	205	229	244	248	236	201
25	171	199	221	236	240	229	196
30	166	192	213	226	230	220	191
35	161	185	204	216	220	211	184
40	155	176	193	205	208	201	177
45	148	167	182	193	196	190	170
50	141	158	171	180	183	178	161
60	126	138	148	154	157	155	144
70	109	117	124	129	131	130	125
80	92.3	96.8	101	104	106	107	105
90	75.2	71.1	79.0	80.8	82.6	84.3	85.6
100	58.8	58.9	59.3	60.3	61.7	63.8	66.8
110	43.6	42.7	43.2	42.6	43.7	45.9	49.4
120	30.3	29.0	28.2	28.2	29.0	30.8	34.1
130	19.2	18.0	17.2	17.0	17.6	19.0	21.5
140	10.8	9.86	9.27	9.08	9.36	10.2	11.9
150	4.95	4.43	4.09	3.96	4.09	4.54	5.39
160	1.59	1.39	1.26	1.21	1.25	1.40	1.70
170	0.216	0.184	0.163	0.155	0.160	0.182	0.224
				$\lambda=0.95$			
0°	261	302	355	359	423	419	386
5	260	301	334	358	421	417	385
10	258	298	330	353	416	412	381
15	254	292	324	346	408	405	375
20	249	286	316	336	397	394	366
25	243	277	305	326	384	382	356
30	235	267	294	313	368	367	344
35	237	256	280	298	351	350	331
40	217	244	266	282	332	332	316
45	207	231	251	266	312	313	300
50	196	217	235	248	292	293	283
60	173	188	202	212	249	252	247
70	149	159	168	176	206	210	209
80	124	130	136	141	165	170	172
90	99.7	103	106	109	127	132	137
100	76.9	77.6	78.8	80.7	93.6	98.0	104
110	56.2	55.6	55.7	56.5	65.3	69.1	74.7
120	38.5	37.3	36.8	37.0	42.6	45.4	50.2
130	24.1	22.9	22.2	22.1	25.3	27.3	30.8
140	13.1	12.4	11.8	11.6	13.2	14.4	16.6
150	6.02	5.47	5.12	5.00	5.66	6.24	7.31
160	1.91	1.69	1.55	1.50	1.69	1.88	2.24
170	0.255	0.220	0.198	0.189	0.211	0.237	0.288
				$\lambda=1.0$			
0°	575	637	695	748	793	827	845
5	573	635	693	745	789	824	842
10	567	628	684	736	780	814	833
15	557	616	671	721	764	798	817
20	543	600	653	701	743	776	794
25	527	580	631	677	780	750	771
30	507	558	605	649	688	719	741
35	485	532	576	617	654	685	707
40	461	504	544	582	617	647	670
45	435	474	511	546	578	607	630
50	408	442	476	507	537	568	588
60	350	377	404	428	454	478	501
70	292	311	330	350	370	391	414

TABLE 5 CONTINUED

α	x_1						
	—1.5	—1.0	—0.5	0.0	0.5	1.0	1.5
80	235	248	261	276	291	309	330
90	182	190	198	208	220	234	252
100	135	139	144	150	158	169	184
110	95.0	96.2	98.5	102	108	116	127
120	62.3	62.1	62.8	64.7	68.1	73.5	81.9
130	37.4	36.6	36.5	37.3	39.2	42.6	48.1
140	19.7	19.0	18.6	18.9	19.8	21.6	24.8
150	8.55	8.04	7.77	7.79	8.15	8.98	10.04
160	2.60	2.38	2.26	2.24	2.34	2.60	3.06
170	0.332	0.297	0.275	0.269	0.280	0.314	0.377

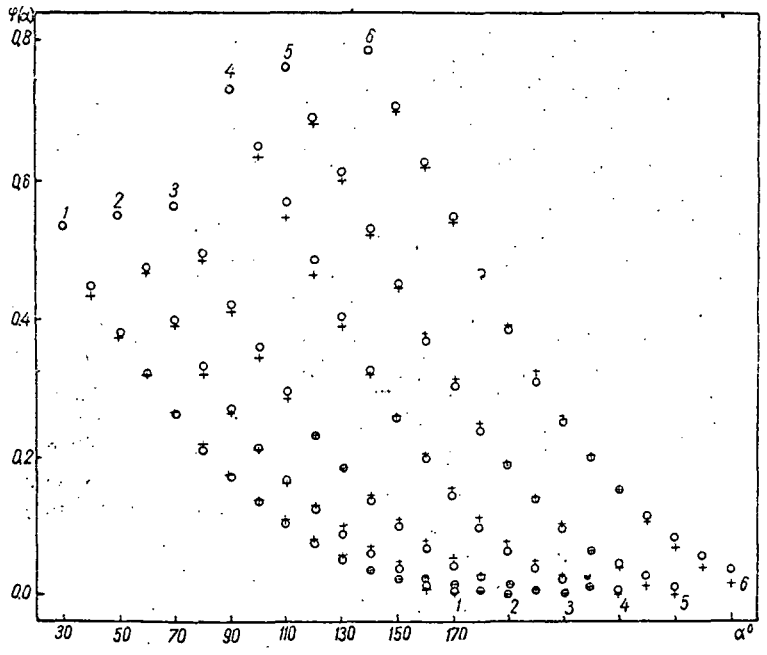

Figure 3. Integral brightness of spheres in terms of phase angle (for $\alpha \geq 30°$). The circles are the observed values, the crosses the calculated values. Each succeeding phase curve was shifted relative to the preceding one 10° with respect to α.

Experimental data show that the derivative $\frac{d\Phi}{d\alpha}\Big|\alpha = \alpha_0$ may be determined with a substantial error, so it is more convenient, initially, to find the value of λ from the disk brightness. Then, using Eq. (11), let us calculate the left side of Eq. (6) and by varying the value of the derivative $\frac{d\Phi}{d\alpha}\Big|\alpha = \alpha_0$ reach equality of both sides of this equation. It was taken that $\alpha_0 = 30°$ for the check made of Eqs. (11) and (12) in terms of sphere measurements. Figure 3 shows the observed (circles) and calculated (crosses) values of the phase function for all six spheres, and as we see, it is only for $\alpha > 150°$ that we find quite large differences between the observed and calculated phase function values for some of the spheres.

The authors wish to thank K. Ye. Skorik and L. A. Bugayenko for their assistance in conducting the experiment.

REFERENCES

1. Morozhenko, A. V., Rubashevskiy, A. A., Yanovitskiy, E. G., Astron. zhur., 47, 1970, 1073.

2. Morozhenko, A. V., Yanovitskiy, E. G., Astron. zhur., 48, 1971, 176.

3. Minin, I. N., Pilinosyan, A. G., Shidlovskaya, I. A., Trudy Astron. obs. LGU, 20, 1964, 12.

4. Yanovitskiy, E. G., V sb: Fizika Luny i planet [In collection: Physics of the Moon and Planets], "Naukova Dumka" Press, 1964, p. 92.

5. Morozhenko, A. V., Yanovitskiy, E. G., Astron. zhur., 48, 1971.

6. Sharonov, V. V., Priroda planet [Nature of the Planets], Fizmatgiz, Moscow, 1958, p. 311.

7. Bugayenko, L. A., et al., V sb: Astrometriya i astrofizika [In collection: Astrometry and Astrophysics], "Naukova Dumka" Press, No. 1, 1968.

8. Akimov, L. A., Barabashov, N. P., Astron. tsirkulyar, 1969, 540.

9. Akimov, L. A., Barabashov, N. P., Vestn. Khar'k. un-ta, seriya astron., 1970, 5.

SPECTROPHOTOMETRIC PECULIARITIES OF SOME SATELLITES OF PLANETS

Yu. D. Davudov, I. K. Koval'

ABSTRACT: Stebbin's and Jacobsen's photoelectric measurements of the solar phase-brightness relationship for Jupiter's Galilean satellites are used to show that the surface layers of the satellites are very porous. The parameter g that characterized relative density of a surface layer is equal to 0.2 for Callisto. Results of spectrophotometric observations of satellites are discussed briefly from the point of view of the possible nature of their surfaces.

Photometric observations of satellites of planets, as a class of objects /49 devoid of atmosphere (with certain exceptions), can be quite adequately used to arrive at a judgment as to the microrelief of the upper layer of their surfaces, and in part, as to the nature of the surface layer itself. In any case, as the long years of experience gained from photometric study of the Moon have shown, data from photometric observations, such as the brightness-phase angle relationship, the spectral variation in the albedo, disk brightness distribution, and other features, had led to rather definite conclusion as to the microrelief of the lunar surface and had made it possible to arrive at certain judgments as to the nature of the material of which the lunar surface layer was comprised.

Unfortunately, as distinguished from the Moon, photometric data on satellites of planets is quite limited because of the small angular sizes of these bodies and the limitations on the phase angles at which they can be observed from the Earth. Moreover, the accuracy of photometric observations is greatly reduced in many cases because the satellites are relatively dim, and are quite close to the central body.

Still, photometric (using light filters) and spectrophotometric observations are a quite effective means for studying this group of objects.

The Brightness-Phase Angle Relationship for the Galilean Satellites of Jupiter

In 1926, Stebbins [1], and in 1927, Stebbins and Jacobsen [2], collected numerous photoelectric measurements of the brightness of the bright satellites of Jupiter for a whole set of observed phase angles (up to 11°). The principal

goal of these observations was to study variations in the brightness of the satellites with phase rotation around a central body. The data obtained are close to B in the color system and unquestionably indicate the variation in the brightness of all four satellites with phase rotation.

The data compiled by Stebbins and Jacobsen have been discussed over and over again, and when these data were supplemented by those obtained in the 1950's at the McDonald Observatory it became conclusive there is a longitudinal effect in the brightness, and sometimes in the color, of the Galilean satellites. The latter evidently is associated with the mottled structure of their surfaces. Callisto is distinguished by maximum changes in brightness with phase rotation when the solar phase angles are large.

Let us pause briefly to consider the results of the observations obtained by Stebbins and Jacobsen as they pertain to the relationship between the brightness of the satellites and the solar phase angle.

Figure 1 shows the brightness of the satellites in terms of phase angle from 20-30 measurements that more or less uniformly cover the phase angles between 0.3° and 11°. The curves approximate well a square-law function of the following type in the case of linear extrapolation of the measurements for the zero phase shown in Figure 1

$$m = m_0 + a\alpha + b\alpha^2$$

when constants a and b have the following values

Jupiter I (Io)	a = 0.046;	b = 0.001;
II (Europa)	0.0312;	0.00125;
III (Ganymede)	0.323;	0.00066;
I (Callisto)	0.090;	0.036.

Callisto's phase function is equated to the wing side of the satellite (the darker side near the opposition). For the leading side

$$m = m_0 + 0.112 + 0.060\alpha - 0.0019\alpha^2.$$

The curve for the lead side in Figure 1 is designated IV.

As will be seen from Figure 1, Callisto's lead side is distinguished by maximum increase in brightness toward the opposition. The brightness differential for the extreme values of α (upon extrapolation of the measurements for α = 0 according to Stebbins and Jacobsen) is $0^m.55$. A more careful consideration

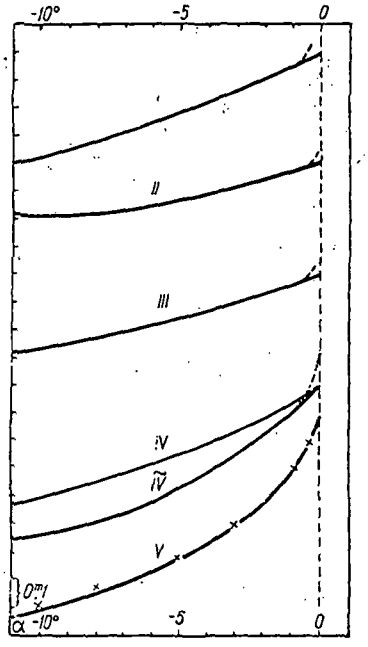

Figure 1. Phase-brightness relationship. I- Io, II- Europa, III- Ganymede, IV- lead and V- wing sides of Callisto. x- asteroid 20 Massalia. x-axis- phase angles; y-axis- brightness, in stellar magnitudes.

of the Stebbins and Jacobsen measurements shows a tendency toward a sharp rise in brightness for all four satellites between 1° and 0° (the broken lines in Figure 1). This effect is particularly well defined in the case of Callisto (lead side) where there are four measurements in the interval of phase angles noted.

So the greater probability is that the actual brightness differential for the satellites should exceed the value taken directly from the Stebbins and Jacobsen phase curves for phase angles between 0° and 11° (Figure 1, solid curves).

The magnitude of the effect of opposition between 1° and 0° can be evaluated for Callisto by using the results obtained by Stebbins and Jacobsen and the procedure detailed in reference [3].

This satellite's geometric albedo is comparatively low ($P(B) \approx 0.2$). We can, therefore, as in the case of the moon, disregard the effects of higher order scattering and make full use of the calculations given in reference [3]. We can, in particular, determine the parameter g, characterizing the relative density of Callisto's surface layer. To do so, let us use the data listed in Table 1 for the planet's phase-brightness relationship for different g values, according to reference [3]. By using the phase-brightness relationship for Callisto between 1° and 11° we obtain $g \simeq 0.2$ for the satellite's lead side (see Figure 1, IV). According to reference [3], $g = 0.25$ for the lunar surface layer (see Figure 1, V). The increase in Callisto's brightness (lead side) is $0^m.28$ between 0° and 1° for the g value found, and the brightness differential for the interval between 0° and 11° is about $0^m.75$.

This conclusion as to the structure of the surface layer on Callisto's lead side is valid only if this layer satisfies the Hapke model, of course [4].

T. Gehrels, in 1955, took photoelectric measurements of the phase-brightness relationship for the asteroid 20 Massalia [5]. Table 2 lists the color characteristics of this asteroid, and Figure 1 shows its phase function in the V system (crosses), which is virtually no different from the lunar phase function or that of Callisto's lead side. /51

TABLE 1. PHASE-BRIGHTNESS RELATIONSHIP FOR A PLANET NEAR OPPOSITION FOR DIFFERENT VALUES OF THE PARAMETER g

α	g					
	0.05	0.1	0.2	0.3	0.4	0.5
0°	0^m00	0^m00	0^m00	0^m00	0^m00	0^m00
1	0.62	0.47	0.28	0.18	0.14	0.11
2	0.68	0.58	0.41	0.30	0.23	0.17
3	0.71	0.63	0.49	0.38	0.30	0.24
4	0.72	0.66	0.54	0.40	0.35	0.29
5	0.73	0.68	0.57	0.48	0.40	0.34
10	0.76	0.74	0.67	0.61	0.59	0.48
15	0.80	0.78	0.73	0.68	0.63	0.58

TABLE 2. SOME CHARACTERISTICS OF PLANETARY SATELLITES

Planet and its satellite	Radius, km	Mean density, g/cm³	Absolute stellar magnitude (V)	$m_{sat} - m_\odot$					A_g (V)
				U	B	V	R	I	
Jupiter									
I - Io	1660	3.9	—1.90	1.70	0.54	0.00	—0.21	—0.24	0.92
II- Europa	1440	4.0	—1.53	0.62	0.24	0.00	—0.12	—0.14	0.83
III- Ganymede	2470	2.5	—2.16	0.56	0.20	0.00	—0.14	—0.16	0.49
IV- Callisto	2340	1.7	—1.20	0.64	0.23	0.00	—0.16	—0.19	0.26
Saturn									
Enceladus	300	0.6	2.22	—	0.01	0.00	—	—	0.54
Tethys	600	0.7	0.72	0.35	0.15	0.00	—	—	0.84
Dione	650	0.85	0.89	0.24	0.08	0.00	—0.03	—0.06	0.94
Rhea	900	0.75	0.21	0.34	0.13	0.00	—0.16	—0.13	0.82
Titan	2500	2.7	—1.16	1.28	0.67	0.00	—0.43	—0.25	0.21
Hyperion	200	3.3	4.61	0.34	0.06	0.00	—	—	—
Iapetus	600	5.5	1.48	0.49	0.08	0.00	—	—	—
Uranus									
Titania	500	—	1.30	0.10	—0.01	0.00	—0.07	—0.19	—
Oberon	400	—	1.49	0.12	0.02	0.00	—0.04	—0.08	—
Neptune									
Triton	2000	4.6	—1.16	0.40	0.14	0.00	—0.13	—0.28	0.36
Nereid	150	3.6	4.00	—	0.17	0.00	—	—	—
Luna	1738	3.34	0.21	0.61	0.29	0.00	—0.35	—0.52	0.11
20	—	—	6.77	0.47	0.19	0.00	—	—	—

The wing side of Callisto is less porous, so the effect of opposition is not as sharply defined. We obtain g = 0.6 directly from curve IV in Figure 1, and by using Table 1. If it is taken that the albedo of the satellite's surface on the wing side is approximately 10 percent less than on the lead side, g = 0.5, roughly, for the wing side, and this is approximately the porosity of the "average Mars" [6].

The high albedo of the first three Galilean satellites is such that it is /52
not as simple to determine g (as in the manner of the foregoing) and this is so because higher order scatterings must be included. But given the same surface layer porosity, there should be a decrease in the magnitude of the observed effect of opposition with increase in surface albedo [7]. If, for example, we take the case of the very high albedo of Io (the geometric albedo in the B system is about 0.6) we find that the satellite's phase curve still shows a brightness differential of about $0^m.4$ between 0° and 11°, and this means its surface porosity also is quite high. This is true to the same degree for the satellites Europa and Ganymede. Overall, this result is in good concordance with Ganymede's low thermal inertia, found by measuring the thermal radiation when the satellite enters Jupiter's shadow [8].

The conclusion as to the high degree of porosity of the surface layers of the Galilean satellites of Jupiter must be considered when analyzing spectrophotometric observations in order to study the nature of the upper covers of satellites.

Albedo and Spectral Energy Distribution for Satellites

Today we put the relationship between the albedo of the Galilean satellites of Jupiter and the wavelength at 0.35-2.5 microns. Photoelectric measurements with light filters [9] are quire reliable in the 0.35-0.82 region. Spectrophotometric data in the visible [10] and IR regions [11] of the spectrum are fragmentary and are in need of refinement. The geometric albedo of the first two satellites in the red region of the spectrum is puzzlingly high (Table 2).

The geometric albedo, p, the apparent albedo in the center of the full disk, ρ, and the smoothness factor for the surface, q, for a planet devoid of atmosphere are linked by the relationship [12]

$$p = \frac{2}{q+2}\rho.$$

Customarily $\rho > p$, but $q \simeq 0$ and $\rho \simeq p$ for Callisto, at least in the short-wavelength region of the spectrum (where the satellite's geometric albedo is approximately that of the Moon's). q increases with increase in the albedo [7, 13], so the differential in the apparent albedo between 0.35 and 0.82 microns should be even greater than that in Table 2 for the geometric albedo differential, and this would apply to all the Galilean satellites, particularly Io.

Attention is drawn to the fact that the high value of the satellite's albedo corresponds to its high mean density (Table 2). The conclusion that suggests itself is that the diameters of Io and Europa are greatly in error as determined (understated) and this is particularly so if it is considered that the angular diameters of these satellites are comparatively small and they are closer to Jupiter than are Ganymede and Callisto, making precise micrometric measurements against Jupiter's background difficult.

Camichel [14] and Dollfus [15] have obtained Io and Europa diameters that are somewhat larger than those accepted earlier, but the corresponding corrections do not change the main point; the albedoes of Io and Europa still are very high.

A high albedo has been determined for Saturn's satellites Tethys, Dione, and Rhea, but these data cannot be trusted because the diameters of these distant satellites cannot be measured directly from the earth. Perhaps the only reliable photometric characteristics of all planetary satellites, with the exception of the moon and the Galilean satellites of Jupiter, are their brightness and spectral energy distribution. /53

V. I. Moroz [16] measured the IR spectrum of the Galilean satellites of Jupiter at 0.7-2.5 microns and has suggested that at the very least much of the surface of Europa and Ganymede can be covered by ice. However, according to reference [17], ice has an inverse albedo behavior with respect to the spectrum as compared to that found by observation. If one attempts to explain the comparatively small drop in energy toward the violet end of the spectrum for Europa by the presence of hoarfrost through which the satellite's own surface is translucent, there is still no way to explain the data for Io. The question of the presence of an atmosphere for the Galilean satellites still is an open one.

The 2-meter reflector at the Shemakha Astrophysical Observatory was used during 1968-1969 by Yu. D. Davudov to obtain some 60 spectrograms of the Galilean satellites of Jupiter and of Titan in the 0.40-0.65 micron band. The observations were made in the Cassegrain focus using a diffraction spectrograph (dispersions 30 and 75 Å/mm). The comparison stars were selected from the Kharitonov catalog [18], and G. F. Sitnik's data [19] were used to effect the photometric tie between the satellite spectrograms and the sun. Mean curves of spectral energy distribution in the spectra of Io (16 spectrograms), Europa (9), Ganymede (7), Callisto (7), and Titan (17), are shown in Figure 2. They are in satisfactory agreement with data by other authors if consideration is given to the fact that the color index for the satellites undergoes change with phase rotation.

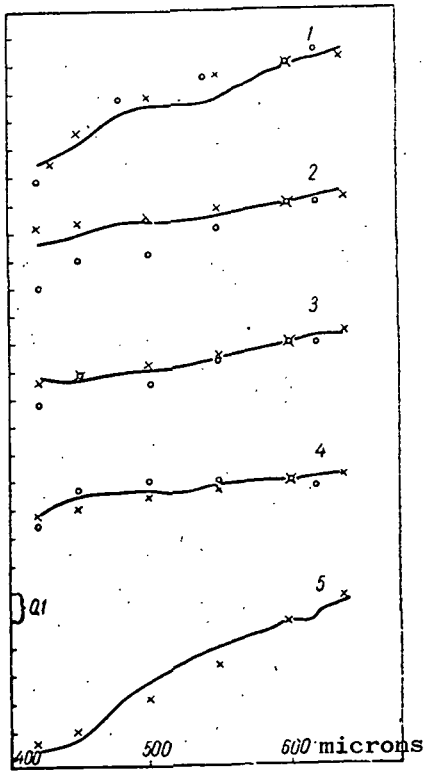

Figure 2. Relative spectral energy distribution. 1- Io; 2- Europa; 3- Ganymede; 4- Callisto; 5- Titan. x- Harris' measurements; o- Priboyeva's measurements; y-axis- logarithms of intensity.

The satellite spectrograms were compared with the lunar spectrum in the region of the 6190 Å CH_4 band. This band is well separated in the Titan spectrum. Its equivalent width is about 20 Å [20]. Careful measurements of the spectrograms for Jupiter's satellites showed no traces of the 6190 Å CH_4 band noted earlier by other observers. We can add to this the fact that the spectral behavior of the Io albedo is, in general, quite difficult to explain by the influence of the atmosphere. If one assumes the satellite to have a neutral surface with a high albedo in this region of the spectrum, it would be necessary to have an atmosphere with a quite complex optical modulus in order to have satisfactory observations. This atmosphere would have to have a relatively great optical thickness and significant true absorption over the whole of the 0.35-0.82 micron band, and this is hard to square with the high albedo of the satellite in the red rays.

Io's color changes greatly with phase rotation, reaching a value of about $0^m.65$ in the U-V ($\simeq 0^m.2$ in B-V and $\simeq 0^m.45$ in U-B). This means that the magnitude of the longitudinal effect on Io's brightness increases from V to U. In other words, the contrast between the dark formations on the satellite's surface and their surroundings increases toward the violet end of the spectrum. So far as /54 the other three Galilean satellites are concerned, the contrast in details in the U, B, and V is almost the same [9]. This effect, which can be observed for Io, could be imparted by an atmosphere in which the true absorption dominates the scattering, and the optical thickness increases toward the violet end of the spectrum. Then it would have to be assumed that there are areas of relief with reduced levels in the longitude region near 300° (corresponding to the minimum brightness of Io near opposition). But the lack of observed atmospheric criteria for Io detracts from the validity of this hypothesis.

Evidently the entire surface is primarily responsible for the observed behavior of spectral values for Io, and this would apply to the overwhelming majority of other planetary satellites as well, although neither asteroids nor meteorites have albedo spectral values similar to those for this satellite [17]. On the other hand, there still is not sufficient grounds for the final rejection of the atmosphere hypothesis. In any case, the comparatively small mass of the Galilean satellites, and the absence in their spectra of CH_4 molecular bands, still is not the deciding argument in favor of this rejection.

REFERENCES

1. Stebbins, J., Lick Obs. Bull., 1927, p. 385.
2. Stebbins, J., Jacobsen, T. S., Lick Obs. Bull., 1928, p. 401.
3. Morozhenko, A. V., Yanovitskiy, E. G., Astron. zhurn., 47, 1970.
4. Hapke, B. W., J. Geophys. Res., 68, 1963, p. 4571.
5. Gehrels, T., Ap. J., 123, 1956, p. 2.
6. Morozhenko, A. V., Yanovitskiy, E. G., Astron. zhurn., 48, 1971.
7. Bugayenko, O. I. et al., Article in this collection.
8. Murray, B. C., Westphal, J. A., Wildey, R. L., Ap. J., 141, 1965, p. 1590.
9. Harris, D., Planets and Satellites, Chapter 8, editors D. Kuiper, B. Middlehurst, Foreign Literature Press, 1963.

10. Priboyeva, N. B., Trudy AI AN Kaz. SSR, IX, 1967.

11. Moroz, V. I., Astron. zhurn., 42, 1965, p. 1287.

12. Koval', I. K., Doctoral Dissertation, Kiev, 1968.

13. Akimov, L. A., Barabashov, N. P., ATs AN SSSR, 1969, p. 540.

14. Camichel, H., Ann. d'Astrophys., 16, 1953, p. 41.

15. Dollfus, A., C. R., 238, 1954, p. 1475.

16. Moroz, V. I., Fizika planet [Physics of Planets], "Nauka" Press, Moscow, 1967, p. 475.

17. Krinov, Ye. L., Astron. zhurn., 17, 1940, p. 4.

18. Kharitonov, A. V., Astron. zhurn., 40, 1963, p. 2.

19. Sitnik, G. F., ATs AN SSSR, 1964, p. 292.

20. Davudov, Yu. D., ATs AN SSSR, 1970, p. 563.

GLOW FROM THE LIMB SIDE OF A SPHERICAL PLANETARY ATMOSPHERE

E. G. Yanovitskiy

ABSTRACT: An approximate formula is derived for calculating the diffuse radiation from the limb side of a spherical planetary atmosphere. The case of an atmosphere adjoining a surface that reflects light istropically is considered. For the case of very small optical thickness of the atmosphere a simple analytical expression is found for computation of diffuse radiation intensity in the assumption that scattering coefficient of the aerosol and gas atmospheric components changes exponentially with altitude. This formula is used for calculation of the limbside radiation intensity of the Martian atmosphere (Figures 2-4).

The glow of the layer of atmosphere directly beyond the limb of a planet's natural surface can be observed when investigating planets from deep space at sufficient close range on the limb side. We understand the planet's natural surface to mean its hard surface (Mars, Earth when there are no clouds) or its cloud cover (Venus, Earth, Jupiter). In many cases it is necessary to take into consideration the distribution of brightness along the above-indicated layer, assigning optical parameters to the atmosphere and to the planetary surface. Then, by comparing the observed distribution of the brightness with the calculated we can determine, for example, the significance of a characteristic such as the change in the concentration of aerosol with altitude for atmospheric optics, for this, in the final analysis, will enable us to build an optical model of the atmosphere. /55

We cannot assume the atmosphere to be plane-parallel when estimating the distribution of brightness along a planet's atmospheric layers, but should take its sphericity into consideration. This is connected with the fact that in the case cited the radiation comes to the observer from a layer of atmosphere, the extent of which is comparable to the radius of the planet. The equation for the transfer of radiation in a spherical atmosphere is described in reference [1]. I. N. Minin and V. V. Sobolev [2] derived the equation for the source function, $B(r, \psi)$ and (r and ψ are the spherical coordinates of the point), for a symmetrical spherical planetary atmosphere illuminated by parallel rays for the case of isotropic scattering[4]. Considered in this same source is the case

4. The problem reviewed is axisymmetrical because the axis is a straight line joining the centers of the planet and the sun.

when the atmosphere is contiguous to an isotropically reflecting surface with specified albedo, A. These same authors, in their articles [3-5], used the approximation method to reduce the problem of diffuse reflection and light transmission by a symmetrical spherical planetary surface to a second order partial differential equation for the corresponding boundary conditions. Numerical calculations for selected special cases were made by way of examples.

Following V. V. Sobolev and I. N. Minin was O. I. Smoktiy [6, 7], who derived an approximate analytical solution of the problem of multiple scattering of light in a spherical atmosphere thus making possible effective numerical calculations, and calculated the intensity of the outgoing radiation for different models of the vertical structure of a symmetrical spherical atmosphere.

The calculation for brightness distribution along the planet's limb side atmospheric layers can be made using the methods in references [3-7]. They are, however, rather complicated when repeated light scattering must be taken into consideration. This paper presents a very simple approximation method for calculating this distribution when the line of sight does not intersect the plane of the terminator. And it is assumed that the atmosphere is contiguous to a surface that is reflecting isotropically. A calculation is made of the brightness distribution along the Martian atmosphere layers as observed directly beyond the limb of its natural surface, for illustrative purposes.

Accordingly, let a spherical, symmetrical atmosphere, the radius of the upper boundary of which is equal to R_A, be illuminated by parallel rays from the Sun. Let us designate the illumination of a unit area at the upper boundary of the atmosphere perpendicular to the incident beams by πS. Let the observer be found at point K (Figure 1). Let us take the current point, T, to be on the line of sight, KB, the radius vector of which is equal to r. The position of the point T on the line of sight can be determined by the segment BT = s, read from point B. Then the intensity of the diffuse radiation, I, reaching the observer from the column of atmosphere located along the line of sight, AB, can be determined from

/56

$$I(s_0) = \int_0^{s_0} B(s) \exp\left[\int_{s_v}^{s} \alpha(z)\, ds\right] \alpha(z)\, ds, \qquad (1)$$

where

B(s) is the source function at point T;

s_0 = AB,

$\alpha(z)$ is the absorption factor;

z is the altitude of point T above the planetary surface (r = R + z).

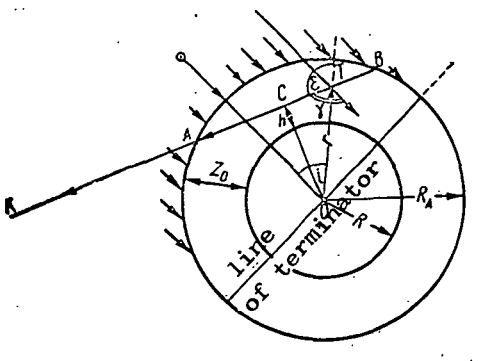

Figure 1.

The thickness of the planetary atmosphere, z_0, is very much less than the planet's radius, R, so we can say that the atmospheric layers are plane-parallel. But we can take it that the quantity of radiant energy from the Sun, and absorbed by an elementary volume of atmosphere, remains as for a spherical atmosphere. In other words, we are considering the change in illumination of the atmosphere along the line of sight, AB. Reference [2] already has used the approximation method described. Now we shall use it to write, in explicit form, an expression for the source function B(s). It is obvious that the above approximation is better justified the smaller z_0/R, and that significant disagreement is to be expected only near the terminator. We shall, therefore, limit ourselves in what follows to the case when the line of sight does not intersect the plane of the terminator within the limits of the atmosphere.

Let us designate the angle between the radius vector r for point T and the direction to the Sun by i = arc cos ζ, and the angle between r and the direction to the observer at point T by ε = arc cos η (Figure 1). Then let us assume that the atmosphere of the planet is purely scattering (that is, it has a single scattering albedo, λ = 1), and is contiguous to a surface with given albedo A that reflects isotropically. Then, if the atmosphere is homogeneous, the approximate expression for source function B in the plane of the atmosphere, given the arbitrary (but not too elongated) scattering indicatrix $\chi(\gamma)$ obtained by V. V. Sobolev (see reference [8], Chapter 10), can be used.

But atmospheric heterogeneity has a significant effect on brightness distribution along atmospheric layers. In this case, the heterogeneity of the

atmosphere for first order scattering can be determined by the scattering indicatrix, $\chi(\gamma)$, in terms of altitude, z (or of optical depth, τ). So far as the component $\Delta B(\tau, \eta, \zeta)$ of the source function, determined by higher order scatterings, is concerned, in this case, as follows from the results of the generalization of the approximate formula from [8] by S. D. Gutshabash [9] we have

$$\Delta B(\tau, \eta, \zeta) = \bar{I}(\tau) + x_1(\tau)\bar{H}(\tau)\eta, \tag{2}$$

where

$$\bar{I}(\tau) = \frac{S\zeta}{2}\left(1+\frac{3}{2}\zeta\right) - \frac{3}{4}S\zeta^2 e^{-\tau/\zeta} - F\left[2+\left(3-\frac{1}{\tau}\int_0^\tau x_1(t)\,dt\right)\tau\right], \tag{3}$$

$$F = \frac{S}{2}\frac{(1-A)R(\zeta,\tau_0)\zeta}{4+\left(3-\frac{1}{\tau_0}\int_0^{\tau_0} x_1(t)\,dt\right)(1-A)\tau_0}, \tag{4}$$

$$x_1(\tau) = \frac{3}{2}\int_0^\pi \chi(\gamma,\tau)\cos\gamma\sin\gamma\,d\gamma, \tag{5}$$

$$\bar{H}(\tau) = F - \frac{S}{4}e^{-\tau/\zeta}\zeta, \tag{6}$$

$$R(\zeta,\tau_0) = 1+\frac{3}{2}\zeta+\left(1-\frac{3}{2}\zeta\right)e^{-\tau_0/\zeta}, \tag{7}$$

and the optical depth is

$$\tau(r) = \int_r^{R_A} \alpha(r)\,dr. \tag{8}$$

Just as in the case of a heterogeneous, purely scattering, atmosphere we have

$$B(\tau,\eta,\zeta,\gamma) = \Delta B(\tau,\eta,\zeta) + \frac{S}{4}\chi(\gamma,r)e^{-\tau/\zeta}. \tag{9}$$

where the function $\Delta B(\tau, \eta, \zeta)$ is found from Eq. (2).

So, converting to a suitable system of coordinates, and substituting Eq.(9) into Eq.(1), we obtain the unknown expression for the intensity of radiation determining the glow of the atmospheric layers on the limb side of the planet.

Let us suppose, for the sake of simplicity, that the line of sight, KB (Figure 1), lies in the plane of the planet's intensity equator. Now the position

of this line with respect to the centers of planet and Sun will be determined by h and the scattering angle γ. Here h is the distance between the line of sight and the planet's surface. And for the current point T on the line of sight

$$s = \sqrt{R_A^2 - r_0^2} \mp \sqrt{r^2 - r_0^2}, \tag{10}$$

where $r_0 = R + h$. The sign is minus for the section BC, and plus for the section AC, of the line of sight. Then

$$ds = \mp \frac{rdr}{\sqrt{r^2 - r_0^2}}. \tag{11}$$

Readily found from Figure 1 are

$$\eta_{1,2} = \cos\varepsilon = \mp \frac{\sqrt{r^2 - r_0^2}}{r}, \tag{12}$$

$$\zeta_{1,2} = \cos i = \frac{r_0}{r}\sin\gamma \pm \frac{\sqrt{r^2 - r_0^2}}{r}\cos\gamma, \tag{13}$$

in which the subscripts 1 and 2 refer to the upper and lower signs in Eqs. (12) and (13), respectively. Substituting Eqs.(10) and (11) into Eq. (1), we obtain

/58

$$I(h, \gamma) = \exp[-\beta(R_A)] \int_{r_0}^{R_A} \{B(\tau(r), \eta_1, \zeta_1)\exp[-\beta(r)] + \tag{14}$$

$$+B(\tau(r), \eta_2, \zeta_2)\exp[\beta(r)]\} \cdot \frac{d\beta(r)}{dr} dr,$$

where

$$\beta(r) = \int_{r_0}^{r} \alpha(r) \frac{rdr}{\sqrt{r^2 - r_0^2}}. \tag{15}$$

Eq. (14) is applicable only when the line of sight does not intersect the terminator. This condition is satisfied when angle $i \leq 90°$. With this in mind, and using Eq. (13), we find that interval of change in the scattering angle, γ, for which the line of sight does not intersect the terminator as

$$\arccos\frac{R}{R_A} \leqslant \gamma \leqslant \pi - \arccos\frac{R}{R_A}. \tag{16}$$

It should be noted that in practice inequality (16) can be strengthened such that the intersection of line of sight and terminator will take place only in the uppermost layers of the atmosphere where, for all practical purposes, solar

radiation is not reradiated.

Finally, let us consider the case of an optically shallow atmosphere, ($\tau_0 \ll 1$), contiguous to a surface with low albedo ($A \ll 1$). Then we are correct in considering only first order scattering; that is, we can take the following expression for the source function

$$B(\tau, \eta, \zeta; \gamma) = \frac{S}{4} \chi(\gamma, r) e^{-\tau/\zeta}. \tag{17}$$

Substituting Eq. (17) into Eq. (14), and considering Eq. (13), after transformations, we obtain

$$I(h, \gamma) = \frac{S}{2} \exp[-\beta(R_A)] \int_{r_0}^{R_A} \chi(\gamma, r) \operatorname{ch}\left[\beta(r) + \right. \\ \left. + \frac{r\tau(r)\sqrt{r^2 - r_0^2 \cos\gamma}}{r_0^2 - r^2 \cos^2\gamma}\right] \exp\left[-\frac{rr_0\tau(r)\sin\gamma}{r_0^2 - r^2\cos^2\gamma}\right] \frac{d\beta(r)}{dr} dr. \tag{18}$$

This latter formula quite obviously is applicable to the Martian atmosphere (the visible region of the spectrum) as well as to a cloudless terrestrial atmosphere (in the long-wavelength region of the visible spectrum).

Let us now move on to the calculation of the brightness distribution along the limb side Martian atmospheric layers. Measurement of brightness distribution along atmospheric layers can yield valuable information on the vertical structure of the planet's atmosphere. In the case of Mars, Yung [10] attempted to use Mariner 4 observations to construct the brightness distribution along the atmospheric aureole. However, the sensitivity of the equipment carried by this space station was such that distribution for sufficiently large h of the line of sight above the planetary surface could not be obtained. Hence it is desirable to have rough a priori estimates of brightness distribution, for these will enable us to establish, in advance, the sensitivity of the equipment designed /59 for such measurements.

It should be pointed out that we cannot, at this point, use Eq. (18) to arrive at sufficiently accurate calculations. The fact is that the distribution of aerosol particles with altitude in the Martian atmosphere is a practically unknown quantity, so that change in the scattering indicatrix and in the aerosol component, τ_a of the optical depth τ, is unknown. We have, therefore, made a number of simplifications, and more or less plausible assumptions, in order to arrive at very rough estimates.

A. V. Morozhenko has calculated [11] the total optical thickness of the Martian atmosphere to be $\tau_0 < 0.05$ for the spectral interval $\lambda \geq 0.4\mu$. This can result in the simplification of Eq. (18). Let us assume, for purposes of definiteness, that the geometric thickness of the Martian atmosphere is $z_0 = 100$ km. If we say that R = 3400 km, then $R_A = 3500$ km. Let us make the calculation for angles $30° \leq \gamma \leq 150°$. Then, from Eq. (13), $0.27 < \zeta \leq 1$, and since $\tau_0 < 0.05$, we can use the following expression instead of Eq. (17) to make the approximate calculation for brightness distribution

$$B(\tau, \eta, \zeta, \gamma) = \frac{S}{4}\chi(\gamma, r). \tag{19}$$

And instead of Eq. (18), we have

$$I(h, \gamma) = \frac{S}{2}\exp[-\beta(R_A)]\int_{r_0}^{R_A}\chi(\gamma, r)\operatorname{ch}[\beta(r)]\frac{d\beta(r)}{dr}dr. \tag{20}$$

As usual (see [6], for example) we assume

$$\chi(\gamma, r) = \frac{\alpha_R(r)}{\alpha(r)}\chi_R(\gamma) + \frac{\alpha_a(r)}{\alpha(r)}\chi_a(\gamma), \tag{21}$$

where

$$\chi_R(\gamma) = \frac{3}{4}(1 + \cos^2\gamma) - \tag{22}$$

is the Rayleigh scattering indicatrix, $\chi_a(\gamma)$ is the aerosol scattering indicatrix

$$\alpha(r) = \alpha_a(r) + \alpha_R(r), \tag{23}$$

and $\alpha_R(r)$ is the Rayleigh scattering factor, $\alpha_a(r)$ is the scattering factor for the aerosol particles. In accordance with Eq. (23), the total optical thickness, τ_0, of the atmosphere can be given in the form

$$\tau_0 = \tau_{0R} + \tau_{0a}. \tag{24}$$

Let us take it that in the atmosphere the aerosol, α_a, and Rayleigh, α_R, scattering factors change exponentially. Let us put (when $z_0 \gg H$ and $z_0 \gg H_a$)

$$\alpha_a(r) = \frac{\tau_{0a}}{H_a}\exp\left(-\frac{r-R}{H_a}\right), \tag{25}$$

$$\alpha_R(r) = \frac{\tau_{0R}}{H}\exp\left(-\frac{r-R}{H}\right), \tag{26}$$

where H and H_a are the altitudes of the homogeneous gas and aerosol components of the atmosphere, respectively.

Substituting Eq. (21) into Eq. (20), and giving consideration to Eqs. (15) and (23) instead of Eq. (20) we find /60

$$I(h,\gamma)=\frac{S}{2}\exp[-\beta(R_A)]\left\{\chi_R(\gamma)\,\mathrm{sh}[\beta(R_A)]+\right.$$
$$\left.+[\chi_a(\gamma)-\chi_R(\gamma)]\int_{r_0}^{R_A}\mathrm{ch}[\beta(r)]\frac{\alpha_a(r)\,rdr}{\sqrt{r^2-r_0^2}}\right\}. \tag{27}$$

Considering Eq. (15), and the fact that ordinarily $H \gg H_a$, and $\tau_{0a} \gg \tau_{0R}$, the integral in the brackets in Eq. (27) can be given in the following approximate form

$$\int_{r_0}^{R_A}\mathrm{ch}[\beta(r)]\frac{\alpha_a(r)\,dr}{\sqrt{r^2-r_0^2}}\approx\int_{r_0}^{R_A}\mathrm{ch}\left[\int_{r_0}^{r}\alpha_a(r')\frac{r'\,dr'}{\sqrt{r'^2-r_0^2}}\right]\times$$
$$\times\frac{\alpha_a(r)\,rdr}{\sqrt{r^2-r_0^2}}=\mathrm{sh}\left[\int_{r_0}^{R_A}\frac{\alpha_a(r)\,rdr}{\sqrt{r^2-r_0^2}}\right]. \tag{28}$$

Using Eq. (26), we can write

$$\int_{r_0}^{R_A}\frac{\alpha_a(r)\,rdr}{\sqrt{r^2-r_0^2}}=\frac{\tau_{0a}}{H_a}e^{\frac{R}{H_a}}\left[r_0K_1\left(\frac{r_0}{H_a}\right)-\int_{R_A}^{\infty}\frac{e^{-\frac{r}{H_a}}rdr}{\sqrt{r^2-r_0^2}}\right], \tag{29}$$

where $K_1(z)$ is a cylindrical first order function of the imaginary argument.

It is obvious that for those r_0 values for which the magnitude

$$\frac{e^{-\frac{R_A-R}{H_a}}}{\sqrt{R_A^2-r_0^2}}\ll 1, \tag{30}$$

we can ignore the second summand in the right-hand side of Eq. (29) as compared to the first. If, moreover, it is considered that for $z \gg 1$ (see [12], p. 977)

$$K_1(z)\sim\sqrt{\frac{\pi}{2z}}e^{-z}\left[1+O\left(\frac{1}{z}\right)\right], \tag{31}$$

instead of Eq. (29), we obtain

$$y=\int_{r_0}^{R_A}\frac{\alpha_a(r)\,rdr}{\sqrt{r^2-r_0^2}}=\tau_{0a}\sqrt{\frac{\pi r_0}{2H_a}}e^{-\frac{h}{H_a}}. \tag{32}$$

as well as

$$x=\int_{r_0}^{R_A}\frac{\alpha_R(r)\,rdr}{\sqrt{r^2-r_0^2}}=\tau_{0R}\sqrt{\frac{\pi r_0}{2H}}e^{-\frac{h}{H}}. \tag{33}$$

Now we can estimate the relative error, $\Delta(h)$, in Eq. (28), providing the Eq. (30) condition is satisfied. Considering Eqs. (15) and (23), we find the following from Eq. (28), with the help of Eqs. (32) and (33)

$$\left\{\int_{r_0}^{R_A} \operatorname{ch}\left[\int_{r_0}^{r} \alpha_a(r')\frac{r'\,dr'}{\sqrt{r'^2-r_0^2}}+\int_{r_0}^{r}\alpha_R(r')\frac{r'\,dr'}{\sqrt{r'^2-r_0^2}}\right]\frac{\alpha_a(r)\,rdr}{\sqrt{r^2-r_0^2}}-\right.$$
$$-\operatorname{sh}\left[\int_{r_0}^{R_A}\frac{\alpha_a(r)\,rdr}{\sqrt{r^2-r_0^2}}\right]\Bigg\}\leqslant\left\{\int_{r_0}^{R_A}\operatorname{ch}\left[\int_{r_0}^{r}\alpha_a(r')\frac{r'\,dr'}{\sqrt{r'-r_0^2}}+\right.\right.$$
$$\left.\left.+\int_{r_0}^{\infty}\alpha_R(r)\frac{rdr}{\sqrt{r^2-r_0^2}}\right]\frac{\alpha_a(r)\,rdr}{\sqrt{r^2-r_0^2}}-\operatorname{sh} y\right\}=\operatorname{sh}(x+y)-\operatorname{sh} x-\operatorname{sh} y, \tag{34}$$

from whence, after uncomplicated transformations, we obtain

$$\Delta(h)\leqslant\frac{2\operatorname{sh}\frac{x}{2}\operatorname{sh}\frac{x+y}{2}}{\operatorname{sh}\frac{y}{2}}. \tag{35}$$

Thus, by using Eqs. (28), (32), and (33) in place of Eq. (27) we obtain the following approximate formula for calculating the intensity of emergent radiation (for an atmosphere with a very small optical thickness)

$$I(h,\gamma)=\frac{S}{2}\exp\left[-\sqrt{\frac{\pi r_0}{2}}\left(\frac{\tau_{0R}}{\sqrt{H}}e^{-\frac{h}{H}}+\frac{\tau_{0a}}{\sqrt{H_a}}e^{-\frac{h}{H_a}}\right)\right]\times$$
$$\times\left\{\chi_R(\gamma)\operatorname{sh}\left[\sqrt{\frac{\pi r_0}{2}}\left(\frac{\tau_{0R}}{\sqrt{H}}e^{-\frac{h}{H}}+\frac{\tau_{0a}}{\sqrt{H_a}}e^{-\frac{h}{H_a}}\right)\right]+\right. \tag{36}$$
$$\left.+[\chi_a(\gamma)-\chi_R(\gamma)]\operatorname{sh}\left(\tau_{0a}\sqrt{\frac{\pi r_0}{2H_a}}e^{-\frac{h}{H_a}}\right)\right\}.$$

The numerical values for $\chi_a(\gamma)$, τ_{0a} and τ_{0R} used for the calculations involving Eq. (36) were taken from A. V. Morozhenko [11]. These data are listed in the table. Further, as per [10], H = 12, H_a = 3 km. Eq. (36) calculations were made for S = 1, and the results are shown in Figures 2-4. We should note that $\Delta(h) < 16$ percent for the numerical values of the optical parameters used [see inequality (35)].

NUMERICAL VALUES OF $\chi_a(\gamma)$, τ_{0a}, and τ_{0R}

γ	$\tilde{\lambda}_\mu$		
	0.4	0.5	0.6
	$\chi_a(\gamma)$	$\chi_a(\gamma)$	$\chi_a(\gamma)$
30°	3.30	3.27	3.24
45	1.89	1.88	1.87
60	1.06	1.06	1.06
90	0.435	0.437	0.440
120	0.321	0.327	0.333
150°	0.385	0.394	0.403
τ_{0R}	0.0100	0.0041	0.0019
τ_{0a}	0.039	0.026	0.019

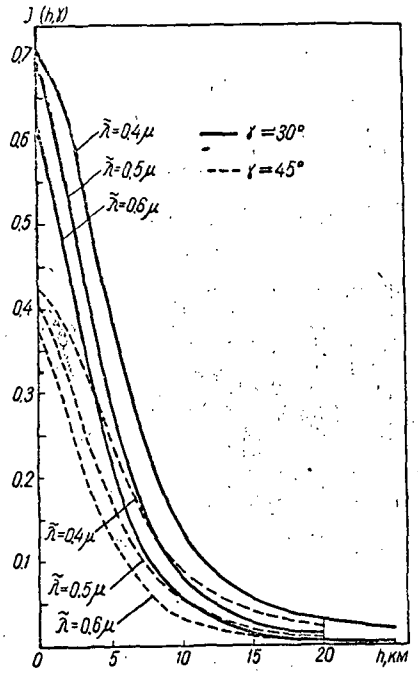

Figure 2.

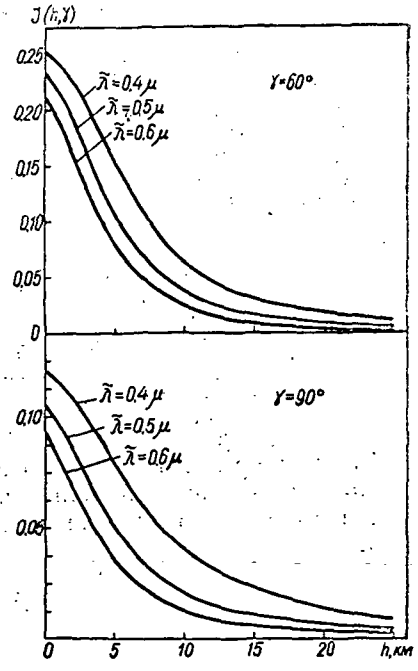

Figure 3.

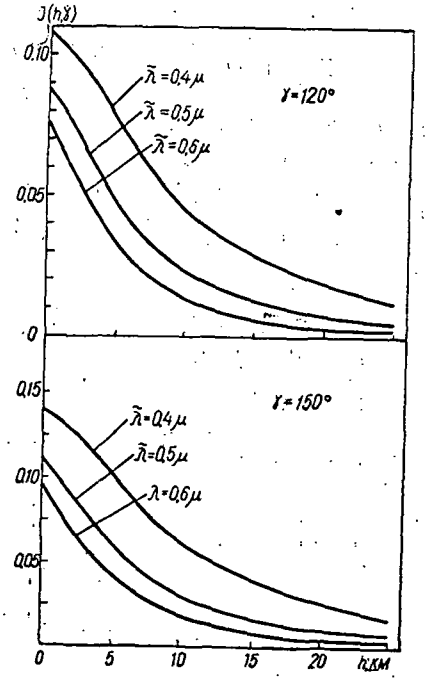

Figure 4.

As will be seen from Figures 2-4, the layers of the atmosphere at the Martian surface with the brightest glow are some 10 km thick. Moreover, as should have been expected, the brightness of the atmospheric layers at a specified altitude, h, is greater the smaller the angle of scatter, γ, all other conditions being equal. This latter evidently is associated with the extensive elongation of the aerosol scattering indicatrix.

In the future, as our concepts of the vertical structure of the Martian atmosphere are refined, it will make sense to repeat the calculations using the more precise Eq. (14). In the meantime, we obviously will have to limit ourselves to the results shown in Figures 2-4 in order to obtain rough estimates.

REFERENCES /63

1. Lenoble, J., Sekera, Z., Pros. Nat. Acad. Sci., USA, 47, 1961, p. 372.

2. Minin, I. N., Sobolev, V. V., Astron. zhur., 40, 1963, p. 496.

3. Sobolev, V. V., Minin, I. N., Iskusstvennyye sputniki Zemli, 14, 1962, p. 7.

4. Minin, I. N., Sobolev, V. V., Kosmicheskiye issledovaniya, 1, 2, 1963, p. 227.

5. Minin, I. N., Sobolev, V. V., Kosmicheskiye issledovaniya, 2, 4, 1964, p. 610.

6. Smoktiy, O. I., Fizika atmosfery i okeana, 1967, 3, 3, p. 245; 4, 383; 5, 496; 1969, 5, 1, 46; 8, 782.

7. Smoktiy, O. I., Vestnik LGU, 1969, p. 10.

8. Sobolev, V. V., Perenos luchistoy energii v atmosferakh zvezd i planet [Radiant Energy Transfer in the Atmospheres of Stars and Planets], Chapter 10, GITTL, Moscow, 1956.

9. Gutshabash, S. D., Uch. zapiski LGU, ser. mat. nauk, No. 153, 1952, p. 25.

10. Yung, A. T., Icarus, 11, 1969, p. 1.

11. Morozhenko, A. V., Astron. zhur., 46, 5, 1969, p. 1087.

12. Gradshteyn I. S., Ryzhik, I. M., Tablitsy integralov, summ, ryadov i proizvedeniy [Tables of Integrals, Sums, Series, and Products], GIFML, Moscow, 1962.

THE POSSIBILITY OF AUTOMATICALLY OBTAINING STATISTICAL MORPHOLOGICAL CHARACTERISTICS OF SECTIONS OF THE LUNAR SURFACE FROM THEIR PHOTOGRAPHIC IMAGES

L. A. Akimov, Yu. V. Korniyenko

ABSTRACT. The problem is formulated mathematically, micro- and macrorelief are determined, possibility is discussed of reproducing relief of a region from its photographic image and obtaining statistical morphological characteristics from this relief. Practical ways of realizing this possibility are analyzed. A possibility is shown of obtaining some statistical morphological characteristics of a region by analogy methods without reproducing its relief using coherent light beam technique or correlation methods. Though a theoretical study of the problems is carried out for the Moon, these results with few exceptions are applicable to other planets, such as the Earth, Mars, Mercury as well.

1. Statement of the Problem

The problem of how to determine the morphological characteristics of sections of the lunar surface will not become completely scientific in nature until it is formulated in qualitative concepts that are strictly mathematical in nature. /63

The first step in solving this problem therefore, is the introduction of the mathematical magnitudes that will be used to describe the surface under investigation, and which must be determined from experimental data.

The question of an adequate description of random surfaces similar to the lunar surface is an extremely complex one (although there are no particular difficulties involved in the case of an agitated sea surface, for example), and this paper will make no attempt to respond to it in full. Instead, a simpler approach is selected, even though not the ideal one, at least from the standpoint of complete correspondence with the real object. It is assumed that a section of the lunar surface can be described by the equation

$$H = \varrho(x, y),$$

where H is the altitude, read from some mean, adequately smooth surface determining the figure of the Moon. This surface can be considered to be a /64

plane within the limits of the section under consideration, and x and y are Cartesian coordinates on this plane. The function $\rho(x, y)$ is a discontinuous function, with the measure of the set of points of the discontinuity equal to zero and integrated over any finite region.

This description is too detailed for practical purposes, so it is convenient to represent $\rho(x,y)$ in the form of the sum of two factors

$$\rho(x, y) = R(x, y) + r(x, y)$$

where $R(x, y)$ characterizes the averaged appearance of the surface, and is obtained by smoothing the function $\rho(x, y)$

$$R(x, y) = \int \rho(x', y')\, g(x - x', y - y')dx'dy'$$

for the entire

section

$g(\xi, \eta)$ is a function significantly different from zero only in the region with characteristic size t such that the value of the function $R(x, y)$ at some point is the result of averaging the function $\rho(x, y)$ for the vicinity of this point with characteristic size t.

Thus, the true relief, $\rho(x, y)$, is broken down into the macrorelief $R(x, y)$ and the microrelief $r(x, y)$ so as to characterize the microrelief by mathematical characteristics, retaining the detailed description for the macrorelief only, or so as to introduce suitable statistical characteristics for the macrorelief as well.

If judicious limitations are imposed on the smoothing function, $g(x, y)$, the appearance of the macrorelief at a scale well in excess of t, and the appearance of the microrelief at a scale well below t, will not depend on the concrete form of $g(\xi, \eta)$, which therefore can be selected solely for convenience. Nevertheless, this breakdown into macro- and microrelief is conditional because it contains an arbitrary magnitude, t, the selection of which is beyond the scope of purely mathematical considerations, and should be made with the concrete goals of the research in mind.

The characteristics of the section of the lunar surface, the macrorelief, and the statistical properties of the microrelief, should include its morphological characteristics.

This is a practically acceptable description of a section of the lunar surface, but can be too detailed, depending on the goals of the research. We may not need a detailed description of the macrorelief, R(x, y), to solve a concrete problem, for example, but instead require its local properties, or, on the other hand, certain integral properties, statistical characteristics in particular. The selection of these latter is entirely dependent on the goals of the research and can be made only after the concrete questions to which answers must be provided during the research have been formulated.

This article is devoted to a preliminary explanation of the possibilities, in principle and in practice, of using photography to obtain the macrorelief, R(x, y), and certain integral characteristics of that relief, that can be useful in solving scientific and technical problems.

2. Restoration of the Relief of a Section of the Lunar Surface from Its Photographic Image.

The apparent brightness of a small section of the lunar surface, which can be taken as approximately flat, depends on its orientation when the positions of Sun and observer are fixed. The optical density of the photographic image /65 therefore contains information at each point as to the magnitude of the slope of the surface at the point. And because the slope is a differential characteristic of the relief, its image provides information on the relief. The completeness and reliability of this information depends entirely on the quality and quantity of original photographic data. Diggelen [1] was first to suggest photometric means for restoring the relief, and further development took place in the work of the Main Astronomical Observatory of the Academy of Sciences of the Ukrainian SSR [2] for lunar application.

Let us review the relationships on which the possibility of solving this problem, in principle, is based.

Let us say we have the image of a small section of the lunar surface, flat on the average, with photometric longitude λ_0 and photometric latitude φ_0. Let

us overlay this section with a Cartesian system of coordinates, x, y, such that the x-axis is oriented along the photometric parallel, and the y-axis along the photometric meridian. If the section under consideration is small enough it can be taken that the photometric coordinates of an infinitely small area of this section have the values λ and φ, which depend solely on the slope of this area, but are not explicitly dependent on its Cartesian coordinates.

Let the photometric properties of the section studied be identical at all points on the surface, and the dependence of the brightness of the area on the lunar surface, I, on the photometric coordinates λ and φ be characterized by the function $B(\lambda, \varphi, \alpha)$, where α is the phase angle for the given position of the Sun, and for the observer, such that

$$I = B(\lambda, \varphi, \alpha) \tag{2.1}$$

Then brightness in terms of x, y can be represented in the following form because of the dependence of the slope on x, y for small $\Delta\lambda = \lambda - \lambda_0$ and $\Delta\varphi = \varphi - \varphi_0$, with an accuracy to magnitudes of the order $(\Delta\lambda)^2$ and $(\Delta\varphi)^2$

$$I(x, y) = B(\lambda_0, \varphi_0, \alpha) + \frac{\partial B(\lambda, \varphi, \alpha)}{\partial \lambda}\Big|_{\substack{\lambda=\lambda_0 \\ \varphi=\varphi_0}} \cdot \Delta\lambda(x, y) + \frac{\partial B(\lambda, \varphi, \alpha)}{\partial \varphi}\Big|_{\substack{\lambda=\lambda_0 \\ \varphi=\varphi_0}} \Delta\varphi(x, y). \tag{2.2}$$

Now, in order to link brightness in terms of the coordinates I(x, y) with the macrorelief of the section, R(x, y), let us take advantage of the fact that

$$\Delta\lambda = -\operatorname{arc\,tg} \frac{\partial R(x, y)}{\partial x}; \quad \Delta\varphi = -\operatorname{arc\,tg} \frac{\partial R(x, y)}{\partial y}, \tag{2.3}$$

or, for small $\Delta\lambda$ and $\Delta\varphi$, approximately

$$\Delta\lambda = -\frac{\partial R(x, y)}{\partial x}; \quad \Delta\varphi = -\frac{\partial R(x, y)}{\partial y}, \tag{2.4}$$

so that Eqs. (2.2) and (2.4) will yield

$$I(x, y) = I_0 - \frac{\partial B(\lambda, \varphi, \alpha)}{\partial \lambda}\Big|_{\substack{\lambda=\lambda_0 \\ \varphi=\varphi_0}} \cdot \frac{\partial R(x, y)}{\partial x} - \frac{\partial B(\lambda, \varphi, \alpha)}{\partial \varphi}\Big|_{\substack{\lambda=\lambda_0 \\ \varphi=\varphi_0}} \frac{\partial R(x, y)}{\partial y} \tag{2.5}$$

where

$I_0 = B(\lambda_0, \varphi_0, \alpha)$, or

$$J(x, y) = b_x \frac{\partial R(x, y)}{\partial x} + b_y \frac{\partial R(x, y)}{\partial y}, \tag{2.6}$$

where

$$J(x, y) = 1 - \frac{J(x, y)}{J_0},$$

$$b_x = \frac{1}{J_0} \cdot \frac{\partial B(\lambda, \varphi; \alpha)}{\partial \lambda}\Big|_{\substack{\lambda=\lambda_0 \\ \varphi=\varphi_0}}, \quad b_y = \frac{1}{J_0} \cdot \frac{\partial B(\lambda, \varphi, \alpha)}{\partial \varphi}\Big|_{\substack{\lambda=\lambda_0 \\ \varphi=\varphi_0}}. \tag{2.7}$$

Eq. (2.6) is a linear partial differential equation that enables us to find R(x, y), knowing the dependence on the coordinates of the relative brightness J(x, y). But Eq. (2.6) must be supplemented by boundary conditions to arrive at an unambiguous localization of R(x, y). The most natural thing to do is to assign the R(x, y) value along some contour in the lunar section investigated that is not a characteristic line of this equation. /66

Numerous observations show [2, 3] that Eq. (2.1) for the lunar surface is such that $b_y = 0$ always is so and that Eq. (2.6) is converted into an ordinary differential equation when the system of coordinates has been selected as above

$$\frac{dR}{dx} = \frac{1}{b_x} J(x, y) \tag{2.8}$$

the solution of which is

$$R(x, y) = R_0(y) + \frac{1}{b_x} \int_0^x J(x', y)\, dx' \tag{2.9}$$

and contains the constant of integration $R_0(y)$. Here the characteristic lines of Eq. (2.6) are straight lines, parallel to the x-axis, and the unambiguous localization of the relief, R(x, y) is possible only in a band parallel to the x-axis and intersecting the contour to which the boundary condition was assigned.

This boundary condition usually is unknown, however. In such cases it can be obtained (within a constant factor) from other photography, obtained under different illumination conditions, when the photometric meridian is in another direction. It is impossible to make an unambiguous determination of the relief if the second photographs are not available to the researcher. Now other information on the nature of the region studied can be used as the basis for plausible assumptions as to its statistical qualities, and these qualities then can be used to find the most plausible form of R(x, y), with consideration given to Eq. (2.8), or Eq. (2.9). There is a broad class of cases when this approach leads to the conclusion that the most plausible relief, R(x, y), satisfies the condition

$$\int R(x, y)dx = 0 \qquad (2.10)$$

within the limits of the region. It replaces the boundary condition and, together with Eq. (2.9), uniquely determines the function R(x, y), which now should be understood to be the most probable, but completely optional, true macrorelief.

This simple arrangement for finding the relief from the image applies only to the case when the image contains no shadows. Ordinarily, however, illumination adequate for discovering the relief forms shadows. It is easy to take this fact into consideration, but in such case only the relief of the illuminated sections can be identified, naturally. By way of illustration, let us consider the simplest, yet extremely common, case of shadows falling along the photometric parallel. This occurs, in particular, when the region studied is in the center of the disk, that is, when the observer views it along a normal to its mean plane.

Let a straight line, parallel to the y-axis, intersect the boundary of the shadows at points x_0, x_1, x_2 ...x_n, and when k is even, x values satisfying the inequality

$$x_k < x < x_{k+1}, \qquad (2.11)$$

correspond to the illuminated points.

Then relief R(x, y) satisfies Eq. (28) [sic] at each of these intervals, remains ambiguous in the intervals

$$x_{k+1} < x < x_{k+2} \qquad (2.12)$$

when k is even. We can relate the R(x, y) values in the different intervals of (2.11) by taking advantage of the fact that the point (x_{k+2}, y) (for even k) is the end of the shadow cast by point (x_k, y) such that

$$R(x_{k+2}, y) - R(x_{k+1}, y) = (x_{k+2} - x_{k+1}) \operatorname{ctg} i, \qquad (2.13)$$

where i is the angle of incidence of the light at the lunar region under study (if the shadow is cast along the x-axis in the positive direction). The angle i is readily reflected in photometric coordinates.

Eqs. (2.8) and (2.13) together form a differential-difference equation, the solution of which in the interval (x_{k+2}, x_{k+3}) can be expressed recursively by a solution in the interval (x_k, x_{k+1}) of the equation

$$R(x, y)=R(x_{k+1}, y)+\frac{1}{b_x}\int_{x_{k+2}}^{x} R(x', y)\,dx'-(x_{k+2}-x_{k+1})\operatorname{ctg} i. \tag{2.14}$$

This solution contains an arbitrary constant, $R(x_0, y)$, quite analogous to the constant $R_0(y)$ in Eq. (2.8). Everything said about $R_0(y)$ applies as well to $R(x_0, y)$. It should be noted, in passing, that analysis of the form of the shadow boundaries could yield additional information about the relief. This question is beyond the scope of this article, however.

The results of the review cited in this section are tentative in nature because Eq. (2.2) was obtained from the approximate replacement of the function $B(\lambda, \varphi, \alpha)$ by the linear part of a Taylor series, and is applicable only to small slopes. This simplification in no way concerns the principle involved, but its rejection will make it necessary to solve a more complex equation than Eq. (2.6).

On the other hand, the effect on the results obtained of random errors, unavoidable in all measurements, has not been included here. Consideration of these errors can disclose additional limitations on the practical possibility of finding the relief from the photometric image.

Finally, this review is based on the assumption of photometric homogeneity of the section studied, something that seldom is the case in fact. Consideration of photometric heterogeneity of a region can require a third round of photographs, if it is necessary to find a unique solution for $R(x, y)$, or additional information of a statistical nature if one is restricted to discovering the statistically plausible form of $R(x, y)$.

Thus, the question reviewed in this section requires additional study, primarily involving expanding the region of applicability of the theory, evaluating the accuracy of the results obtained, seeking the optimum criteria for plausibility when data are inadequate, optimum methods of taking excess information (if available) into consideration, as well as along the lines of a more detailed theoretical and experimental investigation of the law of the reflection of light from the lunar surface.

3. Analog Methods for Obtaining the Correlation Function for the Macrorelief from the Photographic Image of the Region

This section will discuss methods of obtaining the correlation function for altitudes by analog means /68

$$K_R(\xi, \eta) = M[R(x, y) \cdot R(x + \xi, y + \eta)], \tag{3.1}$$

based on its connection with the correlation function for brightness, $C(\xi, \eta)$, determined by the equality

$$C(\xi, \eta) = M[J(x, y) \cdot J(x + \xi, y + \eta)], \tag{3.2}$$

where M is the mathematical expectation. The surface is assumed statistically homogeneous. This connection can be obtained if the relative brightness $J(x, y)$, is expressed in terms of the slope using Eq. (2.6), if $b_y = 0$ for the Moon [3, 4], and if the expression obtained can be substituted into Eq. (3.2). This leads to

$$C(\xi, \eta) = b_x^2 M\left[\frac{\partial R(x, y)}{\partial x} \cdot \frac{\partial R(x + \xi, y + \eta)}{\partial x}\right] \tag{3.3}$$

The following equality can be shown to exist for the mathematical expectation in the right-hand side of Eq. (3.3) for a section characterized by the correlation function for altitudes, $K_R(\xi, \eta)$

$$M\left[\frac{\partial R(x, y)}{\partial x} \cdot \frac{\partial R(x + \xi, y + \eta)}{\partial x}\right] = -\frac{\partial^2 K_R(\xi, \eta)}{\partial \xi^2}, \tag{3.4}$$

such that the unknown relationship has the form

$$\frac{\partial^2 K_R(\xi, \eta)}{\partial \xi^2} = -\frac{1}{b_x^2} C(\xi, \eta), \tag{3.5}$$

and is an ordinary differential equation for $K_R(\xi, \eta)$. The boundary condition for it, permitting the finding of a unique solution, follows from the general properties of the autocorrelation function, evenness, and vanishing at infinity, and has the form

$$K_R(\infty, \eta) = 0, \; K_R(\xi, \eta) = K_R(-\xi, \eta). \tag{3.6}$$

Its solution, boundary conditions considered, has the form

$$K_R(\xi, \eta) = -\frac{1}{b^2}\int\int C(\xi'', \eta)\, d\xi''\, d\xi'. \tag{3.7}$$

So the autocorrelation function for Eq. (3.1) altitudes can be found without image restoration of relief R(x, y) if the Eq. (3.2) correlation function is found by the analog method for the image (this requires an image with a contrast factor of unity).

Two methods are available for determining the Eq. (3.2) autocorrelation function. One, let us call it the correlation method, involves measurement of the integral transparency of a pair of photographic plates with images of the section under investigation so composed that the integral transparency is equal to the product of the brightness in Eq. (3.2) within a constant summand sign and factor. The Eq. (3.2) correlation function, can, for example, be calculated by using the following formula, based on the ergodicity of the realization of the ensemble of random surfaces, /69

$$C(\xi, \eta) \approx \frac{1}{S}\int J(x, y)\cdot J(x+\xi, y+\eta_1)\, dx\, dy,$$

for entire region (3.8)

is obtained as the dependence of the integral transparency of this pair of plates on the magnitude of the shift between them [5]. Here S is the area of the region investigated.

The second method can be called the spectral method because it involves finding the Eq. (3.2) correlation function in terms of the spatial spectrum of the photographic image on the basis of the Weiner-Khinchin theorem

$$C(\xi, \eta) = \int_{-\infty}^{\infty}\int S(\mu, \nu)\, e^{i(\mu\xi+\nu\eta)}\, d\mu\, d\nu, \tag{3.9}$$

where $S(\mu, \nu)$ is the spatial spectrum of the photographic image (with contrast equal to unity) of the region investigated.

There is a simple analog method for obtaining the spectrum of the photographic image that uses the coherent bundles technique [6]. It is based on the fact that the optical image in the focal plane of the objective lens is a

Fourier transform of the amplitude of the light wave in the plane of the objective lens aperture. This spectrum is obtained in the form of blackenings on the photographic plate which then must be subjected to photometry and used to make the Eq. (3.9) calculation.

4. The Possibility of Obtaining Crater Distribution by Size from the Brightness Correlation Function

The analog methods reviewed in the preceding section can, in principle, be used to obtain finer statistical characteristics of the region investigated. This possibility can be illustrated by the example of the distribution of craters by size for the ideal case when there are no other types of formation in a specified region, and all craters are geometrically similar and differ only in size.

Let the distribution of crater brightness be described by the function $i\left(\frac{x - x_0}{a}; \frac{y - y_0}{a}\right)$, where a is the crater diameter and x_0 and y_0 are the coordinates of its center. Then, in the case of uniform displacements along the x-axis, the correlation function for the image of this crater

$$k(\xi, a) = \int_{-\infty}^{\infty}\int i\left(\frac{x}{a}, \frac{y}{a}\right) i\left(\frac{x+\xi}{a}, \frac{y+\eta}{a}\right) dx\, dy \tag{4.1}$$

can be represented in the form

$$k(\xi, a) = a^2 k_0\left(\frac{\xi}{a}\right), \tag{4.2}$$

where

$$k_0(\xi) = k_0(\xi, 1). \tag{4.3}$$

If it is assumed that the density of craters in the area considered is sufficiently low, such that the characteristic distances between them are very much greater than the characteristic sizes, the one-dimensional correlation function $C(\xi)$ for the entire image, found using Eq. (3.2) when $\eta = 0$, is equal to /70

$$C(\xi) = \int_0^\infty k(\xi, a) f(a)\, da, \tag{4.4}$$

where f(a) is the unknown crater size distribution function.

$C(\xi)$ can be represented in the following form, using Eq. (4.2)

$$C(\xi) = \int_0^\infty k_0\left(\frac{\xi}{a}\right) f(a)\, a^2\, da. \tag{4.5}$$

This is an integral equation linking the correlation function for the brightness with the function for the distribution of craters by size. It can be reduced to an integral equation with a difference kernel if a conversion is made from variables ξ, a to the variable

$$X = \ln \xi,\ A = \ln a. \tag{4.6}$$

Then Eq. (6.5) [sic] becomes

$$\int_{-\infty}^{\infty} G(X-A)\cdot F(A)\, dA = Z(X),$$

where

$$G(X) = k_0(e^X),\ F(X) = e^{2X} f(e^X),\quad Z(X) = C(e^X). \tag{4.7}$$

There is no difficulty in finding the solution of Eq. (4.7), if it exists, by using the Fourier method.

The considerations set forth show that it is possible, in principle, but by no means possible in practice, to solve the problem posed because not taken into consideration here is the effect of measurement errors which, in problems of this type, usually are decisive. The question of the practical possibility of solving this problem requires separate investigation.

Conclusion

This article has considered ways to obtain the correlation function for the relief of a region under investigation from its photographic image by using analog type devices.

We have not considered more effective ways to find the statistical and morphological characteristics, accomplishment of which requires the use of electronic digital computers. The most universal method of automating the process of obtaining the statistical and morphological characteristics in this case is to put the image into a computer and obtain an algorithm for recognizing the objects, after which their classification (and comparison) and inclusion using the computer involves no special difficulties, in principle.

However, the object recognition problem is one of the most complex problems of modern cybernetics. It can be solved quite readily as a problem of making a statistical check of a set of hypotheses when posed in abstract form and as applicable to an individual model. The answer lies in finding an object that corresponds to the model with maximum a posteriori probability, but this means calculating the a posteriori probability for every possible object, using Bayes formula, and finding the object to which the maximum probability corresponds. /71 This problem is just as simple, and just as complex, in practice as it is in principle when this approach is taken, although there is a broad class of problems for which this approach can be used, readily, and easily. In the majority of the complex problems it is impossible to apply the a posteriori probability calculated for one object, assuming this can be done, to all objects. Hence the possibility of solving the problem using an optimum formulated algorithm remains a purely abstract possibility that will not lead to a practical solution of the problem. This problem now must be formulated as one of finding a practically realizable recognition algorithm which, if not optimum, is as close to the optimum in effectiveness as possible. The problem considered here is further complicated by the fact that models subject to recognition are not individualized because they have boundaries that are known in advance.

Still, the complexity of the problem considered ought not act as a deterrent to every effort to solve it by using this approach. The first step toward its solution can be a transition from the photographic image of the section investigated to its relief (#2). This eliminates a multiplicity of models corresponding to the same object (because it can be illuminated differently) and significantly simplifies the formulation of criteria distinguishing an object of a particular class from objects of another class. Each of these circumstances can simplify the recognition problem significantly. The complexity and time required to develop this method will pay for itself in full in its great possibilities and high degree of operability in solving newly posed problems.

The work was undertaken on the initiative of the Institute for Space Research of the Academy of Sciences of the USSR.

REFERENCES

1. Diggelen, I., B.A.N., 11, 1951, 423, 283.

2. Lisina, L. R., Fizika Luny i planet [Physics of the Moon and of the Planets], "Naukova Dumka" Press, Kiev, 1968, pp. 7-36.

3. Barabashov, N. P., Yezerskiy, V. I., Prishlyak, N. P., Tsirkulyar Khar'k. astronom. observatorii, No. 25, 1962, pp. 15-21, KhGU Press.

4. Minnaert, M., Planety i sputniki [Planets and Satellites], 1963, IL Press, pp. 192-218.

5. Barabashov, N. P., Akimov, L. A., Vestnik KhGU, seriya astro., No. 5, 1970, KhGU Press.

6. Mareshal, A., Franson, M., Struktura opticheskogo izobrazheniya [The Structure of an Optical Image], "Mir" Press, 1964.

Translated for the National Aeronautics and Space Administration under contract NASw-2038 by Translation Consultants, Ltd., 944 So. Wakefield St., Arlington, Virginia 22204.

NASA-Langley, 1973 —— 30 F-747

NATIONAL AERONAUTICS AND SPACE ADMINISTRATION
WASHINGTON, D.C. 20546

OFFICIAL BUSINESS
PENALTY FOR PRIVATE USE $300

SPECIAL FOURTH-CLASS RATE
BOOK

POSTAGE AND FEES PAID
NATIONAL AERONAUTICS AND
SPACE ADMINISTRATION
451

U.S.MAIL

POSTMASTER: If Undeliverable (Section 158 Postal Manual) Do Not Return

"The aeronautical and space activities of the United States shall be conducted so as to contribute . . . to the expansion of human knowledge of phenomena in the atmosphere and space. The Administration shall provide for the widest practicable and appropriate dissemination of information concerning its activities and the results thereof."

—NATIONAL AERONAUTICS AND SPACE ACT OF 1958

NASA SCIENTIFIC AND TECHNICAL PUBLICATIONS

TECHNICAL REPORTS: Scientific and technical information considered important, complete, and a lasting contribution to existing knowledge.

TECHNICAL NOTES: Information less broad in scope but nevertheless of importance as a contribution to existing knowledge.

TECHNICAL MEMORANDUMS: Information receiving limited distribution because of preliminary data, security classification, or other reasons. Also includes conference proceedings with either limited or unlimited distribution.

CONTRACTOR REPORTS: Scientific and technical information generated under a NASA contract or grant and considered an important contribution to existing knowledge.

TECHNICAL TRANSLATIONS: Information published in a foreign language considered to merit NASA distribution in English.

SPECIAL PUBLICATIONS: Information derived from or of value to NASA activities. Publications include final reports of major projects, monographs, data compilations, handbooks, sourcebooks, and special bibliographies.

TECHNOLOGY UTILIZATION PUBLICATIONS: Information on technology used by NASA that may be of particular interest in commercial and other non-aerospace applications. Publications include Tech Briefs, Technology Utilization Reports and Technology Surveys.

Details on the availability of these publications may be obtained from:

SCIENTIFIC AND TECHNICAL INFORMATION OFFICE

NATIONAL AERONAUTICS AND SPACE ADMINISTRATION

Washington, D.C. 20546